Chem Soc Rev

Current Advances of Lanthanide Ion (Ln3+)-Based UpconversionNanomaterials for Drug Delivery

Journal:	*Chemical Society Reviews*
Manuscript ID:	CS-REV-05-2014-000155.R1
Article Type:	Review Article
Date Submitted by the Author:	15-Jun-2014
Complete List of Authors:	yang, dm ma, pingan; changchun institute of applied chemistry, State key laboratory of application of rare earth resources hou, zy; changchun institute of applied chemistry, State key laboratory of application of rare earth resources cheng, zy; changchun institute of applied chemistry, State key laboratory of application of rare earth resources Li, Chunxia; changchun institute of applied chemistry, State key laboratory of application of rare earth resources lin, j; Changchun inst appl chem, rare earth lab

Chem Soc Rev Chemical Society Reviews Dynamic Article Links ►

Cite this: DOI: 10.1039/c0xx00000x

www.rsc.org/xxxxxx

Invited Review Article

Current Advances of Lanthanide Ion (Ln^{3+})-Based Upconversion Nanomaterials for Drug Delivery

Dongmei Yang, Ping' an Ma, Zhiyou Hou, Ziyong Cheng, Chunxia Li* and Jun Lin*

Received (in XXX, XXX) Xth XXXXXXXXX 20XX, Accepted Xth XXXXXXXXX 20XX
DOI: 10.1039/b000000x

Lanthanide ion (Ln^{3+})-based upconversion nano/micromaterials that emit higher-energy visible light when excited by low-energy NIR light have aroused considerable attention in the forefront of materials science and biomedical fields, which stems from their unique optical and chemical properties including minimum photodamage to living organisms, low autofluorescence, high signal-to-noise ratio and detection sensitivity, and high penetration depth in biological or environmental samples. Thus, Ln^{3+}-based upconversion materials are rising new stars and quickly emerging as potential candidates to revolutionize novel biomedical applications. In this review article, we mainly focus on the recent progress in various chemical syntheses of Ln^{3+}-based upconversion nanomaterials, with special emphasis on their application in stimuli-response controlled drug release and the followed therapy. Functional groups that are introduced into the stimuli-responsive system can respond to external triggers, such as pH, temperature, light, and even magnetic fields, which can regulate the movement of the pharmaceutical cargo and release drug at a desired time and in a desired area. This is crucial to boost drug efficacy in cancer treatment while minimizing side effects of cytotoxic drugs. So many multifunctional (magnetic /upconversion luminescence and porous) composite materials based on Ln^{3+} have been designed for controlled drug delivery and multimodal bioimaging. Finally, the challenges and future opportunities for Ln^{3+}-based upconversion materials are discussed.

1. Introduction

The rare earth elements comprise fifteen lanthanide (Ln) series (from lanthanum to lutetium) as well as yttrium and scandium. Except for La^{3+} and Lu^{3+}, almost all Ln^{3+} ions exhibit distinctive luminescence properties *via* intra-4f or 4f-5d transitions due to abundant and unique energy level structures arising from $4f^n$ inner shell configurations.[1,2] In particular, Ln^{3+}-based upconversion luminescence is one of the most outstanding features of rare earth luminescence, which have provoked extensive attention in past decade years in the forefront of materials sciences. Upconversion is a non-linear anti-Stokes process that efficiently converts two or more low-energy continuous-wave near-infrared (NIR) photons into a higher energy outcome photon (e.g. ultraviolet, visible, and NIR) through the use of long lifetime and real ladder-like energy levels of Ln^{3+} ions embedded in a suitable inorganic host matrix.[3,4] To increase the NIR absorption strength of upconversion Ln^{3+} ions in host lattice, Yb^{3+} is often co-doped with the other ions (Er^{3+} , Tm^{3+}, and Ho^{3+}), as a sensitizer for the upconversion process. The upconversion principles have been studied thoroughly and some excellent reviews have been published by Auzel and Güdel.[5,6] Moreover, Berry and co-workers recently reported the systematic investigation of the optimized geometry and electronic structure of Ln^{3+} doped in hexagonal (β)-$NaYF_4$ nanocrystals in the basis of density functional theory with a spin polarization approach.[7,8]

In the past five years, the focus on Ln^{3+}-doped upconversion nanoparticles (UCNPs) has shifted, away from the controlled synthesis of uniform UCNPs, toward the applications in biomedical fields, as evidenced from the rapidly upsurge of reports on UCNPs for biomedical purposes.[9-19] This stems from their unique advantages, as shown in Fig. 1. Firstly, the excitation wavelength (e.g. 980 nm) for UCNPs is located within the "optical transparency windows" (700-1100 nm),[20] so the use of NIR light holds such advantages as absence of photodamage to live organisms, low autofluorescence background, high signal-to-noise ratio and detection sensitivity, and high penetration depth in biological tissues. In addition, UCNPs have superior chemical stability and remarkable photostability free of on-off blinking and measurable photobleaching under prolonged single-particle excitation (Fig. 1a-d).[21-29] Especially, several recent reports have demonstrated that Nd^{3+} ions, with a large adsorption cross section of at 808 nm, can serve as another sensitizer for upconversion process through the energy migration process like $Nd^{3+} \rightarrow Yb^{3+} \rightarrow$ activators (e.g. Er^{3+}, Tm^{3+} and Ho^{3+}), in which Yb^{3+} ions act as transporting intermediary to make this phenomenon possible.[32-37] Inspiringly, since the adsorption of water at 808 nm is much lower relative to that at 980 nm, the use of Nd^{3+} ions can considerably minimize the overheating effect associated with

conventional 980 nm excitation. Thus this may become another effective solution to reducing potential tissue damage caused by the NIR excitation lasers, especially suitable for NIR photoactivation of biomolecules or phototriggered drug delivery. These intriguing merits impart UCNPs with the capability for *in vitro* and *in vivo* upconversion luminescence (UCL) imaging[28-46] and even NIR light mediated imaging of latent fingerprints based on molecular recognition.[47] Secondly, manifold emission colors can be tuned elaborately by changing host lattices and doping concentration of activators under single NIR light excitation, which provides plenty of room for versatile applications of UCNPs.[48-58] An interesting and exciting example was reported by Liu and co-workers, who fabricated of a series of multicolor-banded upconversion barcodes based on tip-modified β-$NaYF_4$ microrods with different activators doped at the tips (Fig. 1e).[62] Different combinations of three primary colors (blue, green, and red) constructed multicolor upconversion barcodes that are easily readable with conventional optical microscopes. Thirdly, compared with other paramagnetic Ln^{3+} ions (e.g. Dy^{3+} and Ho^{3+}), Gd^{3+} is most preferred for preparing T_1 contrast agents because Gd^{3+} has the highest number of unpaired f electrons with parallel spin. More importantly, the spin-relaxation time of Gd^{3+} can match the Larmor frequency of protons in suitable magnetic field.[63] As a consequence, Gd^{3+}-based UCNPs themselves exhibit optical-magnetic features synergistically and can be used as a new type of multimodal imaging probe that works for both simultaneous upconversion luminescence (UCL) imaging and magnetic resonance imaging (MRI) (Fig. 1f).[64-72] What deserves to be mentioned most is that host lattices barium containing (Ba), ytterbium (Yb) and gadolinium (Gd) are also promising X-ray tomography (CT) contrast agents.[73-81] Finally, a series of both *in vitro* and *in vivo* toxicology studies indicate that UCNPs show good biocompatibility, and so far no evidence demonstrates noticeable biotoxiciy.[82-87] Thus, Ln^{3+}-based upconversion materials are rising new stars and quickly emerging as candidates to revolutionize novel biomedical applications covering multimodal bioimaging, photodynamic therapy, and drug/gene delivery.

The basic concept in utilizing UCNPs for therapeutic purposes originates from the capability to combine other functional nanostructures in one hybrid system, which aim to obtain so-called "theranostic" multifunctional nanomedical platforms for the synergistic diagnosis, therapy and monitoring of the therapeutic progression of the disease. On the other hand, the major obstacles in current chemotherapy include side effects of cytotoxic drugs to healthy tissues, lower therapeutic accumulation concentration at targeted location, and unspecific uptake of normal cells. To ameliorate these hurdles, very clever devices of stimuli-responsive drug delivery systems that deliver a drug in spatial-, temporal-, and dosage-controlled fashions are highly demanded.[88, 89] Recently, spurred by the significant advances in the fabrication of high-quality UCNPs and subsequently elegant surface modification strategies, UCNPs-based nanocomposites have also brought out their captivating advantages in the design and construction of stimuli-responsive drug delivery systems that can response to endogenous or externally specific triggers, such as pH, temperature, magnetic field light, and redox gradients. In particular, UCNPs can serve as nanotransducers to replace the

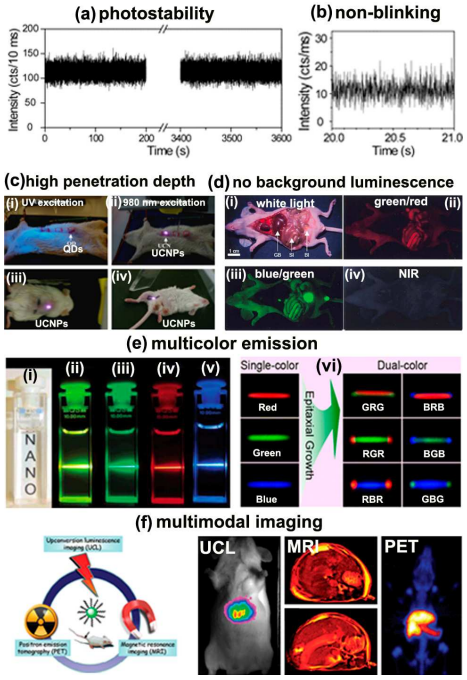

Fig. 1 Unique advantages of UCNPs: (a) Photostability: the time trace of emission intensity from a single UCNP under continuous laser illumination for more than 1 h, suggesting the durable photostability of the UCNPs. (b) Non-blinking: the zoom-in time trace and histogram of emission intensity, showing no on/off behavior non-blinking. (c) High penetration depth: *in vivo* imaging of rat: quantum dots (QDs) injected into abdomen, showing no luminescence (i); PEI-$NaYF_4$:Yb/Er nanoparticles injected below abdominal skin (ii), thigh muscles (iii), or below skin of back (iv), showing obvious luminescence. (d) No background luminescence interference: wavelength-dependent autofluorescence of vital organs and bodily fluids. (i) immediately after sacrifice, the viscera of a hairless, athymic *nu/nu* mouse were exposed. Tissue autofluorescence was then imaged using three different excitation/emission filter sets: (ii) blue/green (460–500 nm/505–560 nm); (iii) green/red (525–555 nm/590–650 nm); and (iv) NIR (725–775 nm/790–830 nm). Arrows in (i) mark the location of the gallbladder (GB), small intestine (SI) and bladder (Bl). (e) Multicolor emission: (i-v) one wt % colloidal solutions of $NaYF_4$:Yb/Er nanocrystals in dichloromethane excited at 977 nm demonstrating upconversion luminescence. (i) $NaYF_4$:Yb/Er solution; (ii) total upconversion luminescence; (iii and iv) $NaYF_4$:Yb/Er upconversion viewed through green and red filters, respectively; (v) $NaYF_4$:Yb/Tm solution; (vi) Single-color emission: optical micrographs of the parent $NaYF_4$ upconversion microrods doped with Yb/Tm (20/0.2 mol%), Yb/Er (5/0.05 mol%), and Yb/Er (50/0.05 mol%), respectively. And dual-color-banded upconversion optical micrographs obtained by varying the composition of the dopants. (f) Multimodal imaging: scheme of a multimodal imaging probe and UCL, MRI and PET (Positron Emission Computed Tomography) multimodal imaging of small animals using $NaYF_4$:Yb/Er. (Adapted from refs. 3, 21, 22, 26, 42, 62. Copyright 2003, 2006, 2008, 2009, 2012, 2014, Highwire press PNAS, Wiley-VCH Verlag GmbH & Co. KGaA, American Chemical Society, Royal Society of Chemistry and Elsevier B. V. Reproduced with permission.)

undesired ultraviolet (UV)-visible source to activate photosensitive therapeutic molecules to fulfill remotely NIR photo-triggered drug release of drug delivery with high spatial/temporal resolution. The majority of the existing photoresponsive drug carriers usually require UV or short visible wavelength excitation, which not only induces severe phototoxicity, but also exhibits low signal-to-noise ratio and significantly limited light-penetration depth. Therefore, such disadvantages would seriously hinder their application in living systems. Hence, NIR-to-UV/visible UCNPs have promising potential in the design of photocontrolled drug delivery at a desired location and specific time. Recently, some UCNPs-based photoresponsive systems have been engineered to achieve on demand drug release in response to irradiation of NIR light.[90-96] So far, quite a few reviews regarding UCNPs-based synthesis, multicolor tuning and applications have been published.[2, 6-16, 27, 30, 40, 97-114] However, taking into account the rapid development of UCNPs in biological applications, it is anticipated that there is still a strong demand for a thorough review with updated and growing literatures related to UCNPs-based composites for controlled drug delivery by means of the rational design of stimuli-response systems. So in this review we mainly highlights the current state-of-the-art for the rational design, fabrication strategies, and application in drug delivery and cancer therapy of UCNPs-based multifunctional nanocomposites based on our and other related research in this area. For the sake of brevity, synthesis, surface modification, biodetection, multimodal bioimgings, and solar cells of UNCPs are not within the principle scope of this review. The readers who are interested in these aspects can refer to other specific reviews[97-114] or representative papers.[115-141]

2. Design philosophy for UCNPs-based drug delivery systems

The principle design philosophy of UCNPs-based drug delivery involves the combination of UCNPs with other functional building blocks (including inorganic and organic materials) into single nanoplatform for the synergistic diagnosis, therapy and monitoring of the therapeutic progression of the disease by taking advantage of special merits of UCNPs. To achieve this goal, three points should be kept in mind. Firstly, the synthesis of high-quality (pure-phase, uniform, monodisperse, and well-shaped) UCNPs is fundamental and crucial in order to integrate effectively other functional nanostructures. From the viewpoint of materials applications, it is particularly attractive because of the possibility to display their respective advantages of each material. Secondly, the composite materials should provide suitable pore structure or linkage site to load antitumor drug molecules by physical absorption or covalent association. Finally, elegant modification strategies should be explored to build up stimuli-responsive devices for drug delivery, which can boost drug efficacy in cancer treatment while minimizing side effects of cytotoxic drugs. In particular, it should be emphasized that the absorption spectra of photosensitive compounds should overlap with the emission band of UNCPs in order to fully utilize the energy transfer between them. In this way, UV/visible light emitted by UCNPs can be exploited to trigger the photoresponsive species anchored to the surface of UCNPs to form NIR light triggered controlled drug delivery. In general, UCNPs-based drug delivery systems mainly include four groups: (i) silica or mesoporous silica coating or encapsulation (UCNPs@SiO_2); (ii) polymer grafting or self-assembly (UCNPs@polymer); (iii) hollow UCNPs with mesoporous surface (hollow UCNPs); and (iv) electrospinning fibers decorated with UCNPs (UCNPs@fibers), as illustrated in Scheme 1. Of course, through rationally design other functional nanostructures (e.g. superparamagnetic Fe_3O_4, ultrasmall CuS and Au nanoparticles) can also been incorporated within UCNPs to obtain symbiosis of the properties of all components. Drug molecules can be conjugated to these carriers by either covalent or non-covalent means. The following section will elaborate the various strategies for these multifunctional UCNPs-based drug delivery systems.

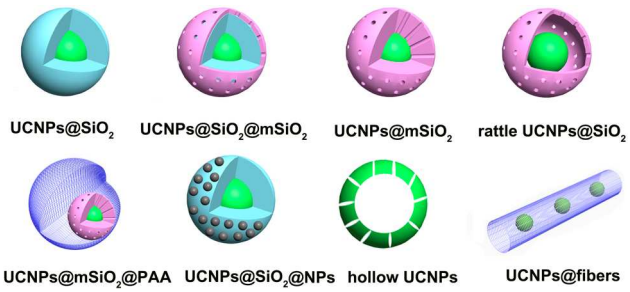

Scheme 1 Schematic Illustration of UCNPs-Based Drug Delivery Carriers. (UCNPs: upconversion nanoparticles, $mSiO_2$: mesoporous silica; PAA: polyacrylic acid; NPs: other functional nanoparticles such as Au, Fe_3O_4, and CuS etc.)

3. Synthetic strategies for UCNPs-based drug delivery systems

Currently, the representative pathways to synthesize four kinds of UCNPs-based drug delivery systems mentioned above can be broadly divided into four categories: (i) sol-gel method; (ii) hydrothermally-assisted template method; (iii) polymer grafting or self-assembly; (iv) electrospinning route.

3.1 Sol-gel method

Sol-gel method is a typical technique for UCNPs-based drug delivery systems without requiring complicated procedures or instruments. The representative sol-gel process involves inorganic precursors (metal salts or metal-alkoxides) that upon reaction with water undergo hydrolysis and condensation, leading to the formation of 3D oxide networks.[142] One of the most well-known examples is the synthesis of uniform colloidal silica spheres that was invented by Stöber in the 1960s.[143] This discovery was called "Stöber method" and produces a profound influence on the synthesis of novel core-shell structured materials with a variety of components, sizes and properties in which silica can be served as either a core or a shell.[144,145] Alternatively, Osseo-Asare and Arriagada opened up a novel water-in-oil reverse microemulsion method for the synthesis of silica nanoparticles with more uniform size.[95] Via microemulsion method (surfactant Trix-100 or Igepal CO-

520/cyclohexane/aqueous solution), a thin and dense silica layer was coated onto the surface of UCNPs to form highly uniform and monodisperse core-shell structured UCNPs@SiO_2 nanospheres.[147,148] The surface of SiO_2 can be readily functionalized with diverse groups such as amines, carboxyl, or thiols, enabling to connect other nanoparticles or photosensitive molecules.[149-153] For examples, Shi and co-workers have demonstrated that the obtained UCNPs@SiO_2 can be integrated with other functional building blocks such as Au nanoparticles (for CT imaging) and ultrasmall CuS (for phototermal therapy) to form multifunctional UCNPs@SiO_2@Au or UCNPs@SiO_2@CuS nanoparticles, which display their respective properties of each component so as to achieve multimodal bioimagings and synergetic therapy (radiotherapy and photothermal ablation).[151,152] Afterwards, taking into account that the dense silica shell has some limitation in drug delivery because of the absence of porous structures, mesoporous silica is used to coat the functional nanoparticles based on modified Stöber method. Mesoporous silica (mSiO_2) possesses intriguing properties including good compatibility, the porous structures with high surface area (providing reserviors for loading various guest molecules), tunable pore size (offering the selectivity for adsorption and controllability of the release of the restricted nanoparticles), and the ease of surface functionalization (providing active site for linking other biological molecules).[154-159] As such, if UCNPs combine with silica or mesoporous silica, a kind of novel core-shell structured nanomaterials for drug delivery can be obtained. By reasonable core-shell structured design and different synthetic strategies, UCNPs can be assembled on, encapsulated within, or combined with other specific nanoparticles to inside and on the surface of silica or mesoporous silica for different application purposes. In this context, dramatic efforts have been devoted to the synthesis of a series of UCNPs-SiO_2 drug delivery systems through sol-gel chemistry.

3.1.1 Two-step sol-gel method

In order to produce mesoporous silica layer, there are two common used structure-directing agents: surfactant cetyltrimethylammonium bromide (CTAB) and organosilanes octadecyltrimethoxysilane (C18TMS). The former can form ordered mesopores while the latter can form disordered and worm-like ones. In the early work, via two-step sol-gel reaction, we fabricated multifunctional nanocomposites using Fe_3O_4 nanospheres as core, with subsequent coating with dense silica and ordered mesoporous silica, and further functionalized by the deposition of $NaYF_4$:Yb/Er (Tm) UCNPs,[160] as shown in Fig. 2. The resultant composite nanomaterials Fe_3O_4@SiO_2@mSiO_2@UCNPs exhibit high magnetization (38.0 emu g^{-1}) and bright UC emission under 980 nm laser excitation. The intermediate solid SiO_2 as a protective matrix plays an important role in protecting the upconversion luminescence from quenching by inner black Fe_3O_4 core while mSiO_2 shell can be used to load drug model ibuprofen (IBU). More importantly, the drug release amount can be monitored by the change of the UC emission intensity. This class of multifunctional system seems to have potential for targeting the tracking drug delivery based on its magnetic and luminescent properties. Following this concept, instead of coating UCNPs at the surface of mSiO_2, UCNPs as inner core was also encapsulated by mSiO_2 to form Gd_2O_3:Er@SiO_2@mSiO_2 (Fig. 3a).[161] In addition, Sun et al. reported the one-pot self-assembly of multifunctional mesoporous nanoprobes with magnetic nanoparticles and hydrophobic upconversion nanocrystals, in which CTAB-stabilized UCNPs (with positive charge) were self-assembled onto Fe_3O_4@SiO_2 (with negative charge) like core–satellites via electrostatic and van der Waals interactions. Then the subsequent co-condensation of tetraethyl orthosilicate (TEOS) and CTAB resulted in the formation of the outer mesoporous silica layer.[162] Apart from CTAB, C18TMS is a common directing agent for the synthesis of disordered mesopore structures. Zhang and our group reported the synthesis of UCNPs@SiO_2@mSiO_2 nanoparticles by using surfactant C18TMS as pore generator via two-step sol-gel reactions,[148,163] as shown in Fig. 3b.

3.1.2 One - step sol-gel method

Despite its success, there are some problems to be addressed for two-step sol-gel method. One of the biggest shortcoming is the inevitable and uncontrolled aggregation of the final nanoparticles, because C18TMS must be removed by high-temperature calcination (550 °C, 6 h), which seemed to the only known way to remove C18TMS from the silica network.[164] Another drawback in two-step sol-gel reaction is that the fabrication of these materials typically requires the intermediate coatings of solid silica followed by further deposition of mesoporous silica layer, which involves the complicated and multistep procedures. To overcome these hurdles, the direct coating of mesoporous silica on the surface of single upconversion nanoparticle is highly demanded via a facile and general strategy. In 2006, Heyon's group reported a typical method for the direct encapsulation of

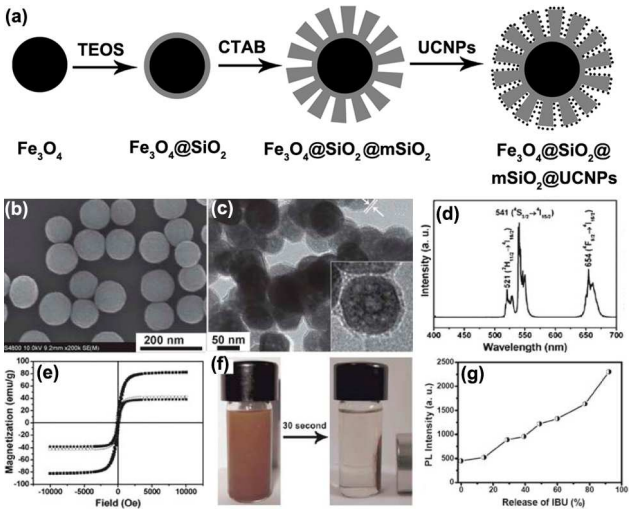

Fig. 2 The formation process of multifunctional Fe_3O_4@SiO_2@mSiO_2@$NaYF_4$:Yb/Er nanocomposites (a), SEM (b) and TEM (c) images, up-conversion emission spectrum (d) of nanocomposites, the magnetic hysteresis loops (e) of pure Fe_3O_4 (O), Fe_3O_4@SiO_2@mSiO_2 (■), Fe_3O_4@SiO_2@mSiO_2@$NaYF_4$:Yb/Er (*), the separation process of the nanocomposites by mamagnet (f), and up-conversion emission intensity of Er^{3+} in IBU-loaded materials as a function of the cumulative released IBU (g). (Adapted from ref. 160. Copyright 2010, Wiley-VCH Verlag GmbH & Co. KGaA. Reproduced with permission.)

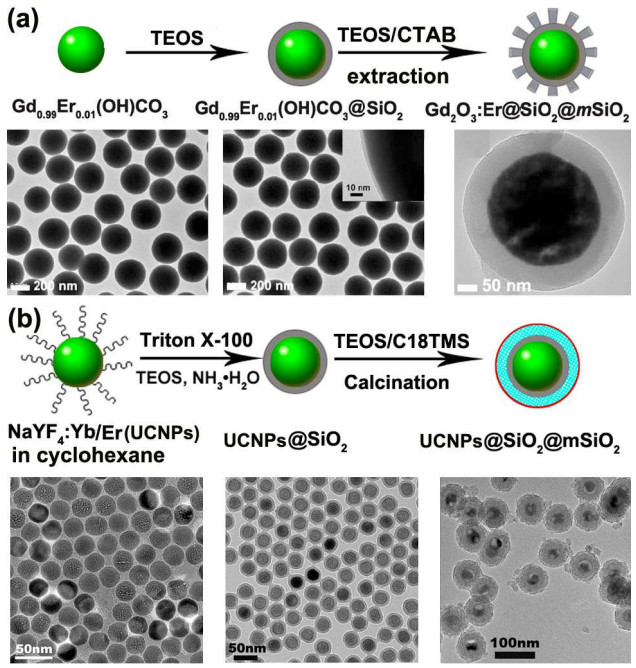

Fig. 3 Schematic illustration for the synthesis of UCNPs@SiO_2@mSiO_2 composite materials via two-step sol-gel strategy by using CTAB (a) or C18TMS (b) as structure-directing agents and the corresponding shape of the product obtained each step. (Adapted from refs. 148, 161. Copyright 2010, 2014, Wiley-VCH Verlag GmbH & Co. KGaA and Royal Society of Chemistry. Reproduced with permission.)

hydrophobic inorganic nanoparticles with mesoporous silica shell.[165] In this method, CTAB not only acts as a capping and phase-transfer agent, but also as the templates for the formation of mesoporous structure in the silica sol-gel reaction. This outstanding work provides a new opportunity for the direct coating of diverse hydrophobic nanoparticles with different compositions, shapes, and sizes with mesoporous silica shells.[166] Enlightened by these researches, our group and Shi's group have reported independently the synthesis of uniform, and monodisperse UCNPs@mSiO_2 nanocomposites by one-step sol-gel process.[168-171] The synthetic procedure for UCNPs@mSiO_2 nanocomposites is shown in Fig. 4.[170] Hydrophobic UCNPs [e.g. $NaYF_4$:Yb/Er or NaY(Gd)F_4:Yb/Er@$NaGdF_4$:Yb] were first transferred from the organic phase to the aqueous phase by using CTAB as a secondary surfactant. Then CTAB-terminated UCNPs can act as the seed for the coating of the mesoporous silica shell via sol-gel process. Finally, the surfaces of the UCNPs@mSiO_2 nanospheres were modified with polyethylene glycol (PEG) in order to enhance the nanocarrier dispersion and long-term stability under physiological conditions, prolong circulation time of the nanocarrier in blood, and facilitate preferential accumulation at the tumor sites by the enhanced permeation and retention (EPR) effect.[172] Thus in this kind of composite nanomaterial, the core imparts it with luminescence and/or magnetic properties for simultaneous UCL and MR imaging, whereas the mesoporous shell afford it suitable to load anticancer drug. The average diameter of nanospheres is determined to be below 100 nm, which is within the acceptable size range for

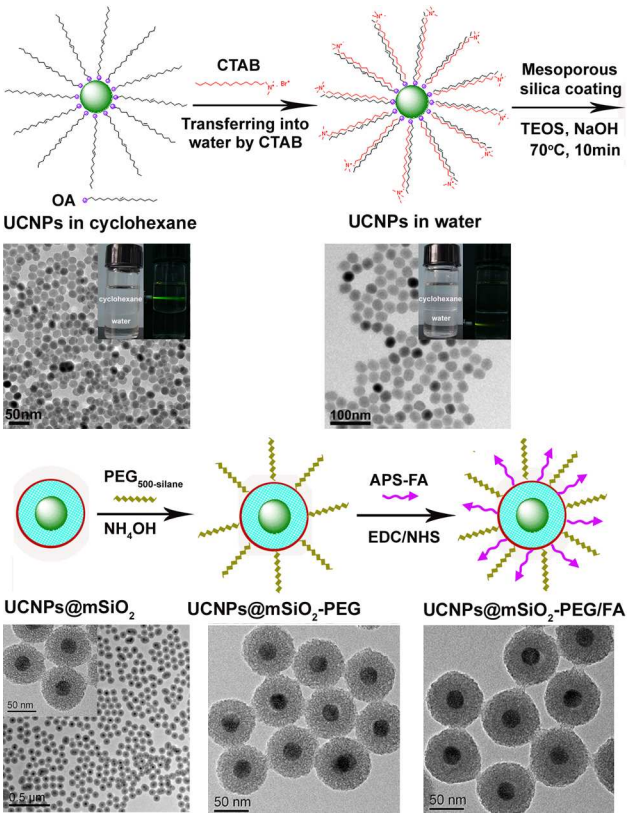

Fig. 4 Schematic illustration for the synthesis of UCNPs@mSiO_2-PEG/FA composite nanospheres via one-step sol-gel reaction and the corresponding shape of products. (Adapted from ref. 170. Copyright 2013, Royal Society of Chemistry. Reproduced with permission.)

biomedical applications *in vivo*.

In addition, CTAB-stabilized UCNPs can be employed to construct pH-responsive drug delivery nanocarriers by using poly(acrylic acid) (PAA), a biodegradable superabsorbent, as a nanoreactor and template. Recently, Wang and co-workers fabricated a novel and unique multifunctional (concentric-UCNPs@mSiO_2)@PAA core-double shell nanostructures (Strategy 1, Fig. 5).[173] The formation of the eccentric PAA shells should be related to the change of the interfacial energy between PAA, UCNPs@mSiO_2 NPs, and the solvent, likely resulting in a minimum interfacial energy. Such material has two specialcharacteristics: ultra high drug storage capacity and sensitive pH-responsive drug release properties. The drug loading content in eccentric-(concentric-UCNPs@mSiO_2)@PAA was 2 mg of DOX per 1 mg nanomaterials. This is because PAA, with an abundance of carboxyl groups, not only effectively loads the positive charged drugs by electrostatic interactions but also has a pH-responsive performance. In the subsequent work, taking into accounts that PAA in the outer layer is unstable in water and prone to swell, the same researchers further improved the experimental protocol. Special eccentric UCNPs@PAA@SiO_2 core-shell nanoclusters consisting of a single $NaYF_4$:Yb/Er/Gd UCNP as core, PAA as intermediate layer, and eccentric SiO_2 as outer layer were manufactured successfully,[174] as shown in Fig. 5 (Strategy 2). In brief, PAA molecules were self-assembled around CTAB-UCNPs nanoparticles to obtain eccentric UCNPs@PAA core-shell nanospheres. During this process, the resulting

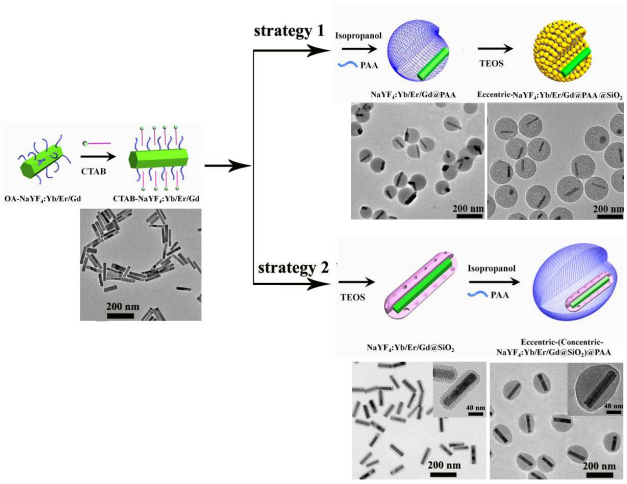

Fig. 5 Schematic illustration of the synthetic procedure for the eccentric $NaYF_4$:Yb/Er/Gd@PAA@SiO_2 core-shell nanoclusters and the corresponding shapes (strategy 1) as well as eccentric-(concentric-$NaYF_4$:Yb/Er/Gd@SiO_2)@PAA core-shell nanostructures and the corresponding shapes (strategy 2). (Adapted from refs. 173, 174. Copyright 2013, Royal Society of Chemistry and American Chemical Society. Reproduced with permission.)

eccentric PAA shell is like a "reservoir" to absorb and retain water molecules inside its net structure because the PAA is a high water-absorbent polymer. Then the hydrolysis reaction of TEOS was confined in the PAA network by sol-gel process, leading to the formation of eccentric UCNPs@PAA/SiO_2 core-shell nanoclusters. Likewise, eccentric UCNPs@PAA/SiO_2 nanomaterial has good capability of drug loading, however, its stability in water has been improved greatly compared to the former.

3.1.3 Combined use of sol-gel method and surface-protected etching method

Apart from the usage of pore-making agents discussed above, UCNPs-based nanoparticles obtained by sol-gel reactions can be further etched to produce rattle-type (or defined as yolk-shell) drug delivery nanocarriers.[175-178] Rattle-type nanostructures have unique interstitial hollow space between core and mesoporous shell, which are attractive as new-generation drug delivery nanoplatform with greatly enhanced drug loading capacity.[179-181] One of the most straightforward synthetic methodologies for rattle-type nanostructures is surface-protected etching method. This approach was first reported by Yin and co-workers to prepare hollow mesoporous SiO_2, where polyvinylpyrrolidone (PVP) as protecting layer was coated solid SiO_2 spheres and subsequent selective etching of the interior SiO_2 using NaOH as etchant by virtue of structural difference between the core and shell of SiO_2.[182] In general, the selection of appropriate etchants and surface protecting agents is critical to obtain high quality yolk-shell structured nanomaterials.[183] The most frequently used etchants include NaOH, HF, $NaCO_3$ and even hot water while the surface protecting agents are PVP, poly(dimethyldiallylammonium chloride) and polyethyleneimine (PEI).

UCNPs-based rattle-type structures are composed of core-shell and hollow structures with special core@void@shell configuration. For instance, Wang et al.[176] employed PEI bearing positive charged networks as surface protecting agent to fabricate UCNPs-based yolk-shell structures, in which hot water was acted as etchant. Li and co-workers[177] reported a rattle-structured Fe_3O_4@void@$NaLuF_4$:Yb/Er nanostructure that can provide the ternary modality of MR, CT and UCL imaging. Bu and co-workers[178] fabricated a multifunctional rattle-structured nanotheranostics with a movable UCNP core, a outer mesoporous SiO_2 shell and a hollow cavity between them, as shown in Fig. 6. Hydrophobic $NaYF_4$:Yb/Er@$NaGdF_4$ (denoted as Gd-UCNP, Fig. 6a) nanoparticles were coated with double dense SiO_2 layers (Fig. 6b, c) by two-step sol-gel method to form Gd-UCNP@d_1-SiO_2@d_2-SiO_2. In order to ensure the reaction to take place exclusively inside the inner SiO_2 layer, PVP was coated the outer SiO_2 layer to protecting it against etching. Then a milder etchant hot water was used to create hollow cavities because it can dissolve the colloidal SiO_2 shell by breaking the internal Si-O-Si bonds at a controllable rate to some extent. As such, via a "surface-protected hot water etching" strategy the intermediate SiO_2 layer was selectively etched away to leave behind a hollow cavity inside the thin porous SiO_2 shell, eventually producing yolk-shell structured UCSNs (Fig. 6d). It is worthwhile noting that traditional alkaline or acidic etchants did not work owing to the difficulty in controlling the etching rates. This design can achieve two major goals: (i) Gd-UCNP core can be acted as UCL/MRI dual-mode imaging probe for locating tumors *in vivo*;

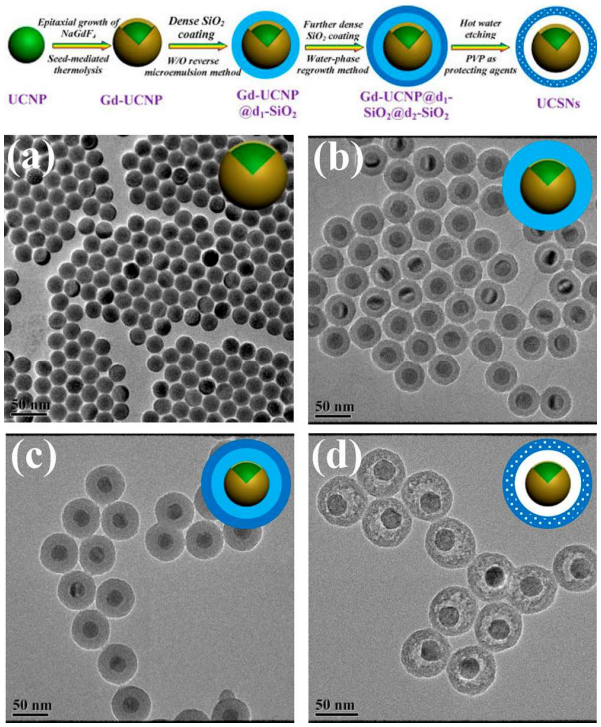

Fig. 6 Schematic Diagram of the Synthetic Procedure of UCSNs and the corresponding TEM images of (a) Gd-UCNP ($NaYF_4$:Yb/Er@$NaGdF_4$), (b) Gd-UCNP@d_1-SiO_2, (c) Gd-UCNP@d_1-SiO_2@d_2-SiO_2, and (d) UCSNs. (Adapted from ref. 178. Copyright 2013, American Chemical Society. Reproduced with permission.)

and (ii) the hollow cavity and porous shell can load drugs cisplatin for localized therapy via synergetic chemo-/radiotherapy.

It should be mentioned that the UCNPs-based rattle-type structures have disordered pore structure and broad pore size distribution because of the lack of structure-directing agents. However, for the controlled drug delivery, ordered, regular and narrow-distributed pores are highly demanded, which facilitates to adjust the transport and release of loading cargos in the pores. Therefore, the search for new and facile strategies to fabricate the UCNPs-based nanomaterials that meets the aforementioned requirements is still an important task faced in the coming years.

3.2 Hydrothermal-assisted template method

Template method is one of the most popular strategies for the synthesis of hollow materials, most of which are synthesized with the help of either hared templates or soft-directing agents.[184,185] In recent reports, melamine formaldehyde,[186,187] carbonaceous nanospheres,[188, 189] poly(acrylic acid sodium salt) microspheres,[190] and sodium poly(4-styrenesulfonate)[191] were acted as templates to prepare upconversion $NaYF_4$:Yb/Er, Y_2O_3:Yb/Er, Gd_2O_3:Yb/Er and $SrMoO_4$:Yb/Er hollow architectures, respectively. Nevertheless, some intrinsic disadvantages of hard template method, such as poor control of the encapsulating materials, time-consuming and cumbersome procedures, and larger size of used template, hinder the development of the research on UCNPs-based hollow structures. To address these problems, if the as-obtained uniform, readily prepared and spherical rare earth oxides are acted as sacrificial templates, the controlled synthesis of hollow UCNPs will become possible under the appropriate conditions. To this purpose, by using Y_2O_3:Yb/Er as templates hollow structured cubic phase $NaYF_4$ spheres with proper particle size (< 200 nm) have been successfully fabricated *via* hydrothermal ion-exchange process.[192] Recently, we used uniform $RE(OH)CO_3$ (RE=Gd, Y and Yb) nanospheres as sacrificial templates to fabricate three kinds of hollow UCNPs: $GdVO_4$:Yb/Er,[193] $Yb(OH)CO_3$@$YbPO_4$,[194] and $NaYF_4$:Yb/Er.[195] In a report, we report the controllable synthesis of monodisperse core-shell structured $Yb(OH)CO_3$@$YbPO_4$:Er hollow spheres as drug carriers by chemical transformation of the sacrificial template $Yb(OH)CO_3$ via the Kirkendall effect (Fig. 7a). In another report, we demonstrate a facile synthesis of $NaYF_4$:Yb/Er hollow mesoporous nanospheres (HMNPs) *via* a hydrothermal process by using $Y(OH)CO_3$:Yb/Er as sacrificial templates (Fig. 7b). From the viewpoints of materials synthesis, our design provides a facile and safe approach to synthesize HMNPs with simple operations and mild experimental conditions. On one hand, $NaBF_4$ was used as fluoride source, which can release gradually H^+ and F^- under high temperature and pressure. Compared with the previous method,[192] it is safer and harmfulless because it avoids direct contacting with HF. On the other hand, PEI, a dendrigraft cationic polymer was coated on the surface of obtained NPs during the hydrothermal process, which played multifarious roles: endowing HMNPs with good water solubility, providing functional groups to conjugate targeted ligand folic acid and protecting the surface of precursors against the etching of H^+. In addition, Anker and co-workers found that during the conversion of the precursor $Gd_2O(CO_3)_2$•H_2O:Yb/Er(Tm) to β- $NaGdF_4$:Yb/Er(Tm) in a teflon-lined autoclave, polyelectrolytes negatively charged sodium alginiate (AL) and positively charged PEI that were then alternately coated onto the outer surface of nanophosphors layer-by-layer can effectively prevent irreversible particle aggregation. Moreover, these polyelectrolytes also provided an amine tag for PEGylation. This method is also employed to fabricate PEGylated magnetic upconversion phosphors with Fe_3O_4 as the core and β-$NaGdF_4$ as a shell.[196] Additionally, $Y_2O_2SO_4$ hollow spheres can be obtained by biomolecule-assisted hydrothermal method followed by calcination. The formation of hollow spheres involves the Ostwald ripening in hydrothermal condition.[197]

In addition to the methods discussed above, electron-beam lithography is also an effective means to obtain hollow rare earth fluorides nanoparticles. The first example comes from Yan et al., who prepared β-$NaYF_4$:Yb/Er hollow-sphere nanocrystals under electron-beam irradiation.[198] The formation mechanism was a heat-induced acid-etching process. Nevertheless, the operation was limited to a small area in transmission electron microscopy, which restricts their practical application in mass-production of hollow-structured materials. In a more recent study, we developed a facile liquid–liquid two-phase hydrothermal approach to one-step synthesize water-soluble $NaREF_4$ (RE=Nd–Lu, Y) nanoparticles with small size (2-28 nm) and uniform morphology by introducing the amphiphilic surfactant sodium dodecylsulfate (SDS) into the reaction system (Fig. 7c).[199]

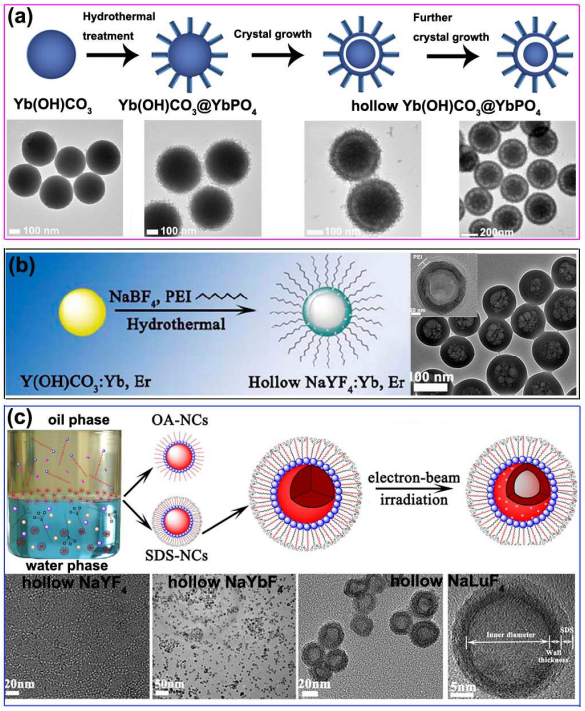

Fig. 7 Schematic diagram and the corresponding shapes of hollow UCNPs nanocarriers: $Yb(OH)CO_3$@$YbPO_4$:Er (a) and (b) $NaYF_4$:Yb/Er hollow spheres via hydrothermal-assisted template method as well as hollow $NaREF_4$ (RE = Y, Yb and Lu) nanospheres (c) via liquid–liquid two-phase hydrothermal approach combined with the electron beam electron-beam lithography. (Adapted from refs. 194, 195, 199. Copyright 2012, 2013, Elsevier B. V. and Wiley-

VCH Verlag GmbH & Co. KGaA. Reproduced with permission.)

Furthermore, it was also found that a large amount of hollow-structured $NaREF_4$ (RE = Y, Yb, and Lu) nanocrystals were produced *in situ* under irradiation of electron-beam. It took only less than one minute for this convenient solid-to-hollow transition process. Moreover, we found that not all of the rare earth ions can form hollow structures. The electron beam acted on only Y, Yb and Lu three species The exact reason for this phenomenon is not still clear at present. The as-prepared hollow-structured nanoparticles can be used as anti-cancer drug carriers for drug storage/release and upconversion cell imaging.

3.3 Polymer grafting or self-assembly

In general, the as-obtained high quality UCNPs by the existing synthetic methods available are hydrophobic in nature owing to the usage of capping surfactants (such as oleic acid), which is far from ideal for the biological application. Therefore, suitable inorganic or organic materials are used to link or encapsulate UCNPs by self-assembling fashion or covalent association. The preceding` two sections mainly focus on the inorganic materials to integrate UCNPs to form nanocomposites. This section will focus on organic polymers used to modify UCNPs for drug carriers. The common used polymers include polyethylene glycol (PEG)-grafted amphiphilic polymer (C18PMH-PEG),[200] PEG phospholipids,[201,202] TWEEN,[203,204] PEI,[205] poly(maleic anhydride-alt-1-octadecene) (PMAO),[206] OQPGA-PEG/RGD/TAT lipid micelles (OQPGA refers to octadecyl-quaternized modified poly glutamic acid),[207] as well as amphiphilic block copolymer such as mPEG-*b*-PCL-*b*-PLL,[208] and poly (styrene-block-allyl alcohol) (PS_{16}-*b*-PAA_{10}).[209] Recently, we designed and synthesized a novel multifunctional upcoversion nanoparticle/polymer composite system for cisplatin (IV) drug delivery and bioimaging. An amphiphilic tri-block copolymer mPEG-*b*-PCL-*b*-PLL conjugated with a cisplatin (IV) prodrug can assembled with hydrophobic UCNPs to form core-shell structured nanocomposites, which could be applied in both delivering cisplatin to cancer cells and monitoring the transport pathway via *in vitro* and *in vivo* imaging.[208] In addition, Liu's group conducted a series of researches on the encapsulation of UCNPs with polymers for drug delivery and multimodal bioimgings. A typical example is that C18PMH-PEG was used to modified $NaYF_4$:Yb/Er UCNPs, in which a hydrophobic OA layer on the surface of UCNPs and beneath the PEG coating to yield "hydrophobic pockets" whereby anticancer drug molecules DOX could be absorbed physically into these pockets via a supramolecular chemistry approach (Fig. 8a).[200] Following the same principle, PEG phospholipids and TWEEN can also be employed to transfer hydrophobic UCNPs into the water to produce water-soluble and biocompatible UCNPs, which were reported by Zhao and Gu.[201,203,204] Meanwhile, DOX and camptothecin (CPT) anticancer drugs could be co-loaded into the "hydrophobic pockets" through hydrophobic interactions (Fig. 8b).[204] Beside these, Liu's group has attempted to synthesize novel nanocomposites with multiple functions by coating or integrating UNCPs with magnetic Fe_3O_4 by different routes. For examples, hydrophobic UCNPs and Fe_3O_4 were simultaneously encapsulated with diblock copolymer PS_{16}-*b*-PAA_{10} via a microemulsion method (Fig. 8c).[209] And Liu's group also reported a novel multifunctional nanoparticles consisting of a UCNP as the inner core, closely packed Fe_3O_4 as the inter-layer,

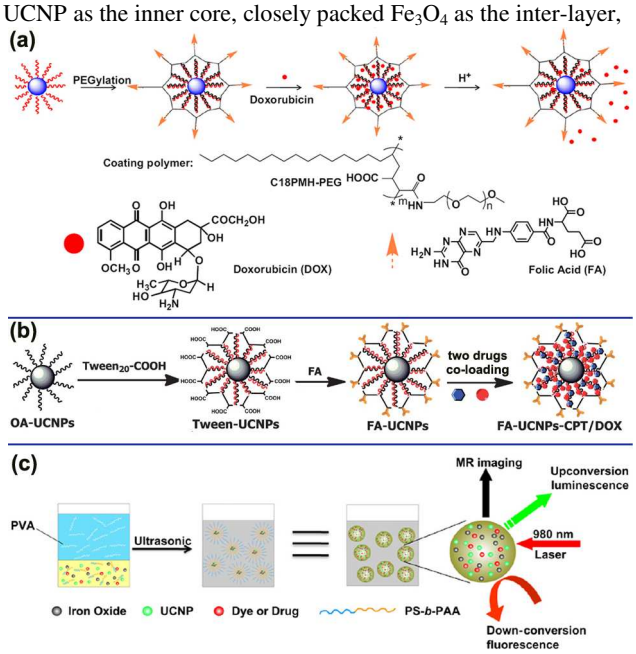

Fig. 8 Schematic diagrams of synthetic procedures of UCNPs@polymer carriers: (a, b) C18PMH-PEG or TWEEN-COOH were used to modified hydrophobic UCNPs to yield "hydrophobic pockets" whereby anticancer drug molecules DOX or CPT could be loaded (or co-loaded) into these pockets through hydrophobic interactions; (c) hydrophobic UCNPs and Fe_3O_4 nanoparticles were simultaneously encapsulated with diblock copolymer PS_{16}-*b*-PAA_{10} via a microemulsion method. (Adapted from refs. 200, 204, 209, copyright 2011, 2014. Elsevier B. V. and Royal Society of Chemistry. Reproduced with permission).

and a thin layer of gold as the shell, which were fabricated via layer-by layer assembly approach.[210,211] These multifunctional nanomaterials can be used for *in vitro* and *in vivo* multimodal biomedical imaging, magnetic-targeted drug delivery and cancer therapy (including chemotherapy and photothermal therapy).

3.4 Electrospinning method

Electrospinning is one of cost-effecive and versatile methods for preparing one dimential (1D) materials including polymers, inorganic materials and hybrid compounds.[212,213] Given that dispersing inorganic rare earth luminescent nanoparticles into polymer hybrid precursors, various 1D rare earth luminescent materials with multiform morphologies such as fiber, wire, belt and tube can be achieved readily via electrospinning route, which have potential applications in fluorescent lamps and color displays.[214-216] Our group has employed this method to prepare various families of 1D luminescence materials. The readers who are interested in this aspect are referred to the review reported by us.[217] More importantly, our group has demonstrated that electrospinning route is also an effective approach to prepare UCNPs/porous multifunctional materials, which can act as promising drug carriers in the biomedical area.[218-223] In our early work, hydrophilic $NaYF_4$:Yb/Er NCs were directly dispersed in electrospining solution containing orthosilicate (TEOS). Then porous SiO_2 fibers decorated UCNPs (UCNPs@SiO_2 fibers) were

obtained after high temperature annealing (550 °C) (Fig. 9a), which served as a carrier to the loading and release of drugs ibuprofen or anticancer DOX as well as upconversion luminescence imaging.[165, 166] Moreover, by controlling fastidiously experimental conditions, UCNPs@SiO_2 tubes can be fabricated successfully (Fig. 9b).[221] The above researches mainly focused on the loading and sustained release of single drug, so the burst release of drug at initial stage during drug delivery is a common question, which is unfavorable for the accumulation of drugs at the tumor site. On the other hand, to accelerate wound healing and decrease postsurgical infection, the release of two or more different drugs at the proper time and in appropriate doses may be required during treatment. To this end, we adopted a novel and ingenious architecture design to obtain a multifunctional dual-drugs delivery system via electrospinning technique by combing the advantages of inorganic materials (UCNPs@$mSiO_2$) and organic materials (polymer).[222] The working principle of our strategy is shown in Fig. 9c. Firstly, antitumor drug DOX delivery carrier UCNPs@$mSiO_2$ nanospheres were fabricated according to a phase transfer assisted surfactant-templating coating process. Subsequently, the as-obtained DOX-UCNPs@$mSiO_2$ nanoparticles were mixed with electrospinning solution including poly(ε-caprolactone) (PCL)-gelatin (PG) and another drug anti-inflammatory (IMC) so as to form dual drugs-loaded composite fibers (denoted as UCNPs@$mSiO_2$@fibers. The two drugs release behaviors *in vitro* presented distinct release properties. Moreover, drug release is a sustained and long-term release behavior, which can solve effectively the problem of drug burst release to some extent. Moreover, the UC luminescent intensity ratios of $^2H_{11/2}/^4S_{3/2}$–$^4I_{15/2}$ (green emission) to $^4F_{9/2}$–$^4I_{15/2}$ (red emission) from Er^{3+} vary with the amount of DOX in the system, and thus drug release can be tracked and monitored utilizing luminescence resonance energy transfer by the change in the green/red intensity ratios.

For the electrospining nanofibers there are some limitation in the *in vivo* therapy application if the tail intravenous injection was adopted for systemic delivery, because nanofibers can not circulate effectively in the blood stream due to their larger size. However, the nanofibers are effective and very attactive for topical treatment of solid tumors and wound healing due to their characteristics including extremely high-specific surface and porosity, air permeability as well as surface wettability. Nanofiberous scaffolds can maintain an appropriately moist environment for the wound by facilitating oxygen permeation and allowing fluid accumulation, effectively protect the wound from bacterial penetration.[224-228] As such, the electrospinning nanofibers are promising materials for facilitating wound healing and skin regeneration. In a further work, we implanted directly UCNPs@$mSiO_2$@fibers patches as dual drugs systems to the solid tumor site of mice by surgical procedures to fulfill the site-specific and high-performance simultaneous diagnosis and therapy for tumors *in vivo* for the first time. An interesting finding is that antiphlogistic drug IMC in composite fibers plays an important role in suppressing the inflammatory responses and helping to heal the wounds *in vivo*, which will be reported separately by us. Besides this, according to a study by Park et al., curcumin (Cur)- loaded poly (lactic acid) (PLA) nanofiber patches has good *in vivo* wound healing apability in a mouse model. It was found that treatment with Cur-PLA nanofibers

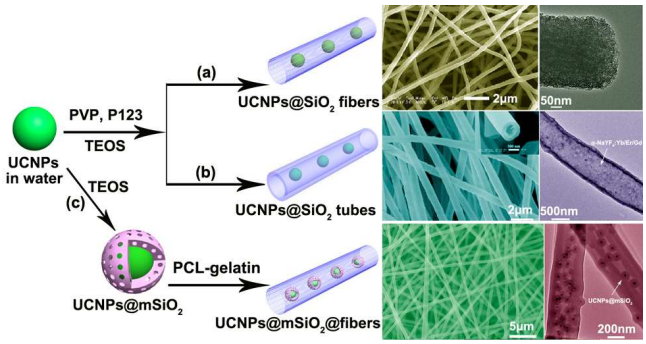

Fig. 9 Schematic diagram of synthetic procedure and the corresponding shapes of diverse UCNPs@SiO_2 fibers (a), UCNPs@SiO_2 tubes (b) and UCNPs@$mSiO_2$@fibers (c). (Adapted from refs. 220-222, copyright 2012, 2013, 2014. Wiley-VCH Verlag GmbH & Co. KGaA, Royal Society of Chemistry and American Chemical Society. Reproduced with permission).

significantly increased the rate of wound closure (87%) by day 7 compared with that of PLA nanofibers (58%).[224] Schneider et al. also reported that a silk nanofiber scaffold electrospun with epidermal growth factor enhanced the wound closure by 90% in an *in vivo* test on mice.[229]

4. Application of UCNPs-based nanomaterials in drug delivery

In recent years, the design and fabrication of multifunctional nanomedical platforms have evoked intensive interest. The major goal is to bridge the gap between the biomaterials and clinical theranostics for simultaneously performing disease diagnosis and therapy within a single nanocarrier. To meet this demand, various UCNPs-based nanocomposites have been exploited as drug delivery system (DDS) for multifunctional upconversion fluorescence bioimaging, drug delivery and monitoring of drugs by fluorescence imaging in real time.

4.1 Luminescence-monitored drug delivery system

One of the major advantage of utilizing UCNPs-based composites as drug carriers is that UCNPs have the ability for tracking and evaluating the efficiency of the drug release in real time. Our group constructed a multifunctional DDS by loading ibuprofen (IBU) into the core-shell structured Fe_3O_4@SiO_2@$mSiO_2$@$NaYF_4$:Yb/Er nanocomposites via a facile two-step sol-gel process. The relationship between the UC luminescence intensity of nanocomposites and the cumulative release of IBU was investigated.[160] It was found that the organic groups in IBU with high vibrational frequencies (1000-3500 cm^{-1}) could significantly quench the luminescence intensity of Er^{3+} to a great extent. With the increase of cumulative release of IBU, more and more drug molecules were liberated from the DDS and the quenching effect will be weakened, resulting in the increase of luminescence intensity.[230] Thus the drug release process could be monitored by the change of UC luminescence intensity. Subsequently, similar relationship was tested and confirmed in

other drug delivery systems by taking IBU as model drug, such as $NaYF_4$:Yb/Er@SiO_2@$mSiO_2$ nanospheres,[231] and porous $NaYF_4$:Yb/Er@silica fiber.[219] As a complementary study, we recently devoted tremendous effort to the doxorubicin (DOX) loaded UCNPs-based nanocarriers for multimodal bioimaging and *in vivo* drug delivery.[169,232] In a typical example,[169] we synthesize highly uniform and monodisperse β-$NaYF_4$:Yb/Er@β-$NaGdF_4$:Yb@$mSiO_2$-PEG (UCNPs@$mSiO_2$-PEG) anticancer DDS (Fig. 10a). The T_1-weighted MRI reveals the concentration-dependent brightening effect due to the presence of Gd^{3+} ions. Upconversion luminescence image of UCNPs@$mSiO_2$-PEG uptaken by cells shows green emission under 980 nm infrared laser excitation (Fig. 10b). *In vitro* cell cytotoxicity tests on cancer cells verified that the DOX-loaded UCNPs@$mSiO_2$-PEG showed comparable cytotoxicity with free DOX at the same concentration of DOX (Fig. 10c). More importantly, *in vivo* antitumor efficacy indicates that the nanocomposites can delivery effectively drug into the tumor site and suppress tumor growth (Fig. 10d). In another study, we reported an anticancer DDS based on DOX-conjugated $NaYF_4$:Yb/Tm UCNPs, in which the quenching and recovery of the luminescence intensity of UCNPs can be applied to monitor the release of DOX by luminescence resonance energy transfer between UCNPs (donor) and DOX (acceptor), as shown in Fig. 11.[233] This correlation between the UC luminescence intensity and the extent of drug release will be potentially used as a probe for monitoring the drug release movement during disease therapy.

4.2 Stimuli-responsive drug delivery system

In conventional DDS, drug molecules are mainly physically absorbed by the porous nanostructure or the hydrophobic ligands of the nanocarriers. The major drawback of these conventional DDS is the irregular drug release, which exhibit burst release in the initial stage. It is well known that the drug efficacy and biodistribution can be altered by the some nonspecific cells and

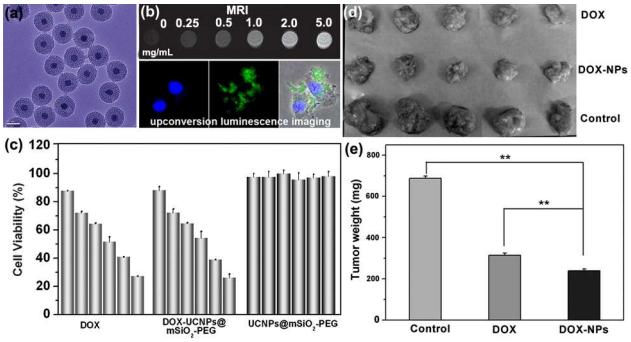

Fig. 10 (a) TEM image and (b) *in vitro* T_1-weighted MR and upconversion luminescence imaging of β-$NaYF_4$:Yb/Er@β-$NaGdF_4$:Yb@$mSiO_2$ (UCNPs@$mSiO_2$) nanoparticles, (c) *in vitro* cytotoxicity of free DOX, DOX-UCNPs@$mSiO_2$-PEG, and pure UCNPs@$mSiO_2$-PEG against HeLa cell after 24 h incubation and (d, e) *in vivo* antitumor efficacy of UNCPs@$mSiO_2$-PEG (labeled as NPs) on H22 cancer subcutaneous model: the photographs (d) of excised tumors from euthanized representative mice after the treatment with saline solution as control, free DOX and DOX-NPs, respectively, and mean tumor weights (e) of each group at the last day of experiment. Two asterisks indicate statistically significant discrepancy (** P< 0.01). (Adapted from ref. 169, copyright 2013. Wiley-VCH Verlag GmbH & Co. KGaA. Reproduced with permission).

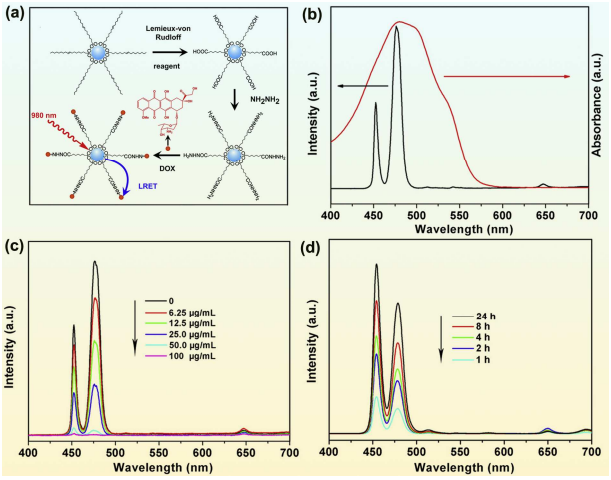

Fig. 11 (a) Schematic illustration of the DOX-conjugated UCNPs. (b) UC emission spectrum of $NaYF_4$:Yb/Tm (black line) and the UV-vis absorption spectrum of DOX (red line). (c) UC emission spectra of $NaYF_4$:Yb/Tm (2 mg mL^{-1}) after reaction with DOX at different concentration. (d) UC emission intensity of DOX conjugated $NaYF_4$:Yb/Tm NPs a function of release time at pH 5.0 and 37 ^oC PBS buffer. (Adapted from ref. 226, copyright 2013. Elsevier B. V. Reproduced with permission).

the physiological conditions. Moreover, some drug molecules cannot distinguish between the diseased and healthy cells, resulting in the collateral damage and undesired side effects.[234,235] Spurred by these problems and challenges, a few "smart" drug delivery systems based on UCNPs have been designed to regulate the release of cargos at a desired time and in a desired site with an appropriate dosage. To achieve the temporal- and dosage-controlled drug release, great efforts have been devoted to design and fabricate the stimuli-responsive systems for drug delivery. These stimuli-responsive DDS can respond to external triggers to control the release of drug from the nanocarriers on demand. Hitherto, several effective strategies such as pH-response, temperature, redox reaction and NIR-light irradiation have been extensively explored to achieve sustained drug release in a controlled manner. Tables 1-3 summarizes of recent works on UCNPs-based stimuli-responsive drug delivery systems including NIR light-induced photolysis of "caged" compounds or photoswitching of photochromic molecules, respectively.

4.2.1 pH-responsive drug delivery system

As the extracellular microenvironment of tumor tissues is more acidic than that in normal tissues and blood, pH-responsive drug delivery vehicles have been widely investigated. In particular, one important design strategy of this pH-responsive DDS is to fabricate charge-conversional system.[236-238] These charge-conversional nanocarriers are negatively charged under neutral and alkaline conditions but switch to positively charged in slightly acidic environment. The fascinating feature of these charge-conversional nanocarriers allows for higher affinity with

negatively charged cell membranes to enhance cellular uptake of nanocarriers. Recently, UCNPs modified with pH-responsive charge switchable polymers such as poly(acrylic acid) (PAA),[173,174,193,239] 2,3-dimethylmaleic anhydride (DMMA),[240] have been developed as controllable and effective DDS. For example, we constructed multifunctional PAA@$GdVO_4$:Yb/Er nanocomposites by filling PAA hydrogel into $GdVO_4$ hollow spheres via photoinduced polymerization. Due to the nature of PAA, positively charged anticancer drug DOX loaded PAA@$GdVO_4$:Yb/Er system exhibits pH-dependent drug releasing kinetics. A lower pH offers a faster drug release rate.[193] Wang's group have reported the PAA-modified $NaYF_4$:Yb/Er (PAA-UCNPs) as pH-activated drug carriers.[239] DOX was introduced into PAA-UCNPs. This PAA-UCNPs nanocomposites exhibited high encapsulation rate at weak alkaline conditions and increased drug dissociation rate in acidic conditions. One can ascribe the results to the intrinsic charge-conversion property of PAA and its interaction with DOX. In neutral medium, negatively charged PAA would bind with the positively charged DOX by the electrostatic interaction. Whereas, PAA was protonized to display positive zeta potential, which lead to the dissociation of electrostatic interaction between PAA and DOX. Subsequently, DOX diffused from the PAA-UCNPs composite. In addition, Wang and co-workers have designed and synthesized novel pH-responsive eccentric-(concentric-UCNPs@SiO_2)@PAA[173] and eccentric UCNPs@PAA@SiO_2 nanocarriers.[174] Likewise, such materials have two special characteristics: ultra high drug storage capacity and sensitive pH-responsive drug release properties.

Besides the above mentioned organic-inorganic hybrid composites, Lu et al. recently reported a pH-activated nanocomposite constructed from mesoporous γ-AlO(OH) and UCNPs (UCNPs-Al) for drug delivery (Fig. 12a-c).[241] It is noted that the UCNPs-Al nanocomposite exhibited charge-conversional behavior from alkaline to acidic medium. It was found that the release of DOX from UCNPs-Al could be controlled by varying the pH values. Under neutral condition (pH = 7.4), the zeta potential of UCNPs-Al was negative, facilitating their electrostatical interaction with DOX molecules. Along with reducing the pH values, UCNPs-Al switched positive charged, resulting in the force between UCNPs-Al and DOX was converted to repulsive from attractive. Then the DOX molecules were pumped out by repulsion of the positive-charged UCNPs-Al. Upon changing pH to 5, the cumulative release of DOX was three-fold larger than that at pH = 7.4 (Fig. 12c). Moreover, the charge-conversional property of DOX loaded UCNPs-Al endowed this nanocomposie with enhanced cellular uptake and suppression effect on cancer cells. Therefore, it is believed that the UCNPs-based nanocomposites that in line with charge-conversion theory are promising platforms to construct pH-responsive DDS for controllable drug release.

The second effective method of constructing pH-responsive DDS is to conjugate drug molecules to the surface of nanoparticles *via* acid-labile linkers, thus the conjugated drugs can be released in weakly acidic environment.[242] We recently demonstrated a pH-triggered DDS based on DOX-conjugated UCNPs nanocomposites.[171,243] For example, DOX was conjugated to the surface of $BaGdF_5$:Yb/Tm@$BaGdF_5$:Yb UCNPs by acid-labile hydrazone bonds (Fig. 12d-g). It is discovered that the total release amount of DOX in acidic condition was more than ten-fold larger than that in neutral medium. This pH-triggered drug release behavior can be ascribed

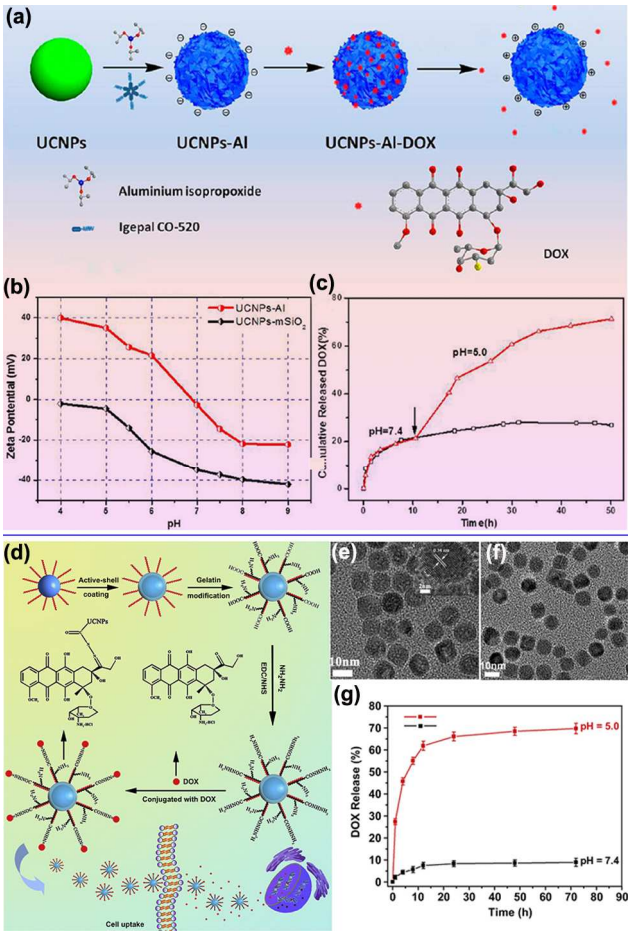

Fig. 12 Two different pH-responsive UCNPs-based drug delivery systems. (a-c) Mesoporous γ-AlO(OH) and UCNPs (UCNPs-Al) system: (a) schematic representation for the synthesis of pH-responsive UCNPs-Al; (b) zeta potential of UCNPs-Al and UCNPs-$mSiO_2$ as a function of pH values; and (c) delayed release of DOX from UCNPs-Al at different pH value. (d-g) DOX-conjugated $BaGdF_5$:Yb/Tm@$BaGdF_5$:Yb (UCNPs) system: (d) the synthesis and DOX-conjugation process of the core-shell structured UCNPs and the drug release behavior; TEM images of (e) UCNPs and (f) gelatin modified UCNPs; and (g) cumulative DOX release from DOX-conjugated UCNPs as function of release time at different pH values. (Adapted from refs. 241, 243. Copyright 2013, 2014. Elsevier B. V. and American Chemical Society. Reproduced with permission.)

to the cleavage of hydrazone bonds in acidic environment (pH = 5~5.85), which is relatively stable in normal physiological environment. Hence the hydrazone bond worked as a "barrier" on the drug release in normal physiological environment, sodecreasing the amount of DOX dissociated from the carrier prior to release in non-target spots during transportation, and reducing the side-effect of chemotherapeutics. Note that the pH-responsive controllable DDS is of practical significance for the clinical cancer therapy since the microenvironments in the extracellular tissues of tumors and intracellular lysosomes and

endosomes are acidic.

4.2.2 Thermo-responsive drug delivery system

Nowadays, another type of stimuli-responsive DDS supported by thermosensitive polymers have been used for controllable drug delivery. Among these smart polymers, poly(N-isopropylacrylamide) (PNIPAM), is the most extensively investigated temperature-sensitive polymer that exhibits a phase transition in aqueous solution at a lower critical solution temperature (LCST) around 32 ^{o}C. Below the LCST, the polymer is expanded and soluble, whereas it is collapsed and insoluble when heated above the LCST. Inspired by their charming thermosensitive characters, PNIPAm hydrogel was integrated with other functional species for thermo-triggered drug release.[244-249] However, in some cases, a positive controllable release that gives faster drug release at higher temperature is more desirable because it can respond to an increased body temperature arising from diseases such as inflammation or cancers. Currently, our group rationally designed and fabricated a bilayer thermosensitive P(PNIPAM-*co*-AAm) hydrogel discs, in which multiwalled carbon nanotubes (MWCNTs) and UCNPs were spatially confined in different layers of hydrogel.[250] In addition, the LCST of the PNIPAM can be flexibly adjusted to near the normal body temperature (37 ^{o}C). In this system, MWCNTs worked as "antenna" of NIR light and convert it the light to heat and transfer it to the surrounding hydrogel. So the NIR light irradiation can cause the shrinking of the hydrogel, thus the drug molecules can be rapidly squeezed out. As the laser is tuned off, the hydrogel will retune to its equilibrium to block the diffusion of drug molecules. In other words, the "turn on" and "turn off" phase of drug release is cycled by manipulating the NIR laser irradiation. Therefore, this temperature-responsive hydrogel can be served as a pulsatile DDS by a NIR laser remotely controllable mode.

Encouraged by these promising results, we continued the studies in order to optimize this thermosensitive DDS for stimuli-responsive drug release. We designed two systems that can response to dual stimuli of pH and thermo. We first reported a new kind of controlled drug release system based on UCNPs/polymer hybrid materials by coating $NaYF_4$:Yb/Er with the smart hydrogel poly(N-isopropylacrylamide-co-(methacrylic acid) [abbreviated as P(NIPAM-*co*-MAA)] shell.[251] An interesting finding involves that the release behavior of antitumor drug DOX in hybrid microspheres was pH-triggered thermally sensitive. Changing the pH to mildly acidic condition at physiological temperature deforms the structure of the polymer shell, thus leading to the rapid release of a significant amount of drugs from the microspheres. In addition, the extent of drug release can be monitored by the change of up-conversion emission intensity. As we know so far, this is the first report on the combination of UCNPs with stimuli-responsive polymers. Later on, as an extension of this work, we architected another novel thermo/pH dual-responsive nanocomposite, in which UCNPs were encapsulated in the mesoporous silica ($mSiO_2$) shell, and then P(NIPAM-*co*-MAA) polymer brushes were grafted onto the mesochannels and the outer shell of the $mSiO_2$ to control of drug molecules (Fig. 13).[252] At low temperature, the mesochannels were blocked with the hydrogel swelling. However, at high temperature, these mesochannels were opened with the shrinking of hydrogel and enable the entrapped drug molecules to diffuse out. Therefore, the unique architecture with

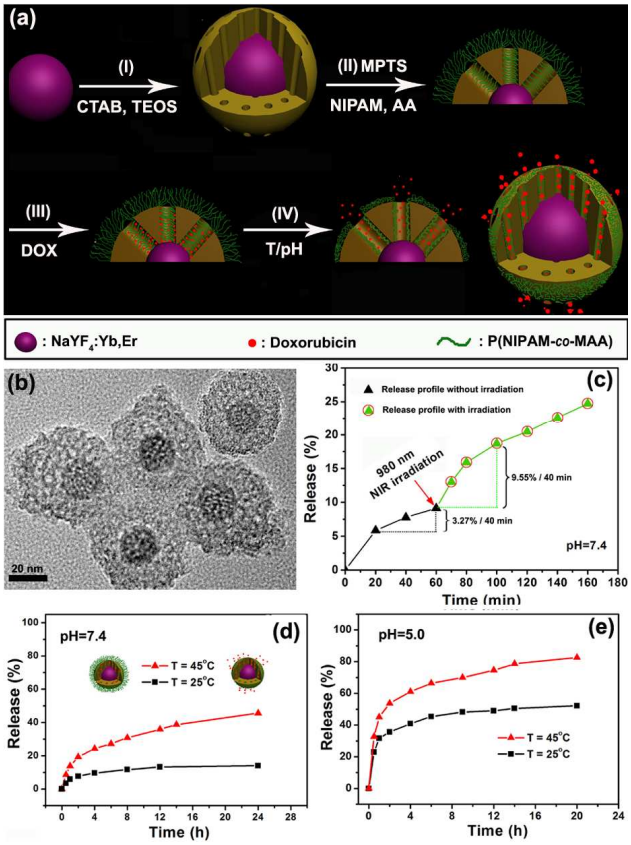

optimal drug **Fig. 13** (a) Synthetic route to UCNPs@$mSiO_2$-P(NIPAM-co-MAA): I) CTAB/TEOS; II) methacryloxypropyltrimethoxysilane (MPTS), N-isopropylacrylamide (NIPAM), methacrylic acid (AA); III) guest (DOX) loading; IV) increase the temperature and decrease the pH value. (b) TEM images of UCNPs@$mSiO_2$-P(NIPAM-co-MAA). Release profiles of DOX from DOX-UCNPs@$mSiO_2$-P(NIPAM-co-MAA) nanocarriers with or without 980 nm laser irradiation at power density of 1.22 W (c) as well as in response to temperature changes at different pH of (d) pH = 7.4 and (e) pH = 5.0. (Adapted from ref. 252. Copyright 2013, Wiley-VCH Verlag GmbH & Co. KGaA. Reproduced with permission.)

release property at high temperature/low pH values is promising candidate for simultaneous cancer therapy and bioimaging.

4.2.3 Redox-responsive drug delivery system

Cisplatin (cis-dichlorodiammineplatinum (II)) has become one of the most widely used anticancer drugs, however, the use of cisplatin is also hampered due to some major problems associated with the lack of tumor specificity, severe side effects and inherent drug resistance. To address these problems, much attention has been paid to octahedrally coordinated Pt(IV)-based counterparts as promising platinum (II) prodrugs. Pt(IV) prodrugs have good chemical inertness and redox properties as well as low cytotoxic side effects to the normal tissues. To achieve effective antitumor treatment, Pt(IV) prodrugs are needed to be activated to form

bioactive Pt(II) species by taking advantage of suitable triggers such as pH, reducing environment of cancer cells, or light.[253] Recently, our group reported the related work on UCNPs-based redox-responsive Pt(IV) prodrugs delivery nanoplatforms by the combination the intriguing merits of UCNPs for the first time.[208,254] We first designed and developed a novel Pt(IV) prodrug conjugated UCNPs for targeted drug delivery and upconversion cell imaging.[254] $NaYF_4$:Yb/Er-PEI nanoparticles were conjugated covalently with Pt(IV) prodrug *cis,cis,tran*-$Pt(NH_3)_2Cl_2(O_2CCH_2CH_2CO_2H)_2$. These Pt(IV) pro-drugs can be reduced by the intracellular reducing agents glutathione (GSH) after internalized by the cancer cells, yielding Pt(II) species to exhibit anticancer activities to bind nuclear DNA in order to kill cancer cells. Based on this preliminary work, we continued to construct a novel multifunctional UCNPs/polymer vectors for cisplatin (IV) drug delivery, which can reduce the drawbacks of cisplatin, circumvent its cellular uptake pathways and give insight in to its fate in *in vitro* and *in vivo* via biomedical imaging (Fig. 14).[208] The schematic illustration of the composite nanomaterials is shown in Fig. 14. Cisplatin (IV) prodrug or fluorescent molecule Rhodamine B (RhB) was conjugated to an amphiphilic tri-block copolymer mPEG-*b*-PCL-*b*-PLL to form two conjugates, which were co-assembled with UCNPs to form the multifunctional core-shell structured nanoparticles (UCNP/P-Pt/RhB). The prepared UCNP@P-Pt/RhB can be used as a luminescent probe for up/down-conversion *in vitro* and *ex/in vivo* imaging. The cisplatin (IV) prodrug system demonstrates anti-cancer activities by releasing toxic cisplatin in the cellular environment or tumor-bearing animal models. Moreover, the expression levels of the tumor apoptotic genes, including Survivin, Bcl-2, and Aif in the cancer cells were regulated by nanoparticles to promote apoptosis. These encouraging results in

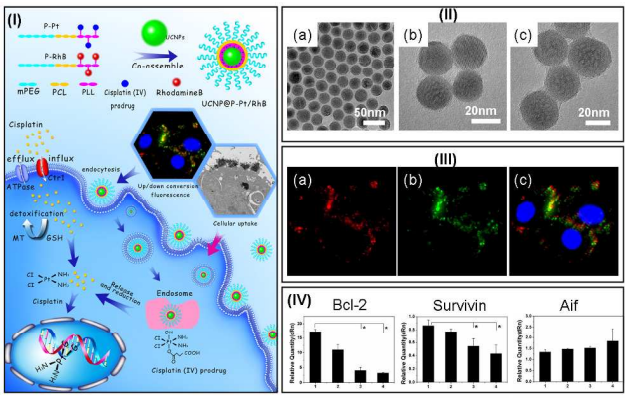

Fig. 14 Rational design of multifunctional upconversion nanocrystals/polymer nanocomposites for cisplatin (IV) delivery and biomedical imaging. (I) Schematic illustration of the preparation of UCNP@P-Pt/RhB nanoparticles and possible cellular pathways for cisplatin and the nanoparticles UCNP@P-Pt/RhB. (II) TEM images of UCNPs (a), UCNP@P (b), and UCNP@P-Pt/RhB (c). (III) Luminescence microscopy images of HeLa cells after incubation with 200 μg ml^{-1} of UCNP@P-Pt/RhB for 6 h at 37 °C. The red fluorescence arises from RhB (a), the green fluorescence arises from UCNPs (b), and the blue fluorescence arises from Hoechst33324 (c). Scale bars: 20 μm. (IV) Quantitative real-time PCR analyses of Bcl-2, Survivin, and Aif mRNA levels of apoptotic genes in MCF-7 cells due to (1) blank control, (2) cisplatin (IV) prodrug, (3) cisplatin, (4) UCNP@P-Pt/RhB exposure for 24 h (n = 3). *P < 0.05. (Adapted from ref. 208. Copyright 2013, Wiley-VCH Verlag GmbH & Co. KGaA. Reproduced with permission.)

the *in vitro* and *in vivo* level highlight the potential of UCNP@P-Pt/RhB nanoparticles as excellent carriers for biomedical imaging and cancer therapeutics.

Apart from chemical reduction method, light also is an effective trigger to activate Pt(IV) to release cytotoxic Pt(II) components. In particular, UCNPs-based nanomaterials as convertors were applied to the remotely controlled photoactivation of antitumor platinum prodrugs, which will be discussed in the following section.

In addition, Zhu et al. reported a novel drug carrier Fe_3O_4@SiO_2/$NaYF_4$:Yb/Er@MnO_2, in which MnO_2 nanosheets served as drug carriers for the loading of the model Congo red (CR) and UC luminescence quenchers. The drug can be released by introducing GSH which reduces MnO_2 to Mn^{2+}, and the drugs can be released at tumor cells accompanied with "turn on" of UC luminescence.[255]

4.2.4 NIR light-triggered drug delivery system

Light-triggered drug delivery platforms have been emerged as an elegant and non-invasive tool for remotely spatiotemporal control for drug payload release at the desired site and time because light can be easily tuned (wavelength, power intensity and irradiation time) and focused (preventing damage to health tissues). This control is considered crucial to boost local effective drug accumulation while minimizing side effects, therefore resulting in improved therapeutic efficacy.[256-258] However, most of the existing light-triggered drug carriers require high energy UV/visible light to activate the photosensitive component. Thus the associated cellular photodamage and poor tissue penetration depth are inevitable, which limit their practical biomedical applications in living systems. Alternatively, multiphoton photoactivation with longer-wavelength excitation is a potential solution to this problem due to the minimal damage and deeper tissue penetration, but the multiphoton photoreactions generally requires an expensive and higher intensity plused laser and has low conversion efficiency owing to narrow absorption cross-sections of the chromophores.[259] Moreover, not all photoresponsive molecules have suitable multi-photon absorption efficencies.[257] To surmount these problems, Ln^{3+}-doped UCNPs offer an excellent choice for this task due to their ability to penetrate deeply into living tissues without causing phototoxic effects. Such a unique and amazing luminescence property allows UCNPs to serve as a powerful NIR-induced mediator (or antenna) to drive the photoreactions of light sensitive compounds anchored to their surface. Hence, introducing UCNPs into light-triggered DDS may find new opportunity in practical applications for remote-controlled release of payload molecules using NIR laser as excitation source. Broadly the approaches can be classified into four categories: (i) NIR light-induced photolysis of photoactivable or "caged" molecules; (ii) NIR light-induced photoswitching of molecules between two structurally and electronically different isomers; (iii) NIR light-triggered redox reaction of photoactivated pro-drug molecules; (iv) NIR light-triggered photodynamic therapy (PDT). This will be elaborated

below.

(i) NIR light-induced photolysis of photoactivable or "caged" molecules for chemotherapy

Generally, a typical photocage refers to a caged molecule rendered biologically inert by a photolabile protecting group. Under the light irradiation with appropriate wavelength, caged group is liberated by photolysis and then restore active forms.[260-263] Scheme 2 shows the general photodecaging process of a bioactive substance.[260] This special property of photosensitive compounds has been harnessed to realize readily controllable release of payload molecules. Recently, major breakthroughs have been achieved successfully to uncage some photocaged molecules such as D-luciferin,[259] carboxylic acid,[264] NO,[265,266] biomolecules,[267] block copolymer,[268] siRNA,[269] and cell adhesion[270] by UV/visible emission of UCNPs. In a typical example, Ford group demonstrated the feasibility of the NIR-triggered release of caged

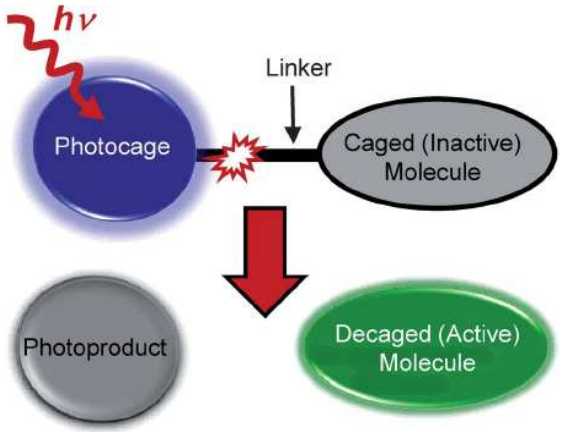

Scheme 2 General photodecaged process: light excitation of the photocage cleaves the covalent bonds with caged molecule, literating it in its active form. (Adapted from ref. 260, copyright 2012. Royal Society of Chemistry. Reproduced with permission).

nitric oxide (NO) using UCNPs by two different strategies,[265,266] given that endogenous mammalian bioregulator NO plays an important role in suppressing tumor growth and immune response.[271,272] In a prior work, Fork et al. prepared silica coated $NaYF_4$:Yb/Er@$NaYF_4$ UCNPs with core-shell structures, which can be further functionalized to attract the NO precursor Roussin'a black salt anion $Fe_4S_3(NO)_7^-$ (RBS) by electrostatic interaction.[265] Then NIR-to-visible upconversion of UCPs can trigger photochemical NO release from RBS due to spectrum overlapping between the absorption of RBS with the emission at 550 nm of UCNPs. In a follow-up study, the same group reported another innovative design for the phototherapeutic release of NO.[266] The new materials consist of poly(dimethylsiloxane) composites with UCNPs that cast into a biocompatible polymer disk (PD). These PDs are then impregnated with the photochemical nitric oxide precursor RBS to give UCNP-RBS-PD devices. When irradiated with 980 nm NIR light through filters composed of porcine tissue, physiologically relevant NO concentrations were released from UCNP-RBS-PD, thus demonstrating the potential of such devices for minimally invasive phototherapeutic applications.

Simultaneously, several research groups demonstrated the rational design and fabrication of UCNPs-based DDS for photo-triggered payloads release and bioimaging, and gained inspiring results *in vitro* and *in vivo*.[91-93,263,273] For instance, Liu and co-workers presented a specific crosslinked mesoporous silica coated upconversion nanoparticles $NaYF_4$:Yb/Tm@$NaYF_4$ as nanocarrier for photo-responsive drug delivery.[91] In this work, photoactivatable o-nitrobenyl derivatives as linker was capped the pore mouths of mesoporous silica. Then antitumor drug DOX was encapsulated into the mesopores of photocaged nanocarrier. Since the spectrum overlap between the absorption band of photocaged DOX nanoconjugate and the upconverted UV emission band of the UCNPs, irradiation with NIR light triggered the cleavage of the caged group, inducing the precisely control drug release from the nanocarriers. This novel and effective drug loaded photocaged nanocarrier may demonstrate new possibility for the selective cell imaging and controlled drug release in the living system with less photo damage and deeper light penetration. Unfortunately, the study is only at the stage of cellular level and efficacy of photo-regulated drug delivery *in vivo* has not been explored. In this context, the photo-regulated drug release in living animal level was demonstrated by Li group.[92] They designed a novel yolk-shell structured nanocomposites (denoted as YSUCNPs, and $NaYF_4$:Yb/Tm@$NaLuF_4$ as the yolk center) as phototrigger-controlled DDS, as shown in Fig. 15. This unique design has two advantages. On the one hand, the hollow cavities can endow the material with a huge loading capacity for prodrug molecules for a sustainable release pattern. On the other hand, the mesoporous silica shell could avoid undesired premature release in living tissue by preventing contact between the adsorbed prodrug molecules. The anticancer drug chlorambucil, which was linked to the hydrophobized phototrigger of amino-coumarin derivative (ACCh) and then loaded into the YSUCNPs. Under NIR excitation, the upconversion UV emission emitted by the UCNPs can effectively drive the cleavage of the amino-coumarin phototrigger, uncaging and releasing the chlorambucil from YSUCNPs. Whereas, the degraded phototrigger molecules were totally retained within the YSUCNPs due to their high hydrophobicity. The *in vitro* drug release behavior indicated that the release dosage could be well tuned by remote control the on-off pattern of the 980 nm NIR laser, even zero premature release can be achieved under physiological conditions. Moreover, photo-regulated drug release in living animal level was successfully carried out for the first time. The results indicated that this YSUCNPs-ACCh nanocomposite can effectively released the anticancer drug into the tumor cells upon NIR irradiation and, hence, promote the drug action to inhibit the growth rate of tumors and prolong the survival time of mice. This work will illuminate the bright prospects of phototriggered DDS in practical biomedicine applications. Another striking example is reported by Yeh and co-workers,[263] who formulated a stimuli-responsive active targeted DDS by using UCNPs as the NIR light-triggered targeting and drug delivery vehicles (Fig. 16). FA was caged using a photolabile protecting molecule and conjugated on UCNPs in order to improve phototargeting selectivity. Upon NIR light irradiation, the emitted UV light from

UCNPs photocleaved the caged group, activated FA, and then allowed FA-modified UCNPs to targeted cancer cells. Moreover, to achieve the chemotherapeutic effect, DOX was thiolated to the surface of UCNPs via a disulfide bond, which can be cleaved by the lysosomal enzymes within cancer cells. The results of *in vivo*

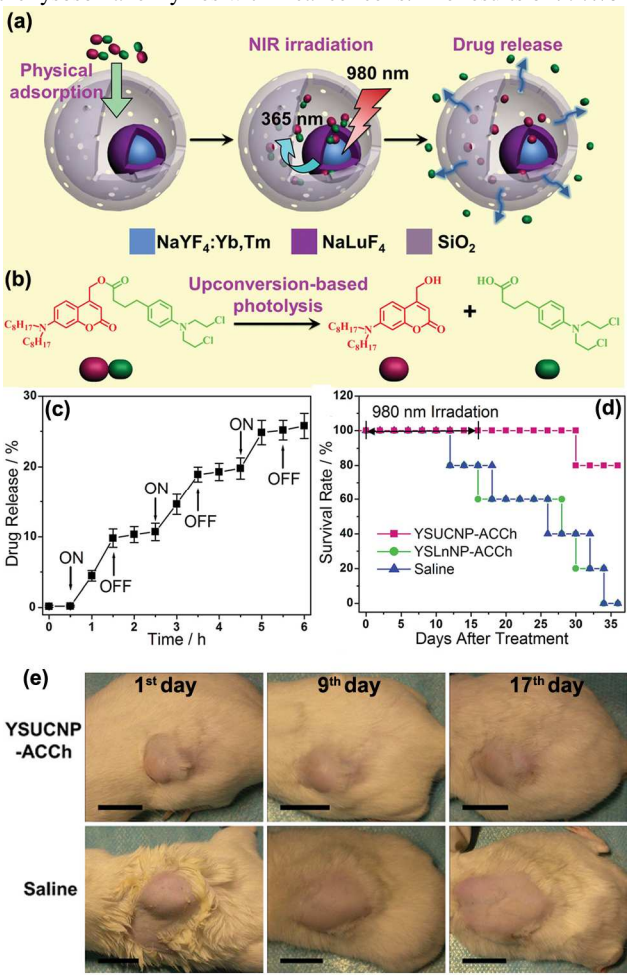

Fig. 15 (a) Schematic illustration of the NIR-regulated UCNPs-based DDS YSUCNPs. (b) The photolysis of the prodrug under NIR emission from the YSUCNPs. (c) Photo-regulated release of drug from YSUCNP-ACCh controlled by a 980 nm laser. (d) Survival rate in mice intratumorally injected with different solutions on the 1st day and on the 9th day. (e) Representative photographs of tumor-bearing mice injected with YSUCNP-ACCh and saline, on the 1st day, and after treatment on the 9th day and 17th day. Scale bars:1 cm. (Adapted from ref. 92. Copyright 2013, Wiley-VCH Verlag GmbH & Co. KGaA. Reproduced with permission.)

imaging and therapeutic efficacy exhibited highly selective targeting behaviors in a controlled manner. This stimuli-responsive active targeted DDS may be a new paradigm for increasing local effective therapeutic concentration of drugs and minimizing adverse side effects from chemotherapy, subsequently enhancing therapeutic efficacy. Table 2 summarizes recent works on NIR light-induced photolysis of "caged" compounds.

(ii) NIR light-induced photoswitching of molecules between two structurally and electronically different isomers

In addition to the photocaged compounds, some photochromic compounds can undergo a reversibly change in their molecular structure or conformation upon exposure to light with different excitation wavelengths accompanied with the variation of

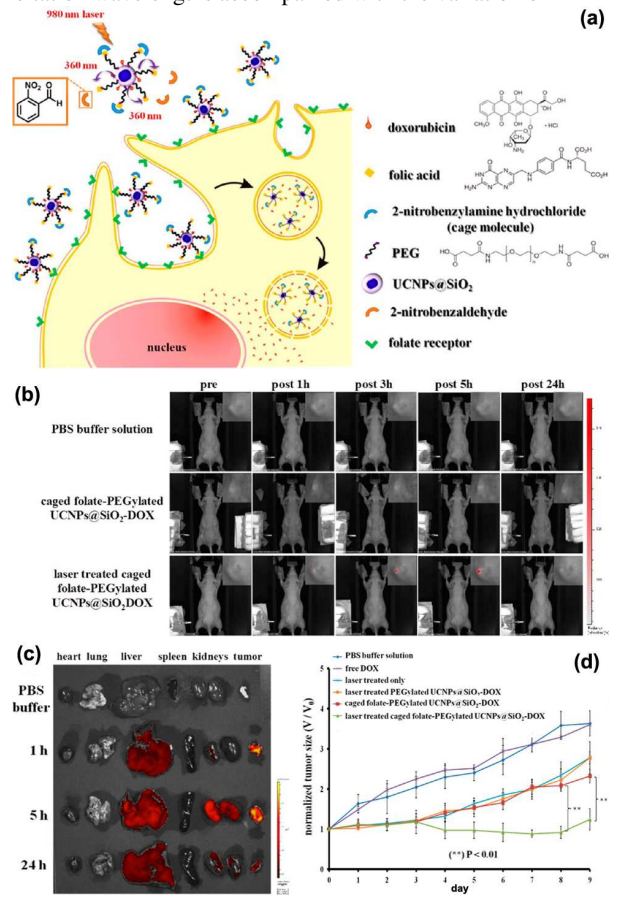

Fig. 16 (a) Illustration of photocaged UCNPs following NIR laser activation to remove cage molecules and subsequent targeting of cancer cells. (b) Time course upconversion NIRluminescence (emission 800 nm) images of caged folate-PEGylated UCNPs@SiO_2-DOX nanoparticles without NIR laser irradiation. Insets show the enlarged tumor region. (c) *Ex vivo* DOX fluorescence (emission 580 nm) images of the dissected organs and tumor from the group of laser-treated caged folate-PEGylated UCNPs@SiO_2-DOX nanoparticles of (b). (d) Tumor growth suppression monitored interms of tumor volume changes. Error bars are based on five mice per group (n = 5). **$P < 0.01$ calculated and compared to caged folate-PEGylated UCNPs@SiO_2-DOX (without laser irradiation). (Adapted from ref. 263. Copyright 2013, American Chemical Society. Reproduced with permission.)

absorption spectrum of the compounds.[274,275] In this context, photochromic compounds can be utilized to photocontrolled drug delivery. Probably, one of the most spectacular works in this area was done by Tanaka group in 2003 with the use of photosensitive coumarin derivatives that are attached to the pore outlets of MCM-41.[276] Under exposure to UV light (> 310 nm), coumains undergo dimerization to form dimer, which leaded to sealing of the pore openings, effectively preventing guest molecules release from the mesoporous silica. In turn, coumarin dimers disintegrate

to open up pore mouths to initiate the diffusion controlled release of the enclosed active compounds with UV light of 250 nm. As far as our knowledge, this is the first report about mesoporous silica for efficient and reversible photocontrol over guest molecules. Keeping in mind the shortcomings of UV or visible light, NIR light has become a good choice to trigger the photochemical reaction of photoswitches. The main families of organic photochromic compounds whose absorption can overlap with UV or visible emission generated UCNPs include coumarin, azobezenes, spiropyrans and dithienylethene. For instances, Branda et al. employed core-shell-shell UCNPs to reversibly toggle dithienylethene (DTE) photoresponsive molecules between their two isomers in a "remote-control" fashion by modulating merely the intensity of the 980 nm excitation light.[277,278] By virtue of the property of DTE, Li et al. further reported photoswitchable upconversion nanophosphors for small animal UCL imaging *in vivo* based on $NaYF_4$:Yb/Er/Tm and DTE trapped in one nanosystem using BSA-*graft*-dextran copolymer as a shell.[279] Capobianco et al. reported the photoswitching of bis-spiropyran (BSP) by direct anchoring BSP into the surface of $LiYF_4$:Yb/Tm UCNPs, in which fluorescence resonance energy transfer from NIR-to-UV UCNPs to BSP can drive reversible interconversion of BSP molecules from ring-closed bis-spiropyran form to the ring-open bis-merocyanine form upon NIR excitation.[280] More recently, an unprecedented and new reversible 980 nm NIR light-driven reflection in a self-organized helical superstructure loaded with UCNPs only by modulating the power density of 980 nm laser was reported by Yan and co-workers.[281] These successful investigations provide the possibility for the NIR photocontrolled drug delivery based on UCNPs-based nanocomposites through the reversible transformation in the molecular structure of photochromic compounds. For instance, the UV-visible reversible photoisomerization of the azobenzene group (and its derivaties) enables photoregulated control of drug release.[89] Following this concept, Shi et al. reported a novel NIR light triggered anticancer carriers based on $mSiO_2$ coated $NaYF_4$:Yb/Tm@$NaYF_4$ UCNPs (Fig. 17).[93] Photoactive azobenzene (azo) groups were installed into the mesopores of SiO_2 layer. Upon NIR laser irradiation, the UV (350 nm) and visible (450 nm) light emitted by UCNPs caused reversible *trans-cis* photoisomerization of azo molecules in the mesopores, creating a continuous rotation-inversion movement to trigger the release of chemotherapeutic molecules. This wagging motion of azo molecule will worked as an "impeller" to trigger the drug release in a controllable fashion. *In vitro* drug release behavior of this smart DDS indicated that the amount of released anticancer drug can be well regulated by varying the intensity and time duration of NIR exposure, thus realizing NIR light-controlled precise drug release. Another strategy for obtaining nanoparticles with photoswitchable drug release is to take advantage of visible upconversion emission light from $NaYF_4$:Yb/Er hollow spheres to trigger isomerization between ring-closed spiropyran and ring-opened merocyanine, which is reported by Qu group recently.[68] Table 3 summarizes recent works on NIR light-induced photoswitching of photochromic molecules.

(iii) NIR light-triggered photoactivation of platinum(IV) antitumor prodrug

As discussed in Section 4.2.3, the usage of Pt(IV) prodrugs with good chemical inertness, redox properties and low cytotoxic side effects to the normal tissues is a good solution to overcome the disadvantages of Pt(II). Apart from chemical reduction method,

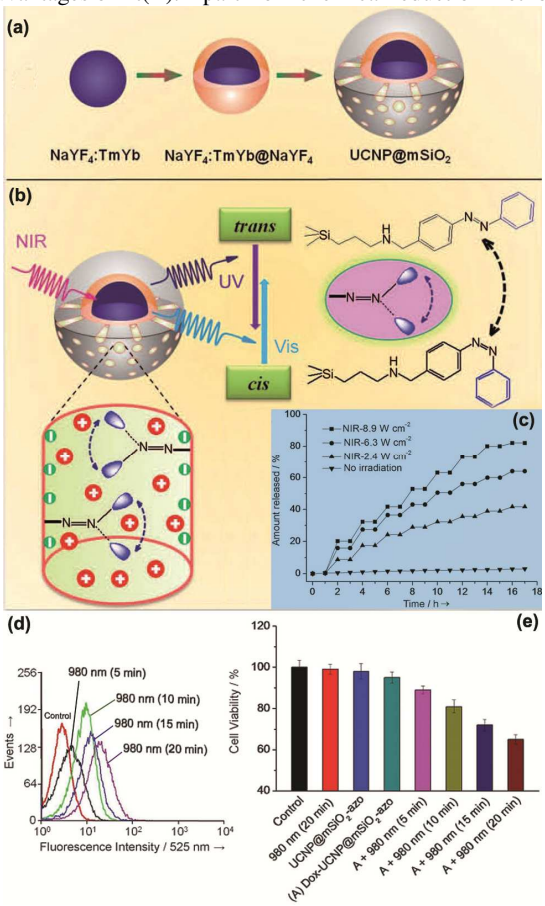

Fig. 17 (a) Synthetic procedure for upconverting nanoparticles coated with a mesoporous silica outer layer. (b) NIR light-triggered DOX release by making use of the upconversion property of UCNPs and *trans-cis* photoisomerization of azo molecules grafted in the mesopore network of a mesoporous silica layer. (c) Drug release in PBS under NIR light irradiation and dark conditions, alternatively. Every duration of NIR irradiations is 1 h. (d) Flow cytometry histograms under excitation of 488 nm laser light shows the DOX fluorescence intensity in HeLa cell nuclei separated from the whole cell after treatment with NIR light exposure for different times. (e) Inhibition of HeLa cell growth at different conditions. The concentration of the MSN materials was 1 mg mL^{-1}, and the NIR light exposure intensity was 2.4 W cm^{-2}. (Adapted from ref. 93. Copyright 2013, Wiley-VCH Verlag GmbH & Co. KGaA. Reproduced with permission.)

light also is an effective trigger to photoactivate Pt(IV) to release cytotoxic Pt(II) components.[282,283] Considering the intrinsic hurdles of UV, Xing and our groups independently developed new and personalized NIR light-mediated drug delivery nanoplatform by combining Pt(IV) antitumor prodrug with the Yb/Tm co-doped UCNPs for remote control of prodrug activation.[95,96] In one report, we develop a multifunctional nanomedicine system UCNP-DPP-PEG which combines cancer

diagnosis and therapy together (Fig. 18).[95] The core-shell structured $NaYF_4$:Yb/Tm@$NaGdF_4$/Yb UCNPs are used as the drug carriers. Meanwhile, the dicarboxyl light-activated platinum(IV) pro-drugs *trans,trans,trans*-[$Pt(N_3)_2(NH_3)(py)(O_2CCH_2CH_2COOH)_2$] (DPP) were conjugated to the surface of UCNPs followed by further PEG modification to obtain UCNP-DPP-PEG. The novelty of this study involves: (1) it provides a novel strategy by using the NIR-to-UV UCNPs to activate the platinum pro-drug for the first time. The UCNPs can absorb NIR light and convert it into the UV to activate the pro-drug to platinum (II) drugs to kill the cancer cells. Most importantly, the pro-drug conjugated nanoparticles under 980 nm NIR light exhibit higher *in vivo* antitumor therapy efficacy than that under UV light. This NIR-to-UV strategy can be served as a new way to utilize UV to treat cancer in deep tissue. (2) The UCL/MR/CT tri-modality imaging has been realized in one nanomedical system, which integrates the advantages of different imaging modality techniques together to avoid the shortcomings of single imaging modality. Therefore, this multifunctional nanocomposite can be used as multi-modality bioimaging contrast agents and transducers by converting NIR light into UV for control of drugs activity in practical cancer therapy. Around

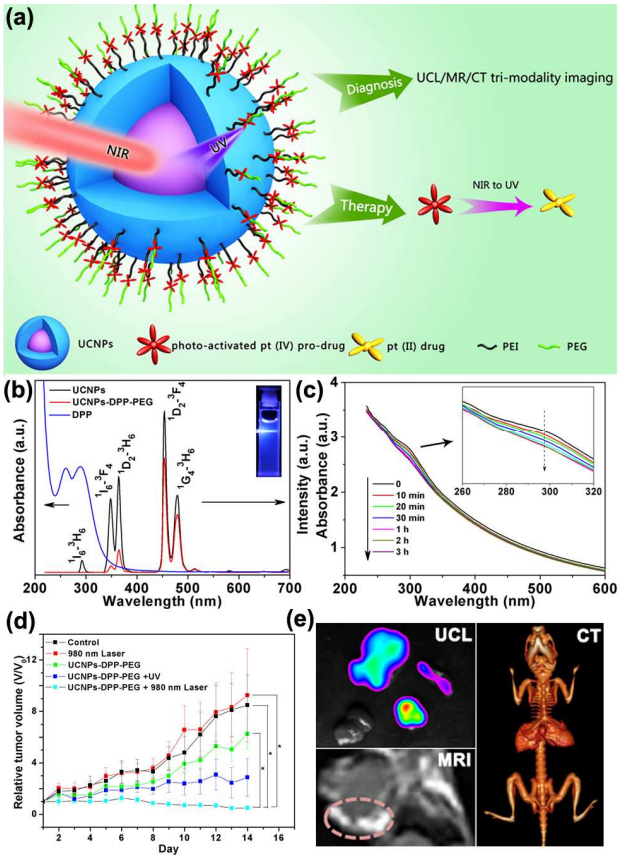

Fig. 18 (a) Schematic illustration of the characterization of UCNP-DPP-PEG nanoparticles. (b) Absorption spectrum of the DPP (blue line), emission spectra of pure UCNPs (black line), and DPP-conjugated UCNPs (red line) under 980 nm laser. (c) Absorption spectra of the UCNP-DPP-PEG as a function of time under 980 nm laser irradiation. (d) *in vivo* tumor volume changes of Balb/c mice on different groups after various treatments, 980 nm laser irradiation for 30 min (2.5 W cm^{-2}, 5 min break after 5 min irradiation), UV (365 nm) irradiation for 30 min, or without any irradiation. (e) *In vivo* UCL/MR/CT trimodality imaging of a tumor-bearing Balb/c mouse after injection of nanoparticles at the tumor site. (Adapted from ref. 95. Copyright 2013, American Chemical Society. Reproduced with permission.)

the same time, Xing et al. conjugated both photoactivatable Pt(IV) prodrug *trans,trans,trans*-[$Pt(N_3)_2(OH)(O_2CCH_2CH_2CO_2H)(py)_2$] and a caspase imaging peptide with a flanking activatable fluorescence resonance energy transfer pair consisting of a far-red fluorescence donor (Cy5) and a NIR quencher (Qsy21) to the surface of UCNP@SiO_2 (Fig. 19).[96] Upon NIR light irradiation, the converted UV emission from UCNPs@SiO_2 could locally activate the Pt(IV) prodrug and thus efficiently induced potent antitumor cytotoxcity in both cisplatin-sensitive and resistant tumor cells. Moreover, such NIR light-controlled tumor

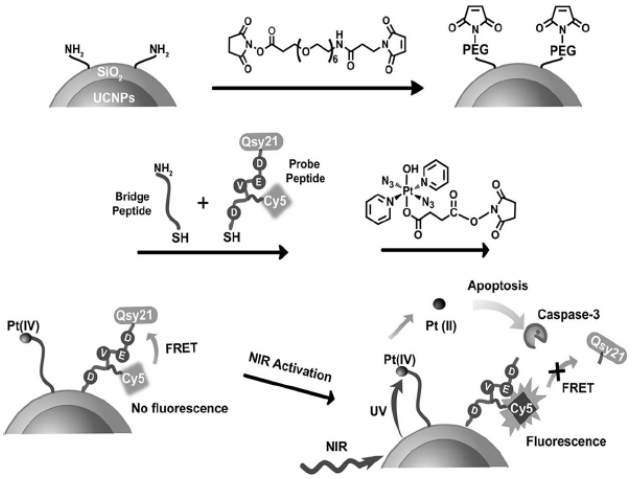

inactivation triggers the cellular apoptosis and the highly activated caspase could cleave the NIR imaging peptide probe from the nanoparticle surface, thus greatly turning on the quenched NIR fluorescence of Cy5, whereby which the real-time imaging of apoptosis in living cells by activated cytotoxicity can be monitored.

Fig. 19 Schematic illustration of NIR light activation of platinum(IV) prodrug and intracellular apoptosis imaging through UCNPs. (Adapted from ref. 96. Copyright 2013, Wiley-VCH Verlag GmbH &Co. KGaA. Reproduced with permission.)

(iv) NIR light-triggered photodynamic therapy (PDT)

PDT is a special light-triggered DDS, which is emerged as a non-invasive therapeutic modality for local treatment of diseases. Typical PDT system involves three key components: the photosensitizer (PS) molecules, appropriate excitation light, and oxygen within the tissue at the disease site. Upon excitation by the light with appropriate wavelength, PS molecules are activated in the presence of oxygen, producing singlet oxygen ($^1O_2$) or cytotoxic reactive oxygen species (ROS) to kill the nearby abnormal cells with little or no effect on the surrounding tissues. Over the past decades, PDT techniques have been proved to be a viable treatment option for early stage cancer and an adjuvant for surgery in late-stage cancer. However, a major challenge of this treatment methodology in clinical applications is the limited tissue penetration of the light needed for its activation, resulting

in ineffective therapeutic efficacy when treating large and deep-seated tumors. Alternatively, UCNPs capable of converting NIR light into UV-visible light provide potential strategy to make up for the defects of current PDT. Moreover, fruitful emission properties of UCNPs provide an additional benefit to simultaneously excite two or more types of PSs in a single platform under a single excitation wavelength. Following this concept, UCNPs open a new way to utilize the PS upon NIR irradiation. Recently, the use of UCNPs for PDT treatment has attracted considerable interest due to the greater penetration depths of NIR light in biological tissues.[284-290] Table 4 summarizes recent works on UCNPs-based photodynamic therapy system.

For the first time, Zhang' team demonstrated the UCNPs-based PDT treatment by incorporating merocyanine 540 (MC540) into $NaYF_4$:Yb/Er@SiO_2 nanocomposite.[291] To further improve the therapeutic efficiency, these NPs were functionalized with a tumor targeting antibody, which exhibited primary PDT effects on MCF-7/AZ cancer cells after 45 min irradiation. However, the efficiency of PDT was still low because the non-porous SiO_2 layer interfered the release of generated ROS. In the further studies, some novel nanostructures were designed in an attempt to assist the release of ROS from the nanocarriers. Zhang and co-workers reported core-shell structured $NaYF_4$:Yb/Er@SiO_2@mSiO_2 nanospheres with zinc phthalocyanine (ZnPc) PS loaded into the mesoporous silica shell.[163] They discovered that the ZnPc molecules were retained in the porous silica shell while they continuously produced $^1O_2$ under the irradiation of NIR laser. *In vivo* PDT treatment on MB49 bladder cancer cells demonstrated that the generated ROS can be easily released out to kill the cancer cells. Subsequently, other groups developed UCNPs-mSiO_2 structured nanocomposites for NIR light triggered PDT, acquired inspiring *in vitro* cancer killing results.[292,293] More recently, by incorporating two types of PS molecules into a single nanoplatform, Zhang's group extended their studies to *in vivo* tumor-targeted PDT treatment in small animals (Fig. 20).[294] Two different PSs, ZnPc and MC540, were simultaneously activated by the two UC emission peaks of $NaYF_4$:Yb/Er under a single excitation wavelength, fully utilizing the upconverted energy to maximize the PDT efficiency. Compared with single-PS loaded PDT system, this dual-PS loaded approach showed a greater PDT efficacy due to the enhanced generation of $^1O_2$ after NIR light irradiation. Importantly, ZnPc/MC540 co-loaded UCNPs were further modified with cancer-specific targeting agents, and intravenously injected into the tumor-bearing mice. *In vivo* targeted PDT treatment of melanoma tumors exhibited great tumor regression effect. This work presented the first proof-of-concept for the PS-loaded UCNPs for actively tumor-targeted PDT treatment *in vivo*. In addition to this silica encapsulation approach, Liu' group developed a non-covalent physical adsorption strategy to upload PS molecules onto UCNPs.[295] Chlorin e6 (Ce6), a PS molecule, was incorporated onto PEGlated UCNPs through hydrophobic interaction, yielding UCNPs-Ce6 nanocomplex as PDT agent. Upon intratumoral injection of UCNPs-Ce6 and NIR light exposure in a mouse model, excellent tumor destruction was achieved. Very recently, by loading double-layered Ce6 and charge-reversible polymer onto $NaYF_4$:Yb/Er/Mn UCNPs *via* a layer-by-layer self-assemble process, this group for the first time realized pH-responsive PDT cancer treatment.[240] At pH 6.8, the charge-reversible nanocomplexe showed remarkably increased *in vitro* intracellular uptake due to their interaction with negatively charged cell membranes. Enhanced PDT cancer killing efficacy was observed

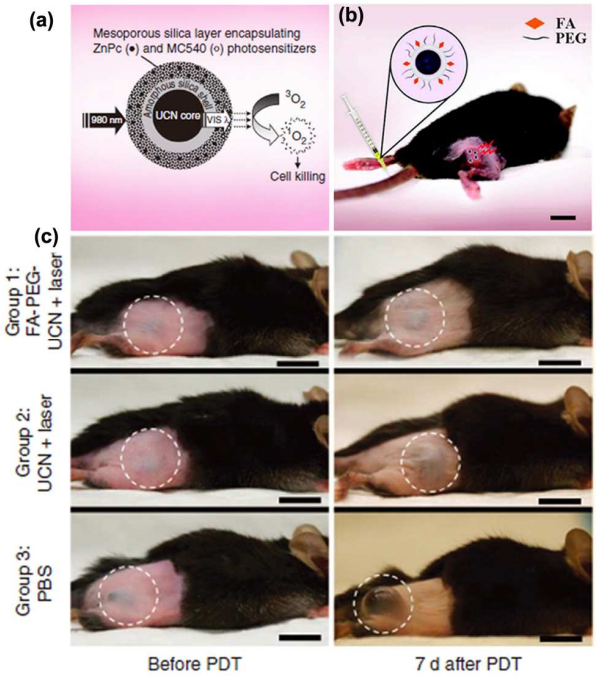

Fig. 20 (a) Schematic of mesoporous-silica–coated UCNs coloaded with ZnPc and MC540 photosensitizers for PDT. (b) Schematic diagram showing UCN-based targeted PDT in a mouse model of melanoma intravenously injected with UCNs surface modified with folic acid (FA) and PEG moieties. (c) Representative gross photos of a mouse from each group 1-3 intravenously injected with FA-PEG-UCNs, unmodified UCNs or PBS showing the change in tumor size (highlighted by dashed white circles) before and after PDT treatment. Scale bars:10 mm. (Adapted from ref. 294. Copyright 2012, Highwire press PNAS. Reproduced with permission.)

in both *in vitro* and *in vivo* results, owing to the slightly acidic tumor microenvironment.

However, the generally used physical encapsulation and adsorption methods suffer from premature leakage or desorption of PS molecules from the nanocarriers during the circulation in the blood, which can lead to a reduced PDT efficiency and unwanted side effects.[296,297] Alternatively, covalent coupling PS molecules onto the UCNPs should be a good choice to eliminate these defects, as well as improve energy transfer (ET) efficiency between PS and UCNPs. Zhang et al. demonstrated a covalent bonding strategy to link the Rose Bengal (RB),[297]monomalonic fullerene (C60MA),[298] or ZnPc[299] PS molecules onto UCNPs. In another study, Hyeon and co-workers synthesized an unique theranostic agent by attaching Ce6 molecules on UCNPs *via* both physical adsorption and chemical conjugation for bimodal imaging and PDT.[300] The above mentioned covalent conjugation strategy effectively reduced the leakage of PS molecules and simultaneously improved the ET efficiency from PS to UCNPs.

Nevertheless, the limited drug loading capacity in this method is still a big concern for *in vivo* PDT treatment.

Here it should be pointed out that one important advantage of using NIR light to trigger PDT in the UCNPs-based systems mainley relies on the higher penetration depth of NIR light. There are several researches to explore the imging penetration depth that UCNPs can reach and their advantage in photodynamic therapy. Li reported that high-contrast UCL imaging of a whole-body black mouse with a penetration depth of ~2 cm was achieved by using sub-10 nm β-$NaLuF_4$:Gd/Yb/Tm nanocrystals as a UCL probe.[40] Prasad and Han also demonstrated high contrast UCL imaging of deep tissues by using the NIR_{in}-NIR_{out} (980 nm-800 nm) α-$NaYbF_4$:Tm/CaF_2 core-shell nanoparticles-loaded synthetic fibrous mesh wrapped around rat femoral bone and a cuvette with nanoparticle aqueous dispersion covered with a 3.2 cm thick animal tissue (pork).[301] Additionally, Liu compared the tissue penetration abilities between 980 nm NIR light induced UCNPs-based PDT and traditional visible light (660 nm) triggered PDT by blocking irradiated subjects using pork tissues with different thicknesses.[295] It was found that although the $^1O_2$ generation efficiency of the NIR-induced PDT using UCNPs-Ce6 was much lower than the direct exposure of Ce6 to the 660 nm light, $^1O_2$ formation of the free Ce6 sample was dramatically reduced by ~80% if the 660 nm light was blocked by a 3 mm thick pork tissue and completely eliminated once the light was blocked by 8 mm pork. In contrast, the $^1O_2$ generation decreased by ~5% and ~50% when the 980 nm light was blocked by 3 mm and 8 mm thick tissue, respectively. *In vivo* experiments further confirmed that NIR-induced PDT exhibits terrifically increased tissue penetration depth relative to the traditional visible light excited PDT, offering significantly improved treatment efficacy for tumors blocked by thick biological tissues. These outcomings highlight the promise of UCNPs for *in vivo* bioimaing and cancer treatment.

4. 3 Targeted drug delivery system

After overcoming the problems of controllable release of drugs via the stimuli-responsive strategy, another key challenge for enhancing disease therapy is the precise release of the therapeutic agents at specific site. An effective method to accomplish this goal is to develop targeted drug delivery systems to improve the therapeutic index of drug molecules and minimize the toxic side effects on healthy cells and tissues. Nowadays, tremendous effort has been dedicated to the fabrication of targeted DDS to achieve disease site-specific drug payload delivery with elevated local dosages. The existing targeted DDS can be divided into two categories: (i) specific molecules-targeted drug delivery vehicles by covalently conjugating UCNPs-based nanocarriers with specific biomolecules; (ii) magnetic field-guided targeting drug release.

4. 3.1 Specific biomolecules-targeted drug delivery system

Target-specific recognition is the most popular method to construct targeted DDS by modifying drug delivery vehicles with some specific ligands or biomolecules (e.g. FA, antibodies, RGD peptide, TAT peptide, and aptamers etc.). These acceptor-labeled nanocarriers can specifically recognize the receptor existing on the surface of target cells. Thus site-specific drug release can be realized through a receptor-mediate endocytosis pathway. Folic acid (FA) has emerged as an attractive agent for targeted anticancer drug release, because folate receptors (FR) are overexpressed in a large variety of human cancer cells but absent in normal cells, including cancers of the ovary, lung, breast, kidney, brain, endometrium, colon and renal.[302-304] Meanwhile, FA possesses high stability, low cost, non-immunogenic, capability to be conjugated with a wide variety of molecules or nanoparticles and high affinity to FR even after conjugated to therapeutic/diagnostic cargo. Combining with the advantages of UCNPs, FA-coupled UCNPs have been widely investigated for simultaneous diagnosis and therapy.[170,195,200,204,305,306] For instance, we recently conjugated FA to the surface of $NaYF_4$:Yb/Er hollow nanospheres as anticancer drug carriers. After FA-modified composites were incubated with HeLa cells, significant suppression effect on cancer cells as well as increased luminescence signal arising from UCNPs could be observed. Gu and co-workers constructed FA-chitosan coated UCNPs (FASOC-UCNPs) as carriers for *in vivo* targeted deep-tissue imaging and photodynamic therapy.[288] A hydrophobic photosensitizer, ZnPc, was loaded into the hydrophobic layer of FASOC-UCNPs by physical encapsulation. Furthermore, a NIR fluorescent dye ICG-Der-01 was also encapsulated in the FASOC-UCNPs to track their *in vivo* biodistribution and targeting imaging capacity. Both the *in vitro* and *in vivo* results indicated that these FA-modified nanocarriers could be selectively accumulated in FR-overexpressed tumor cells by FR-mediate active targeting, resulting in the enhanced NIR fluorescence in tumor site and remarkable therapeutic efficacy over traditional PDT (Fig. 21).

In addition to FA molecules, a nuclear localizing signal peptide (TAT) has been proved to be a promising specific agent for nuclear-targeted translocation. TAT peptide can be recognized by nuclear pore complexes, leading to the active nuclear entry of cargos. For instance, Shi and co-workers synthesized TAT-conjugated $mSiO_2$ for nuclear-targeted drug delivery.[307] It was found that TAT-modified nanocarriers with smaller particle size could efficiently target the nucleus and deliver the active DOX into the targeted nucleus, inducing apoptosis of cancer cells with higher efficiencies. Following this study, the same group developed TAT-conjugated $NaYF_4$:Yb/Er@$NaGdF_4$-PEG (UCNPs-PEG/TAT) as active nuclear-targeted theranostics.[308] It is noted that the DOX-loaded UCNPs-PEG/TAT could easily migrate into HeLa cells for direct nuclear drug delivery because TAT protein was effective in nuclear translocation of recombinant fusion proteins, resulting in an enhanced activity in killing the cancer cells (Fig. 22a). *In vitro* confocal observations in HeLa cells incubated without and with TAT for 24 h clearly show that in the presence of TAT, the stronger fluorescent emissions from both UCNPs and DOX can be found mostly from nuclei, indicating the effective internalization of the NPs into the cell nucleus compared to the DOX-UCNPs-PEG (without TAT) (Fig. 22b).

As mentioned above, this nuclear-targeted DDS may open up new insight into the targeted cancer therapy and diagnosis. However, in such nuclear-targeted theranostic system, the size of TAT-bonded NPs is a critical factor in the intra-nuclear translocation. In particular, the size of NPs should be smaller than that of nuclear pore complexes to ensure than the NPs can be step

across the nuclear pore. In addition, Yan et al. demonstrated the design and fabrication of a dual-targeting upconversion nanoplatform for two-color fluorescence imaging-guided PDT. The nanoplatform was prepared from 3-aminophenylboronic acid(APBA) functionalized upconversion nanocrystals (APBA-UCNPs) and hyaluronated fullerene (HAC_{60}) via a specific diol-

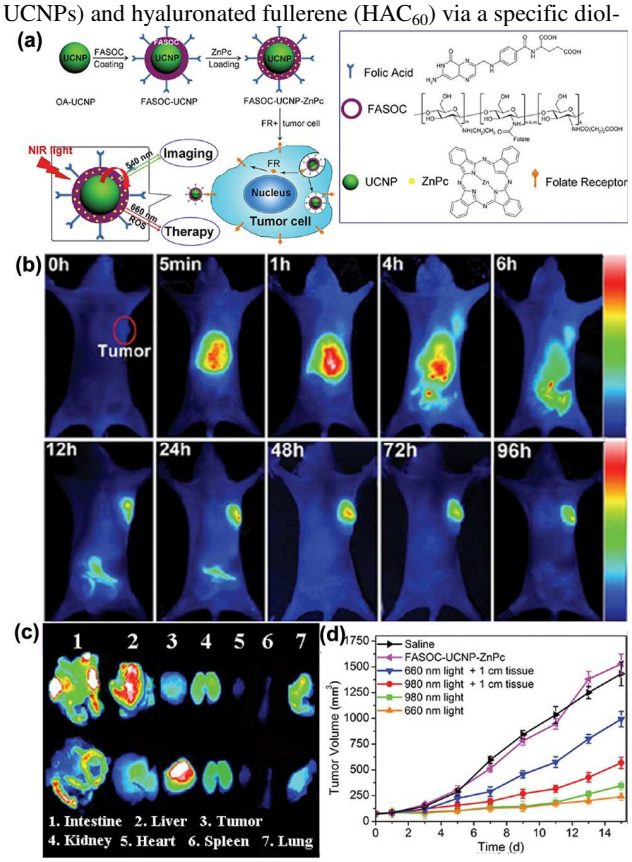

Fig. 21 (a) Schematic of the synthesis of FASOC-UCNP-ZnPc nanoconstruct and folate-mediated binding of tumor cells with folate receptor expression; (b, c) *In vivo* tumor-targeting of the nanoconstructs. (b) Fluorescence images of nude mice bearing Bel-7402 tumors with intravenously injection of FASOC-UCNP-ICG; (c) fluorescence images of isolated organs separated from Bel-7402 tumor-bearing mice in different groups at 24 h postinjection. (d) Comparison of the therapeutic efficacy of deep-tissue PDT triggered by 980 and 660 nm light: tumor growth of mice in different treatment groups within 15 days. (Adapted from ref. 288. Copyright 2013, American Chemical Society. Reproduced with permission.)

borate condensation. The two specific ligands of APBA and hyaluronic acid (HA) provide synergistic targeting effects, high target ability, and hence a dramatically elevated uptake of the nanoplatform by cancer cells. The high generation yield of $^1O_2$ due to multiplexed Förster resonance energy transfer between APBA-UCNPs (donor) and HAC_{60} (acceptor) allows effective therapy. The present nanoplatform shows great potential for highly selective tumor-targeted imaging-guided PDT.[309]

Besides FA and TAT, in recent years, aptamers consisted of single-stranded oligonucleotides have also become an important class of targeted biomolecules for drug delivery and cancer treatment, which originates from their good properties including flexible design, synthetic accessibility, easy modification, chemical stability, and rapid tissue penetration.[310,311] Very recently, Tan et al. developed a specific aptamer-guided G-quadruplex DNA nanoplatform for targeted upconversion bioimaging and PDT, in which G4-aptamer is bioconjugated to $NaLuF_4$:Gd/Yb/Er UCNPs, then photosensitizer TMPyP4 intercalated within the G4-aptamer structure, allowing the

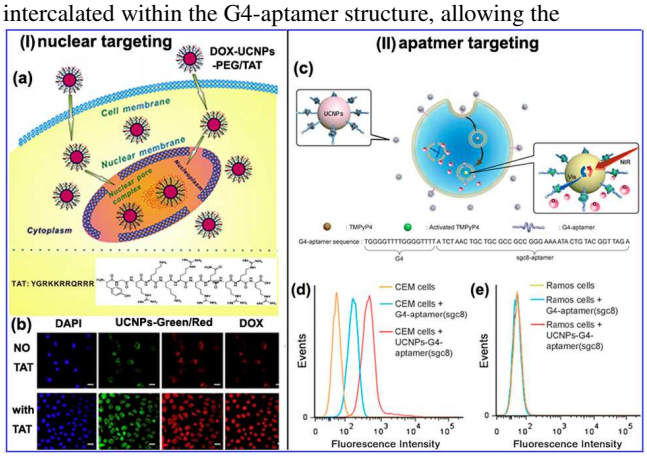

Fig. 22 Two kinds of specific biomolecules-targeted drug delivery system. (I) Nuclear targeting. (a) Schematic illustration of the nuclear-targeting of UCNPs-based theranostic system for nuclear imaging and direct intranuclear anticancer drug delivery. (b) *In vitro* confocal observations of UCNPs and DOX in Hela cells incubated with DOX-UCNPs-PEG (without TAT) and DOX-UCNPs-PEG/TAT for 24 h. The blue fluorescence is from DAPI used to stain the nuclei. The green and red fluorescences are from UCNPs under 980 nm laser excitation, while DOX emits red fluorescence under 488 nm laser excitation. Without TAT, UCNPs can be found within the cytoplasm, but not in the nucleus, and DOX accumulate mostly within the cytoplasm with a negligible DOX fluorescence within nuclei. In contrast, in the presence of TAT, the stronger fluorescent emissions from both UCNPs and DOX can be found mostly from nuclei, indicating the effective internalization of the NPs into the cell nucleus. Scale bar: 20 mm. (II) Aptamer targeting: (c) Engineering of a targeted photodynamic therapy nanoplatform using an aptamer-guided G-quadruplex DNA carrier and 980 nm NIR irradiation. Flow cytometry histograms to monitor the binding of the G4-aptamer and UCNP-G4-aptamer with (d) CEM cells and (e) Ramos cells, respectively, demonstrating that UCNP-G4-aptamer has high selectivity and targeting specificity sgc8 toward CEM cells but shows little affinity to nontarget Ramos cells. (Adapted from refs. 308, 312. Copyright 2012, 2013, and Elsevier B. V. and Wiley-VCH Verlag GmbH & Co. KGaA. Reproduced with permission.)

occurrence of energy transfer from UCNPs to TMPyP4 (Fig. 22c). In this case, once the nanoplatform is delivered into cancer cells, the emitted visible light produced by UCNPs can activate TMPyP4 to generate sufficient ROS to efficiently kill cancer cells.

Flow cytometry histograms demonstrate clearly that UCNP-G4-aptamer has high selectivity and targeting specificity sgc8 toward CEM cells but shows little affinity to nontarget Ramos cells (Fig. 22d, e). This design has capability of selective recognition and imaging of cancer cells, controllable and effective activation of the photosensitizer, and improvement of the therapeutic effect.[312]

4. 3. 2 Magnetic targeted drug delivery system

Besides specific biomolecular targeting, magnetic-field-guided drug delivery is proposed to be a more convenient and attractive strategy of delivering payload molecules to the area of interest. Superparamagnetic iron oxide (Fe_3O_4) is one of the most promising targeted agents due to its prominent advantages of magnetic-responsive property, biocompatibility and biodegradability.[211,313-316] Following these features, considerable interest has been focused on the synthesis of magnetic-optical multifunctional nanoplatforms by integrating Fe_3O_4 and UCNPs into a single nanocarrier for simultaneous diagnosis and therapy purposes. The major design strategies are to encapsulate these two moieties into the block copolymer or construct a core-shell structure. For example, Liu and co-workers demonstrated a polymer encapsulated UCNPs/Fe_3O_4/DOX nanocomposite for multi-model imaging and targeted drug delivery.[211] In the presence of a magnetic field, the cancer cells near the magnet were mostly killed by the DOX-loaded UCNPs/Fe_3O_4 nanocomposites, while those far from the magnet were largely survived. This could be attributed to the higher cell uptake of the nanocomposites guided under an external magnetic field. In addition, Stucky et al. synthesized a nanorattle structured spheres Fe_3O_4@SiO_2@volid@Y_2O_3:Yb/Er consisted of a moveable Fe_3O_4@SiO_2 inner particle and Y_2O_3:Yb/Er shells, which provide a high drug-loading capacity (Fig. 23).[175] An active accumulation

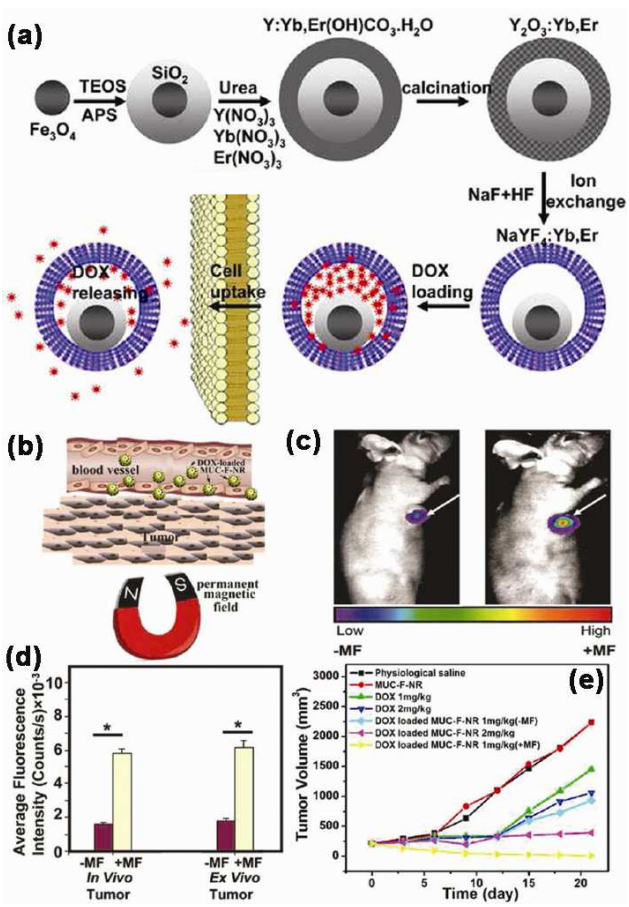

Fig. 23 Multifunctional UCNPs-based "nanorattle" for magnetic-targetted therapy. (a) Synthetic procedure for the Drug-Loaded Fe_3O_4@SiO_2@volid@Y_2O_3:Yb/Er nanorattles. (b) Schematic illustration of targeting of DOX loaded multifunctional drug carrier to tumor cells assisted by an externally applied magnetic field (MF). (c) *In vivo* mice imaging after 1 h magnetic field treatment. (d) The luminescence signal was measured from the whole tumor *in vivo* and *ex vivo*. (e) Tumor volume changes of mice under different treatments. (Adapted from ref. 175. Copyright 2012, American Chemical Society. Reproduced with permission.)

of DOX-loaded Fe_3O_4@SiO_2@volid@Y_2O_3:Yb/Er nanocomposite in tumors could be observed from the increased UC luminescence intensity when an external magnetic field was applied. *In vivo* therapeutic experiments on marine hepatocarcinoma (H22) tumor-bearing mice exhibited excellent tumor inhibition effect due to the effective tumor targeting in the presence of a magnetic field. This magnetic guided drug delivery may be a unique targeted therapeutic approach that is specific and selective to localized regions.

5. Conclusions and perspectives

This review mainly presents a survey on the rational design, various synthetic strategies and application in drug delivery and cancer therapy of UCNPs-based composite nanomaterials in the last five years. Despites these successes, there exists the major challenges for these nanomaterials that need to be resolved in order to fulfill the translation from the bench to bedside.

Firstly, since the vast majority of photosensitive compounds do not absorb NIR light directly, the efficiency of NIR light triggered controlled drug delivery systems has strongly related to UV intensity emitted by UCNPs. Therefore, the development of highly efficient NIR-to-UV UCNPs will be of great importance by elaborate design of core-shell structure and the choice of host lattices. More recently, an investigation by Liu and co-workers found that minimizing the migration of excitation energy to defects in KYb_2F_7:2% Er UCNPs can generate an unusual four-photon-promoted violet upconversion emission from Er^{3+} with an intensity that is more than eight times higher than previously reported $NaYF_4$: 20%Yb/2%Er.[317] This finding provides new clue for enhancing upconversion luminescence through energy clustering at the sublattice level.

Secondly, an excellent photoresponsive drug delivery system should possess the properties of zero-premature release, near-infrared light excitation, clean photolysis without side products, and external precise manipulations.[257] Moreover, the safety, and biodegradability of photoresponsive compounds such as azobenzene, o-nitro benzyl derivatives is questionable. Therefore, the search for biocompatible photosensitive materials will be critical in photo-controlled drug delivery.

Thirdly, among the photocontrolled drug delivery systems available, 980 nm NIR light is usually used to control drug delivery, however, the overheating effect associated with 980 nm excitation is a major limitation for *in vivo* application. UCNPs that can be effectively excited by other NIR wavelengths (e.g. 915 nm[20] and 808 nm[32-37]) can considerably minimize the overheating effect and reduce potential tissue damage compared with 980 nm NIR laser. Thus other NIR lights break a new park for the application of UCNPs in biomedical fields, especially suitable for NIR photoactivation of biomolecules or phototriggered drug delivery, which is one of the important

research directions of UCNPs-based nanomaterials in near future.

Fourthly, during the drug delivery, multimodal bioimagings of UCNPs-based nanomaterials were often used for disease diagnosis. However, UCL/MR/CT images *in vivo* are often observed by *in situ* tumor injection of naomaterials. Very few studies on *in vivo* bioimagings are performed by tail intravenous injection due to low accumulation concentration of nanomaterials at the specific tumor location. Although promising in usage of target molecules, the density of the target molecules on the surface of nanoparticles needs to be precisely optimized to facilitate the balance between tissue biodistribution and cellular uptake. In this context, the better design of target molecules modified UCNPs-based drug delivery nanomaterials is highly demanded in order to achieve real-time monitoring of treatment progress by the tail intravenous injection.

Finally, the engineering of multifunctional UCNPs-based nanocomposites is still an incipient area, so their bio-safety systematical and rigorous evaluations *in vivo*, especially the degradability are one of the prominent problems due to their complex biodistributions and elimination pathways.[318] These problems involve interdisciplinary research areas ranging from chemistry, biology to medicine, which needs close collaborations of the experts from various fields. If these problems are solved satisfactorily in the near future, the UCNPs-based multifunctional nanomaterials will open up new opportunities for simultaneous diagnosis and the efficient treatment of diseases.

Taken together, the investigations on UCNPs-based drug delivery systems are still in the early stage, and there is plenty of room for innovative research in this exciting field. It is believed that this highly dynamic research field will certainly continue to produce breakthrough discoveries for the disease diagnosis and treatment in near future.

Acknowledgements

This project is financially supported by the National Natural Science Foundation of China (NSFC 51332008, 51372243), National Basic Research Program of China (2010CB327704, 2014CB643803).

Notes and references

State Key Laboratory of Rare Earth Resource Utilization, Changchun Institute of Applied Chemistry, Chinese Academy of Sciences, Changchun, 130022, Jilin, China. E-mail: cxli@ciac.ac.cn; jlin@ciac.ac.cn; Fax: +86-431-85698041; Tel: +86-431-85262031.

References

1 S. V. Eliseeva and J.-C. G. Bünzli, *Chem. Soc. Rev.*, 2010, **39**, 189-227.
2 F. Wang and X. G. Liu, *Chem. Soc. Rev.*, 2009, **38**, 976-989.
3 J.-C. Boyer, F. Vetrone, L. A. Cuccia and J. A. Capobianco, *J. Am. Chem. Soc.*, 2006, **128**, 7444-7445.
4 J. B. Zhao, D. Y. Jin, E. P. Schartner, Y. Q. Lu, Y. J. Liu, A. Z. Zvyagin, L. X. Zhang, J. M. Dawes, P. Xi, J. A. Piper, E. M. Goldys and T. M. Monro, *Nat. Nanotechnol.*, 2013, **8**, 729-734.
5 D. R. Gamelin and H. U. Güdel, *Acc. Chem. Res.*, 2000, **33**, 235-242.
6 F. Auzel, *Chem. Rev.*, 2004, **104**, 139-174.
7 R. Anderson, S. Smith, S. May and M. Berry, *J. Phys. Chem. Lett.*, 2013, **5**, 36-42.
8 G. Yao, M. T. Berry, P. S. May and D. Kilin, *J. Phys. Chem. C*, 2013, **117**, 17177-17185.
9 D. K. Chatterjee, M. K. Gnanasammandhan and Y. Zhang, *Small*, 2010, **6**, 2781-2795.
10 C. X. Li and J. Lin, *J. Mater. Chem.*, 2010, **20**, 6831-6847.
11 C. Bouzigues, T. Gacoin and A. Alexandrou, *ACS Nano*, 2011, **5**, 8488-8505.
12 M. Wang, G. Abbineni, A. Clevenger, C. B. Mao and S. K. Xu, *Nanomed-Nanotechnol.*, 2011, **7**, 710-729.
13 A. Gnach and A. Bednarkiewicz, *Nano Today*, 2012, **7**, 532-563.
14 Y. S. Liu, D. T. Tu, H. M. Zhu and X. Y. Chen, *Chem. Soc. Rev.*, 2013, **42**, 6924-6958.
15 W. Feng, C. M. Han and F. Y. Li, *Adv. Mater.*, 2013, **25**, 5287-5303.
16 Z. J. Gu, L. Yan, G. Tian, S. J. Li, Z. F. Chai and Y. L. Zhao, *Adv Mater.*, 2013, **25**, 3758-3579.
17 J. Shen, L. Zhao and G. Han, *Adv. Drug Delivery Rev.*, 2013, **65**, 744-755.
18 S. L. Gai, C. X. Li, P. P. Yang and J. Lin, *Chem. Rev.*, 2014, **114**, 2343-2389.
19 G. Y. Chen, H. L. Qiu, P. N. Prasad and X. Y. Chen, *Chem. Rev.*, 2014, **114**, 5161-5214.
20 Q. Zhan, J. Qian, H. Liang, G. Somesfalean, D. Wang, S. He, Z. Zhang and S. Andersson-Engels, *ACS Nano*, 2011, **5**, 3744-3757.
21 J. Frangioni, *Curr. Opin. Chem. Biol.*, 2003, **7**, 626-634.
22 S. W. Wu, G. Han, D. J. Milliron, S. Aloni, V. Altoe, D. V. Talapin, B. E. Cohen and P. J. Schuck, *Proc. Natl. Acad. Sci. U.S.A.*, 2009, **106**, 10917-10921.
23 D. K. Chatterjee, A. J. Rufaihah and Y. Zhang, *Biomaterials*, 2009, **29**, 937-943.
24 G. Y. Chen, T. Y. Ohulchanskyy, A. Kachynski, H. Ågren and P. N. Prasad, *ACS Nano*, 2011, **5**, 4981-4986.
25 Q. Q. Zhan, S. L. He, J. Qian, H. Cheng and F. H. Cai, *Theranostics*, 2013, **3**, 306-316.
26 Z. Song, Y. Anissimov, J. Zhao, A.V. Nechaev, A. Nadort, D. Y. Jin, T. W. Prow, M.S. Roberts and A. Zvyagin, *J. Biomed. Opt.*, 2013, **18**, 061215-061215.
27 D. J. Gargas, E. M. Chan, A. D. Ostrowski, S. Aloni, M. V. P. Altoe, E. S. Barnard, B. Sanii, J. J. Urban, D. J. Milliron, B. E. Cohen and P. J. Schuck, *Nat. Nanotech.*, 2014, **9**, 300-305.
28 S. H. Nam, Y. M. Bae, Y. I. Park, J. H. Kim, H. M. Kim, J. S. Choi, K. T. Lee, T. Hyeon and Y. D. Suh, *Angew. Chem., Int. Ed.*, 2011, **50**, 6093-6097.
29 A. D. Ostrowski, E. M. Chan, D. J. Gargas, E. M. Katz, G. Han, P. J. Schuck, D. J. Milliron and B. E. Cohen, *ACS Nano*, 2012, **6**, 2686-2692.
30 D. Q. Chen, Y. L. Yu, F. Huang, H. Lin, P. Huang, A. P. Yang, Z. X. Wang and Y. S. Wang, *J. Mater. Chem.*, 2012, **22**, 2632-2640.
31 X. M. Li, R. Wang, F. Zhang, L. Zhou, D. K. Shen, C. Yao and D. Y. Zhao, *Sci. Rep.*, 2013, **3**, 3536.
32 J. Shen, G. Chen, A. M. Yu, W. Fan, O. S. Bilsel, C. C. Chang and G. Han, *Adv. Optical Mater.*, 2013, **1**, 644-650.
33 X. Xie, N. Gao, R. Deng, Q. Sun, Q. Xu and X. Liu, *J. Am. Chem. Soc.*, 2013, **135**, 12608-12611.
34 Y. F. Wang, G. Y. Liu, L. D. Sun, J. W. Xiao, J. C. Zhou and C. H.

Yan, *ACS Nano*, 2013, **7**, 7200-7206.
35 H. Wen, H. Zhu, X. Chen, T. F. Hung, B. Wang, G. Zhu, S. F. Yu and F. Wang, *Angew. Chem., Int. Ed.*, 2013, **52**, 13419-13423.
36 U. Rocha, K. U. Kumar, C. Jacinto, I. Villa, F. Sanz-Rodríguez, M. Del Carmen Iglesias de la Cruz, A. Juarranz, E. Carrasco, F. C. J. M. van Veggel, E. Bovero, J. G. Solé and D. Jaque, *Small*, 2014, **10**, 1141-1154.
37 L. D. Sun, Y. F. Wang and C. H. Yan, *Acc. Chem. Res.*, 2014, **47**, 1001-1009.
38 S. A. Hilderbrand, F. W. Shao, C. Salthouse, U. Mahmood and R. Weissleder, *Chem. Commun.*, 2009, 4188-4190.
39 B. Dong, S. Xu, J. Sun, S. Bi, D. Li, X. Bai, Y. Wang, L. P. Wang and H. W. Song, *J. Mater. Chem.*, 2011, **21**, 6193-6200.
40 Q. Liu, Y. Sun, T. S. Yang, W. Feng, C. G. Li and F. Y. Li, *J. Am. Chem. Soc.*, 2011, **133**, 17122-17125.
41 Q. Liu, T. S. Yang, W. Feng and F. Y. Li, *J. Am. Chem. Soc.*, 2012, **134**, 5390-5397.
42 J. Zhou, Z. Liu and F. Y. Li, *Chem. Soc. Rev.*, 2012, **41**, 1323-1349.
43 Y. Sun, X. J. Zhu, J. J. Peng and F. Y. Li, *ACS Nano*, 2013, **7**, 11290-11300.
44 Z. L. Wang, J. H. Hao, H. L. W. Chan, W.-T. Wong and K.-L. Wong, *Small*, 2012, **8**, 1863-1868.
45 X. Teng, Y. H. Zhu, W. Wei, S. C. Wang, J. F. Huang, R. Naccache, W. B. Hu, A. J. Y. Tok, Y. Han, Q. C. Zhang, Q. L, Fan, W. Huang, J. A. Capobianco and L. Huang, *J. Am. Chem. Soc.*, 2012, **134**, 8340-8343.
46 F. Y. Liu, X. X. He, L. Liu, H. P. You, H. M. Zhang and Z. X. Wang, *Biomaterials*, 2013, **34**, 5218-5225.
47 J. Wang, T. Wei, X. Li, B. Zhang, J. Wang, C. Huang and Q. Yuan, *Angew. Chem. Int. Ed.*, 2014, **53**, 1616-1620.
48 H. X. Mai, Y. W. Zhang, L. D. Sun and C. H. Yan, *J. Phys. Chem. C*, 2007, **111**, 13721-13729.
49 F. Wang and X. G. Liu, *J. Am. Chem. Soc.*, 2008, **130**, 5642-5643.
50 O. Ehlert, R. Thomann, M. Darbandi and T. Nann, *ACS Nano*, 2008, **2**, 120-124.
51 V. Mahalingam, F. Vetrone, R. Naccache, A. Speghini and J. A. Capobianco, *Adv. Mater.*, 2009, **21**, 4025-4028.
52 N. Niu, P. P. Yang, H. He, X. Zhang, S. L. Gai, C. X. Li and J. Lin, *J. Mater. Chem.*, 2012, **22**, 10889-10899.
53 E. M. Chan, G. Han, J. D. Goldberg, D. J. Gargas, A. D. Ostrowski, P. J. Schuck, B. E. Cohen and D. J. Milliron, *Nano Lett.*, 2012, **12**, 3839-3845.
54 Y. S. Liu, D. T. Tu, H. M. Zhu, R. F. Li, W. Q. Luo and X. Y. Chen, *Adv. Mater.*, 2010, **22**, 3266-3271.
55 H. H. Gorris, R. Ali, S. M. Saleh and O. S. Wolfbeis, *Adv. Mater.*, 2011, **23**, 1652-1655.
56 X. Zhang, P. P. Yang, C. X. Li, D. Wang, J. Xu, S. L. Gai and J. Lin, *Chem. Commun.*, 2011, **47**, 12143-12145.
57 H. H. Gorris and O. S. Wolfbeis, *Angew. Chem., Int. Ed.*, 2013, **52**, 3584-3600.
58 Q. Q. Dou, N. M. Idris and Y. Zhang, *Biomaterials*, 2013, **34**, 1722-1731.
59 S. Wilhelm, T. Hirsch, W. M. Patterson, E. Scheucher, T. Mayr and O. S. Wolfbeis, *Theranostics*, 2013, **3**, 239-248.
60 Y. Q. Lu, J. B. Zhao, R. Zhang, Y. J. Liu, D. M. Liu, E. M. Goldys, X. S. Yang, P. Xi, A. Sunna, J. Lu, Y. Shi, R. C. Leif, Y. J. Huo, J. Shen, J. A. Piper, J. P. Robinson and D. Y. Jin, *Nat. Photonics*, 2014, **8**, 32-36.
61 F. Wang and X. G. Liu, *Acc. Chem. Res.*, 2014, **47**, 1378-1385.
62 Y. H. Zhang, L. X. Zhang, R. R. Deng, J. Tian, Y. Zong, D. Y. Jin and X. G. Liu, *J. Am. Chem. Soc.*, 2014, **136**, 4893-4896.
63 P. Caravan, J. J. Ellison, T. J. McMurry and R. B. Lauffer, *Chem. Rev.*, 1999, **99**, 2293-2352.
64 Y. I. Park, J. H. Kim, K. T. Lee, K. S. Jeon, H. B. Na, J. H. Yu, H. M. Kim, N. Lee, S. H. Choi, S. I. Baik, H. Kim, S. P. Park, B. J. Park, Y. W. Kim, S. H. Lee, S. Y. Yoon, I. C. Song, W. K. Moon, Y. D. Suh and T. Hyeon, *Adv. Mater.*, 2009, **21**, 4467-4471.
65 R. Kumar, M. Nyk, T. Y. Ohulchanskyy, C. A. Flask and P. N. Prasad, *Adv. Funct. Mater.*, 2009, **19**, 853-859.
66 M. He, P. Huang, C. L. Zhang, H. Y. Hu, C. C. Bao, G. Gao, R. He and D. X. Cui, *Adv. Funct. Mater.*, 2011, **21**, 4470-4477.
67 Noah J. J. Johnson, Wendy. Oakden, Greg J. Stanisz, R. Scott Prosser and F. C. J. M. van Veggel, *Chem. Mater.*, 2011, **23**, 3714-3722.
68 C. Y. Cao, H. K. Yang, J. W. Chung, B. K. Moon, B. C. Choi, J. H. Jeong and K. H. Kim, *J. Mater. Chem.*, 2011, **21**, 10342-10347.
69 C. H. Dong, A. Korinek, B. Blasiak, B. Tomanek and F. C. J. M. van Veggel, *Chem. Mater.*, 2012, **24**, 1297-1305.
70 Y. Y. Hou, R. R. Qiao, F. Fang, X. X. Wang, C. Y. Dong, K. Liu, C. Y. Liu, Z. F. Liu, H. Lei, F. Wang and M. Y. Gao, *ACS Nano*, 2013, **7**, 330-338.
71 Y. X. Liu, D. S. Wang, J. X. Shi, Q. Peng and Y. D. Li, *Angew. Chem., Int. Ed.*, 2013, **52**, 4366-4369.
72 D. L. Ni, J. W. Zhang, W. B. Bu, H. Y. Xing, F. Han, Q. F. Xiao, Z. W. Yao, F. Chen, Q. J. He, J. N. Liu, S. J. Zhang, W. P. Fan, L. P. Zhou, W. J. Peng and J. L. Shi, *ACS Nano*, 2014, **8**, 1231-1242.
73 Y. L. Liu, K. L. Ai, J. H. Liu, Q. H. Yuan, Y. Y. He and L. H. Lu, *Angew. Chem., Int. Ed.*, 2012, **51**, 1437-1442.
74 S. J. Zeng, M.-K. Tsang, C.-F. Chan, K.-L. Wong and J. H. Hao, *Biomaterials*, 2012, **33**, 9232-9238.
75 H. R. Liu, W. Lu, H. B. Wang, L. Rao, Z. G. Yi, S. J. Zeng and J. H. Hao, *Nanoscale*, 2013, **5**, 6023-6029.
76 H. Y. Xing, X. P. Zheng, Q. G. Ren, W. B. Bu, W. Q. Ge, Q. F. Xiao, S. J. Zhang, C. Y. Wei, H. Y. Qu, Z. Wang, Y. Q. Hua, L. P. Zhou, W. J. Peng, K. L. Zhao and J. L. Shi, *Sci. Rep.*, 2013, **3**, 1751.
77 F. Li, C. G. Li, J. H. Liu, X. M. Liu, L. Zhao, T. Y. Bai, Q. H. Yuan, X. G. Kong, Y. Han, Z. Shi and S. H. Feng, *Nanoscale*, 2013, **5**, 6950-6959.
78 S. J. Zeng, H. B. Wang, W. Lu, Z. G. Yi, L. Rao, H. R. Liu and J. H. Hao, *Biomaterials*, 2014, **35**, 2934-2941.
79 Z. G. Yi, S. J. Zeng, W. Lu, H. B. Wang, L. Rao, H. R. Liu and J. H. Hao, *ACS Appl. Mater. Interfaces*, 2014, **6**, 3839-3846.
80 Y. Z. Min, J. M. Li, F. Liu, P. Padmanabhan, E. K. L. Yeow and B. G. Xing, *Nanomaterials*, 2014, **4**, 129-154.
81 Wang and F. Zhang, *J. Mater. Chem. B*, 2014, **2**, 2422-2443.
82 J. R. Abdul and Y. Zhang, *Biomaterials*, 2008, **29**, 4122-4128.
83 L. Xiong, T. Yang, Y. Yang, C. Xu and F. Li, *Biomaterials*, 2010, **31**, 7078-7085.
84 J. C. Zhou, Z. L. Yang, W. Dong, R. J. Tang, L. D. Sun and C. H. Yan, *Biomaterials*, 2011, **32**, 9059-9067.
85 L. Cheng, K. Yang, X. Lu, M. Shao and Z. Liu, *Nanomedicine*, 2011, **6**, 1327-1340.
86 K. Wang, J. B. Ma, M. He, G. Gao, H. Xu, J. Sang, Y. X. Wang, B. Q.

Zhao and D. X. Cui, *Theranostics*, 2013, **3**, 258-266.
87 C. Y. Liu, Y. Hou and M. Y. Gao, *Adv. Mater.*, 2014, DOI:10.1002/adma.201305535.
88 J. Yang, *Adv. Drug Delivery Rev.*, 2012, **64**, 965-966.
89 S. Mura, J. Nicolas and P. Couvreur, *Nat. Mater.*, 2013, **12**, 991-1003.
90 N. C. Fan, F. Y. Cheng, J. A. Ho and C. S. Yeh, *Angew. Chem., Int. Ed.*, 2012, **51**, 8806-8810.
91 Y. M. Yang, B. Velmurugan, X. G. Liu and B. G. Xing, *Small*, 2013, **9**, 2937-2944.
92 L. Z. Zhao, J. J. Peng, Q. Huang, C. Y. Li, M. Chen, Y. Sun, Q. N. Lin, L. Y. Zhu and F. Y. Li, *Adv. Funct. Mater.*, 2014, **24**, 363-371.
93 J. N. Liu, W. B. Bu, L. M. Pan and J. L. Shi, *Angew. Chem.*, *Int. Ed.*, 2013, **52**, 4375-4379.
94 L. Zhou, Z. W. Chen, K. Dong, M. L. Yin, J. S. Ren and X. G. Qu, *Adv. Mater.*, 2014, **26**, 2424-2430.
95 Y. L. Dai, H. H. Xiao, J. H. Liu, Q. H. Yuan, P. A. Ma, D. M. Yang, C. X. Li, Z. Y. Cheng, Z. Y. Hou, P. P. Yang and J. Lin, *J. Am. Chem. Soc.,* 2013, **135**, 18920-18929.
96 Y. Z. Min, J. M. Li, F. Liu, E. K. L. Yeow and B. G. Xing, *Angew. Chem., Int. Ed.*, 2014, **53**, 1012-1016.
97 G. F. Wang, Q. Peng and Y. D. Li, *Acc. Chem. Res.*, 2011, **44**, 322-332.
98 M. Haase and H. Schfer, *Angew. Chem., Int. Ed.*, 2011, **50**, 5805-5829.
99 Heike S Mader, Peter Kele, Sayed M Saleh and Otto S Wolfbeis, *Curr. Opin. Chem. Biol.*, 2010, **14**, 582-596.
100 P. P. Fedorov, A. A. Luginina, S. V. Kuznetsov and V. V. Osiko, *J. Fluorine Chem.*, 2011, **132**, 1012-1039.
101 F. C. J. M. van Veggel, C. H. Dong, N, J. J. Johnson and J. Pichaandi, *Nanoscale*, 2012, **4**, 7309-7321.
102 A. Kar and A. Patra, *Nanoscale*, 2012, **4**, 3608-3619.
103 T. Liu, L. N. Sun, Z. Liu, Y. N. Qiu and L. Y. Shi, *Prog. Chem.*, 2012, **24**, 304-317.
104 J. Chen and J. X. Zhao, *Sensors*, 2012, **12**, 2414-2435.
105 D. Q. Chen and Y. S. Wang, *Nanoscale*, 2013, **5**, 4621-4637.
106 P. Y. Qiu, N. Zhou, H. Y. Chen, C. L. Zhang, G. Gao and D. X. Cui, *Nanoscale*, 2013, **5**, 11512-11525.
107 Y. S. Liu, D. T. Tu, H. M. Zhu, E. Ma and X. Y. Chen, *Nanoscale*, 2013, **5**, 1369-1384.
108 D. T. Tu, Y. S. Liu, H. M. Zhu and X. Y. Chen, *Chem. Eur. J.*, 2013, **19**, 5516-5527.
109 C. Wang, L. Cheng and Z. Liu, *Theranostics*, 2013, **3**, 317-330.
110 X. M. Li, D. Y. Zhao and F. Zhan, *Theranostics*, 2013, **3**, 292-305.
111 W. GJHM van Sark, J. de Wild, J. K. Rath, A. Meijerink, R. EI Schropp, *Nanoscale Res. Lett.*, 2013, **8**, 81-90.
112 H. Z. Lian, Z. Y. Hou, M. M. Shang, D. L. Geng, Y. Zhang and J. Lin, *Energy*, 2013, **57**, 270-283.
113 Y. M. Yang, *Microchim. Acta*, 2014, **181**, 263-294.
114 T. D. Tu, W. Zheng, Y. S. Liu, H. M. Zhu and X. Y. Chen, *Coord. Chem. Rev.*, 2014, **273-274**, 13-29.
115 X. Wang and Y. D. Li, *Nature*, 2005, **437**, 121-124.
116 H. X. Mai, Y. W. Zhang, R. Si, Z. G. Yan, L. D. Sun, L. P. You and C. H. Yan, *J. Am. Chem. Soc.*, 2006, **128**, 6426-6436.
117 F. Zhang, Y. Wan, T. Yu, F. Q. Zhang, Y. F. Shi, S. H. Xie, Y. G. Li, L. Xu, B. Tu and D. Y. Zhao, *Angew. Chem., Int. Ed.*, 2007, **46**, 7976-7979.
118 Z. Q. Li, Y. Zhang and S. Jiang, *Adv. Mater.*, 2008, **20**, 4765-4769.
119 H. Q. Wang and T. Nann, *ACS Nano*, 2009, **3**, 3804-3808.
120 F. Wang, Y. Han, C. S. Lim, Y. H. Lu, J. Wang, J. Xu, H. Y. Chen, C. Zhang, M. H. Hong and X. G. Liu, *Nature* 2010, **463**, 1061-1065.
121 X. C. Ye, J. E. Collins, Y. J. Kang, J. Chen, D. T. N. Chen, A. G. Yodh and C. B. Murray, *Proc. Natl. Acad. Sci.*, 2010, **107**, 22430-22435.
122 D. Q. Chen, Y. L. Yu, F. Huang, P. Huang, A. P. Yang and Y. S. Wang, *J. Am. Chem. Soc.*, 2010, **132**, 9976-9978.
123 F. Zhang, G. B. Braun, Y. F. Shi, Y. C. Zhang, X. H. Sun, N. O. Reich, D. Y. Zhao and G. Stucky, *J. Am. Chem. Soc.*, 2010, **132**, 2850-2851.
124 D. T. Tu, L. Q. Liu, Q. Ju, Y. S. Liu, H. M. Zhu, R. F. Li and X. Y. Chen, *Angew. Chem., Int. Ed.*, 2011, **50**, 6306-6310.
125 N. J. J. Johnson, A. Korinek, C. H. Dong and F. C. J. M. van Veggel, *J. Am. Chem. Soc.*, 2012, **134**, 11068-11071.
126 B. Voss and M. Haase, *ACS Nano*, 2013, **7**, 11242-11254.
127 C. Zhang and J. Y. Lee, *ACS Nano*, 2013, **7**, 4393-4402.
128 Y. S. Liu, D. T. Tu, H. M. Zhu, E. Ma and X. Y. Chen, *Nanoscale*, 2013, **5**, 1369-1384.
129 J. Shen, G. Chen, T. Y. Ohulchanskyy, S. J. Kesseli, S. Buchholz, Z. Li, P. N. Prasad and G. Han, *Small*, 2013, **9**, 3213-3231.
130 X. S. Zhai, S. S. Liu, Y. L. Zhang, G. S. Qin and W. P. Qin, *J. Mater. Chem. C*, 2014, **2**, 2037-2044.
131 S. J. Zeng, Z. G. Yi, W. Lu, C. Qian, H. B. Wang, L. Rao, T. M. Zeng, H. R. liu, H. J. Liu, B. Fei and J. H. Hao, *Adv. Funct. Mater.*, 2014, DOI: 10.1002/adfm.201304270.
132 P. Huang, W. Zheng, S. Y. Zhou, D. T. Tu, Z. Chen, H. M. Zhu, R. F. Li, E. Ma, M. D. Huang and X. Y. Chen, *Angew. Chem. Int. Ed.*, 2014, **53**, 1252-1257.
133 W. W. Ye, M. K, Tsang, X. Liu, M. Yang and J. H. Hao, *Small*, 2014, DOI: 10.1002/smll.201303766.
134 R. Martín-Rodríguez, S. Fischer, A. Ivaturi, B. Froehlich, K. W. Krämer, J. C. Goldschmidt, B. S. Richards and A. Meijerink, *Chem. Mater.*, 2013, **25**, 1912-1921.
135 A. Ivaturi, S. K. W. Macdougall, R. M. Rodriguez, M. Quintanilla, J. Marques-Hueso, K. W. Krämer, A. Meijerink and B. S. Richards, *J. Applied. Phys.*, 2013, **114**, 1-10.
136 T. Liu, X. Bai, C. Miao, Q. L. Dai, W. Xu, Y. H. Yu, Q. D. Chen and H. W. Song, *J. Phys. Chem. C*, 2014, **118**, 3258-3265.
137 H. P. Paudel, L. L. Zhong, K. Bayat, M. F. Baroughi, S. Smith, C. K. Lin, C. Y. Jiang, M. T. Berry and P. S. May, *J. Phys. Chem. C*, 2011, **115**, 19028-19036.
138 S. Schietinger, T. Aichele, H.Q. Wang, T. Nann and O. Benson, *Nano Lett.*, 2010, **10**, 134-138.
139 W. Ge, X. R. Zhang, M. Liu, Z. W. Lei, R. J. Knize and Y. L. Lu, *Theranostics*, 2013, **3**, 282-288.
140 Qi-C. Sun, H. Mundoor, J. C. Ribot,V. Singh, I. I. Smalyukh and P. Nagpal, *Nano Lett.*, 2014, **14**, 101-106.
141 Q. Luu, A. Hor, J. Fisher, R. B. Anderson, S. Liu, T.-S. Luk, H. P. Paudel, M. F. Baroughi, P. S. May and S. Smith, *J. Phys. Chem. C*, 2014, **118**, 3251-3257.
142 W. Li and D. Y. Zhao, *Adv. Mater.*, 2013, **25**, 142-149.
143 W. Stöber, A. Fink and E. Bohn, *J. Colloid Interface Sci.*, 1968, **26**, 62-69.
144 N. Erathodiyil and J. Y. Ying, *Acc. Chem. Res.*, 2011, **44**, 925-935.
145 A. Guerrero-Martínez, J. Pérez-Juste and L. M. Liz-Marzán, *Adv.*

Mater., 2010, **22**, 1182-1195.
146 F. J. Arriagada and K. Osseo-Asare, *J. Colloid Interface Sci.*, 1999, **211**, 210-220.
147 F. F. Li, C. G. Li, X. M. Liu, Y. Chen, T. Y. Bai, L. Wang, Z. Shi and S. H. Feng, *Chem. Eur. J.*, 2012, **18**, 11641-11646.
148 B. Liu, C. X. Li, D. M. Yang, Z. Y. Hou, P. A. Ma, Z. Y. Cheng, H. Z. Lian, S. S. Huang and J. Lin, *Eur. J. Inorg. Chem.*, 2014, 1906-1913.
149 Z. Q. Li, L. M. Wang, Z. Y. Wang, X. H. Liu and Y. J. Xiong, *J. Phys. Chem. C* , 2011, **115**, 3291-3296.
150 X. G. Yu, Y. Shan, G. C. Li and K. Z. Chen, *J. Mater. Chem.*, 2011, **21**, 8104-8109.
151 Q. F. Xiao, X. P. Zheng, W. B. Bu, W. Q. Ge, S. J. Zhang, F. Chen, H. Y. Xing, Q. G. Ren, W. P. Fan, K. L. Zhao, Y. Q. Hua and J. L. Shi, *J. Am. Chem. Soc.*, 2013, **135**, 13041-13048.
152 H. Y. Xing, W. B. Bu, S. J. Zhang, X. P. Zheng, M. Li, F. Chen, Q. J. He, L. P. Zhou, W. J. Peng, Y. Q. Hua and J. L. Shi, *Biomaterials*, 2012, **33**, 1079-1089.
153 S. Liu, G. Y. Chen, T. Y. Ohulchanskyy, M. T. Swihart and P. N. Prasad, *Theranostics*, 2013, **3**, 275-281.
154 M. Vallet-Regí, A. Rámila, R. P. del Real and J. Pérez-Pariente, *Chem. Mater.*, 2001, **13**, 308-311.
155 P. P. Yang, Z. W. Quan, C. X. Li, X. J. Kang, H. Z. Lian and J. Lin, *Biomaterials*, 2008, **29**, 4341-4347.
156 P. P. Yang, Z. W. Quan, Z. Y. Hou, C. X. Li, X. J. Kang, Z. Y. Cheng and J. Lin, *Biomaterials*, 2009, **30**, 4786-4795.
157 J. E. Lee, N. Lee, T. Kim, J. Kim and T. Hyeon, *Acc. Chem. Res.*, 2011, **44**, 893-902.
158 J. M. Rosenholm, C. Sahlgren and M. Lindén, *Curr. Drug Targets*, 2011, **12**, 1166-1186.
159 C. Argyo, V. Weiss, C. Bräuchle and T. Bein, *Chem. Mater.*, 2014, **26**, 435-451.
160 S. L. Gai, P. P. Yang, C. X. Li, W. X. Wang, Y. L. Dai, N. Niu and J. Lin, *Adv. Funct. Mater.*, 2010, **20**, 1166-1172.
161 Z. H. Xu, C. X. Li, P. A. Ma, Z. Y. Hou, D. M. Yang, X. J. Kang and J. Lin, *Nanoscale*, 2011, **3**, 661-667.
162 Z. Liu, L. N. Sun, F. Y. Li, Q. Liu, L. Y. Shi, D. S. Zhang, S. Yuan, T. Liu and Y. N. Qiu, *J. Mater. Chem.*, 2011, **21**, 17615-17618.
163 H. S. Qian, H. C. Guo, P. C. Ho, R. Mahendran and Y. Zhang, *Small*, 2009, **5**, 2285-2290.
164 S. X. Shi, F. Chen and W. B. Cai, *Nanomedicine*, 2013, **8**, 2027-2039.
165 J. Kim, J. E. lee, J. lee, J. H. Yu, B. C. Kim, K. An, Y. Hwang, C. H. Shin, J. G. Park, J. Kim and T. Hyeon, *J. Am. Chem. Soc.*, 2006, **128**, 688-689.
166 J. E. Lee, N. Lee, T. Kim, J. Kim and T. Hyeon, *Acc. Chem. Res.*, 2011, **44**, 893-902.
167 C. X. Li, J. L. Liu, S. Alonso, F. Y. Li and Y. Zhang, *Nanoscale*, 2012, **4**, 6065-6071.
168 J. N. Liu, W. B. Bu, S. J. Zhang, F. Chen, H. Y. Xing, L. M. Pan, L. P. Zhou, W. J. Peng and J. L. Shi, *Chem. Eur. J.*, 2012, **18**, 2335-2341.
169 C. X. Li, D. M. Yang, P. A. Ma, Y. Y. Chen, Y. Wu, Z. Y. Hou, Y. L. Dai, J. H. Zhao and C. P. Sui, *Small*, 2013, **9**, 4150-4159.
170 C. X. Li, Z. Y. Hou, Y. L. Dai, D. M. Yang, Z. Y. Cheng, P. A. Ma and J. Lin, *Biomater. Sci.*, 2013, **1**, 213-223.
171 L. N. Sun, T. Liu, Y. N. Qiu, J. L. Liu, L. Y. Shi and O. S. Wolfbeis, *Microchim. Acta*, 2014, **181**, 775-781.
172 L. L. Li, F. Q. Tang, H. Y. Liu, T. L. Liu, N. J. Hao, D. Chen, X. Teng and J. Q. He, *ACS Nano*, 2010, **4**, 6874-6882.
173 L. Li, C. Liu, L. Y. Zhang, T. T. Wang, H. Yu, C. G. Wang and Z. M. Su, *Nanoscale*, 2013, **5**, 2249-2253.
174 L. L. Chen, L. Li, L. Y. Zhang, S. X. Xing, T. T. Wang, Y. A. Wang, C. G. Wang and Z. M. Su, *ACS Appl. Mater. Interfaces*, 2013, **5**, 7282-7290.
175 F. Zhang, G. B. Braun, A. Pallaoro, Y. C. Zhang, Y. F. Shi, D. X. Cui, M. Moskovits, D. Y. Zhao and G. D. Stucky, *Nano Lett.*, 2012, **12**, 61-67.
176 L. Y. Zhang, T. T. Wang, L. Yang, C. Liu, C. G. Wang, H. Y. Liu, Y. A. Wang and Z. M. Su, *Chem. Eur. J.*, 2012, **18**, 12512-12521.
177 X. J. Zhu, J. Zhou, M. Chen, M. Shi, W. Feng and F. Y. Li, *Biomaterials*, 2012, **33**, 4618-4627.
178 W. P. Fan, B. Shen, F. Chen, K. L. Zhao, S. J. Zhang, L. P. Zhou, W. J. Peng, Q. F. Xiao, H. Y. Xing, J. N. Liu, D. L. Ni, Q. J. He and J. L. Shi, *J. Am. Chem. Soc.*, 2013, **135**, 6494-6503.
179 Y. F. Zhu, T. Ikoma, N. Hanagata and S. Kaskel, *Small*, 2010, **6**, 471-478.
180 X. J. Kang, Z. Y. Cheng, D. M. Yang, P. A. Ma, M. M. Shang, C. Peng, Y. L. Dai and J. Lin, *Adv. Funct. Mater.*, 2012, **22**, 1470-1481.
181 F. Q. Tang, L. L. Li and D. Chen, *Adv. Mater.*, 2012, **24**, 1504-1534.
182 Q. Zhang, T. R. Zhang, J. P. Ge and Y. D. Yin, *Nano Lett.*, 2008, **8**, 2867-2871.
183 X. L. Fang, X. J. Zhao, W. J. Fang, C. Chen and N. F. Zheng, *Nanoscale*, 2013, **5**, 2205-2218.
184 J. Liu, F. Liu, K. Gao, J. S. Wu and D. F. Xue, *J. Mater. Chem.*, 2009, **19**, 6073-6084.
185 X. J. Kang, C. X. Li, Z. Y. Cheng, P. A. Ma, Z. Y. Hou and J. Lin, *Wiley Interdiscip. Rev. Nanomed. Nanobiotechnol.*, 2014, **6**, 80-101.
186 G. Jia, H. P. You, K. Liu, Y. H. Zheng, N. Guo and H. J. Zhang, *Langmuir*, 2010, **26**, 5122-5128.
187 Y. H. Han, S. L. Gai, P. A. Ma, L. Z. Wang, M. L. Zhang, S. H. Huang and P. P. Yang, *Inorg. Chem.*, 2013, **52**, 9184-9191.
188 G. Tian, Z. J. Gu, X. X. Liu, L. J. Zhou, W. Y. Yin, L. Yan, S. Jin, W. L. Ren, G. M. Xing, S. J. Li and Y. L. Zhao, *J. Phys. Chem. C*, 2011, **115**, 23790-23796.
189 L. Dong, D. An, M. Gong, Y. Lu, H. L. Gao, Y. J. Xu and S. H. Yu, *Small*, 2013, **9**, 3235-3241.
190 H. Ren, L. Y. Zhang, T. T. Wang, L. Li, Z. M. Su and C. G. Wang, *Chem. Commun.*, 2013, **49**, 6036-6038.
191 Y. Wang, P. P. Yang, P. A. Ma, F. Y. Qu, S. L. Gai, N. Niu, F. He and J. Lin, *J. Mater. Chem. B*, 2013, **1**, 2056-2065.
192 F. Zhang, Y. F. Shi, X. H. Sun, D. Y. Zhao and G. D. Stucky, *Chem. Mater.*, 2009, **21**, 5237-5243.
193 X. J. Kang, D. M. Yang, Y. L. Dai, M. M. Shang, Z. Y. Cheng, X. Zhang, P. A. Ma and J. Lin, *Nanoscale*, 2013, **5**, 253-261.
194 Z. H. Xu, P. A. Ma, C. X. Li, Z. Y. Hou, X. F. Zhai, S. S. Huang and J. Lin, *Biomaterials*, 2011, **32**, 4161-4173.
195 D. M. Yang, X. J. Kang, P. A. Ma, Y. L. Dai, Z. Y. Hou, Z. Y. Cheng, C. X. Li and J. Lin, *Biomaterials*, 2013, **34**, 1601-1612.
196 H. Y. Chen, B. Qi, T. Moore, D. C. Colvin, T. Crawford, J. C. Gore, F. Alexis, O. T. Mefford and J. N. Anker, *Biomaterials*, 2014, **10**, 160-168.

197 G. Chen, F. S. Chen, X. H. Liu, W. Ma, H. M. Luo, J. H. Li, R. Z. Ma and G. Z. Qiu, *Nano Res.*, 2014, DOI: 10.1007/s12274-014-0472-5.
198 W. Feng, L. D. Sun, Y. W. Zhang and C. H. Yan, *Small*, 2009, **5**, 2057-2060.
199 D. M. Yang, Y. L. Dai, P. A. Ma, X. J. Kang, Z. Y. Cheng, C. X. Li and J. Lin, *Chem. Eur. J*, 2013, **19**, 2685- 2694.
200 C. Wang, L. Cheng and Z. Liu, *Biomaterials*, 2011, **32**, 1110-1120.
201 G. Tian, Z. J. Gu, L. J. Zhou, W. Y. Yin, X. X. Liu, L. Yan, S. Jin, W. L. Ren, G. M. Xing, S. J. Li and Y. L. Zhao, *Adv. Mater.*, 2012, **24**, 1226-1231.
202 L. L. Li, R. B. Zhang, L. L. Yin, K. Z. Zheng, W. P. Qin, P. R. Selvin and Y. Lu, *Angew. Chem. Int. Ed.*, 2012, **51**, 6121-6125.
203 W. L. Rem, G. Tian, S. Jian, Z. J. Gu, L. J. Zhou, L. Yan, S. Jin, W. Y. Yin and Y. L. Zhao, *RSC Adv.*, 2012, **2**, 7037-7041.
204 G. Tian, W. Y. Yin, J. J. Jin, X. Zhang, G. M. Xing, S. J. Li, Z. J. Gu and Y. L. Zhao, *J. Mater. Chem. B*, 2014, **2**, 1379-1389.
205 F. Wang, D. K. Chatterjee, Z. Li, Y. Zhang, X. Fan and M. Wang, *Nanotechnology*, 2006, **17**, 5786-5791.
206 X. Zhang, Y. M. Wang and J. Zhu, *Chem. Mater.*, 2011, **21**, 12132-12318.
207 H. J. Wang, R. Shrestha and Y. Zhang, *Part. Part. Syst. Charact.*, 2014, **31**, 228-235.
208 P. A. Ma, H. H. Xiao, X. Li, C. X. Li, Y. L. Dai, Z. Y. Cheng, X. B. Jing and J. Lin, *Adv. Mater.*, 2013, **25**, 4898-4905.
209 H. Xu, L. Cheng, C. Wang, X. X. Ma, Y. G. Li and Z. Liu, *Biomaterials*, 2011, **32**, 9364-9373.
210 L. Cheng, K. Yang, Y. Li, J. Chen, C. Wang, M. Shao, S.-T. Lee and Z. Liu, *Angew. Chem., Int. Ed.*, 2011, **50**, 7385-7390.
211 L. Cheng, K, Yang, Y. G. Li, X. Zeng, M. W. Shao, S. T. Lee and Z. Liu, *Biomaterials*, 2012, **33**, 2215-2222.
212 P. Wang, Y. P. Wang and M. Li, *Light Sci. Appl.*, 2013, **2**, e102.
213 Q. L. Ma, J. X. Wang, X. T. Dong, W. S. Yu and G. X. Liu, *J. Nanopart. Res.*, 2014, **16**, 2239.
214 B. Dong, H. W. Song, H. Q. Yu, H. Zhang, R. F. Qin, X. Bai, G. H. Pan, S. Z. Lu, F. Wang, L. B. Fan and Q. L. Dai, *J. Phys. Chem. C*, 2008, **112**, 1435-1440.
215 G. G. Li, Z. Y. Hou, C. Peng, W. X. Wang, Z. Y. Cheng, C. X. Li, H. Z. Lian and J. Lin, *Adv. Funct. Mater.*, 2010, **20**, 3446-3456.
216 Z. Y. Hou, P. P. Yang, C. X. Li, L. L. Wang, H. Z. Lian, Z. W. Quan and J. Lin, *Chem. Mater.*, 2008, **20**, 6686-6696.
217 Z. Y. Hou, G. G. Li, H. Z. Lian and J. Lin, *J. Mater. Chem.*, 2012, **22**, 5254-5276.
218 Z. Y. Hou, C. M. Zhang, C. X. Li, Z. H. Xu, Z. Y. Cheng, G. G. Li, W. X. Wang, C. Peng and J. Lin, *Chem. Eur. J.*, 2010, **16**, 14513-14519.
219 Z. Y. Hou, C. X. Li, P. A. Ma, G. G. Li, Z. Y. Cheng, C. Peng, D. M. Yang, P. P. Yang and J. Lin, *Adv. Funct. Mater.*, 2011, **21**, 2356-2365.
220 Z. Y. Hou, C. X. Li, P. A. Ma, Z. Y. Cheng, X. J. Li, X. Zhang, Y. L. Dai, D. M. Yang, H. Z. Lian and J. Lin, *Adv. Funct. Mater.*, 2012, **22**, 2713-2722.
221 X. J. Li, X. J. Li, C. X. Li, Y. L. Dai, P. A. Ma, X. Zhang, X. J. Kang, Z. Y. Cheng and J. Lin, *RSC Advances*, 2013, **3**, 8517-8526.
222 Z. Y. Hou, X. J. Li, C. X. Li, Y. L. Dai, P. A. Ma, X. Zhang, X. J. Kang, Z. Y. Cheng and J. Lin, *Langmuir*, 2013, **29**, 9473-9482.
223 M. Liu, H. Liu, S. F. Sun, X. J. Li, Y. M. Zhou, Z. Y Hou and J. Lin, *Langmuir* 2014, **30**, 1176-1182.
224 T. T. T. Nguyen, C. Ghosh, S.-G. Hwang, L. D. Tran and J. S. Park, *J. Mater. Sci.*, 2013, **48**, 7125-7133.
225 J. S. Choi, K. W. Leong and H. S. Yoo, *Biomaterials*, 2008, **29**, 587-596.
226 N. Bölgen, I. Vargel, P. Korkusuz, Y. Z. Menceloğlu and E. Pişkin, *J. Biomed. Mater. Res. B*, 2007, **81B**, 530-543.
227 P. Zahedi, I. Rezaeian, S. O. Ranaei-Siadat, S. H. Jafari and P. Supaphol, *Polym. Adv. Technol.*, 2010, **21**,77-95.
228 Z. G. Chen, P. W. Wang, B. Wei, X. M. Mo and F. Z. Cui, *Acta Biomater.*, 2010, **6**, 372-382.
229 A. Schneider, X. Y. Wang, D. L. Kaplan, J. A. Garlick and C. Egles, *Acta Biomater.*, 2009, **5**, 2570-2578.
230 C. M. Zhang, C. X. Li, S. S. Huang, Z. Y. Hou, Z. Y. Cheng, P. P. Yang and J. Lin, *Biomaterials*, 2010, **31**, 3374-3383.
231 X. J. Kang, Z. Y. Cheng, C. X. Li, D. M. Yang, M. M. Shang, P. A. Ma, G. G. Li, N. Liu and J. Lin, *J. Phys. Chem. C,* 2011, **115**, 15801-15811.
232 Y. Y. Chen, P. A. Ma, D. M. Yang, Y. Wu, Y. L. Dai, C. X. Li and J. Lin, *Chem. Asian J.*, 2014, **9**, 506-513.
233 Y. L. Dai, D. M. Yang, P. A. Ma, X. J. Kang, X. Zhang, C. X. Li, Z. Y. Hou, Z. Y. Cheng and J. Lin, *Biomaterials*, 2012, **33**, 8704-8713.
234 J. Zhang, Z. F. Yuan, Y. Wang, W. H. Chen, G. F. Luo, S. X. Cheng, R. X. Zhuo and X. Z. Zhang, *J. Am. Chem. Soc.*, 2013, **135**, 5068-5073.
235 K. K. Cotí, M. E. Belowich, M. Liong, M. W. Ambrogio, Y. A. Lau, H. A. Khatib, J. I. Zink, N. M. Khashab and J. F. Stoddart, *Nanoscale*, 2009, **1**, 16-39.
236 J. Z. Du, T. M. Sun, W. J. Song, J. Wu and J. Wang, *Angew. Chem., Int. Ed.*, 2010, **49**, 3621-3626.
237 A. F. Radovic-Moreno, T. K. Lu, V. A. Puscasu, C. J. Yoon, R. Langer and O. C. Farokhzad, *ACS Nano*, 2012, **6**, 4279-4287.
238 J. Z. Du, X. J. Du, C. Q. Mao and J. Wang, *J. Am. Chem. Soc.*, 2011, **133**, 17560-17563.
239 X. K. Jia, J. J. Yin, D. G. He, X. X. He, K. M. Wang, M. Chen and Y. H. Li, *J. Biomed. Nanotechnol.*, 2013, **9**, 2063-2072.
240 C. Wang, L. Cheng, Y. M. Liu, X. J. Wang, X. X. Ma, Z. Y. Deng, Y. G. Li and Z. Liu, *Adv. Funct. Mater.*, 2013, **23**, 3077-3086.
241 Y. Chen, K. L. Ai, Y. L. Liu and L. H. Lu, *ACS Appl. Mater. Interfaces*, 2014, **6**, 655-663.
242 F. H. Chen, L. M. Zhang, Q. T. Chen, Y. Zhang and Z. J. Zhang, *Chem. Commun.*, 2010, **46**, 8633-8635.
243 D. M. Yang, Y. L. Dai, J. H. Liu, Y. Zhou, Y. Y. Chen, C. X. Li, P. A. Ma and J. Lin, *Biomaterials*, 2014, **35**, 2011-2023.
244 Y. Z. You, K. K. Kalebaila, S. L. Brock and D. Qupicky, *Chem. Mater.*, 2008, **20**, 3354-3359.
245 Y. H. Lien, T. M. Wu, J. H. Wu and J. W. Liao, *J. Nanopart. Res.*, 2011, **13**, 5065-5075.
246 Y. F. Yang, A. J. Mijalis, H. Fu, C. Agosto, K. J. Tan, J. D. Batteas and D. E. Bergbreiter, *J. Am. Chem. Soc.*, 2012, **134**, 7378-7383.
247 K. S. Soppimath, D. C. W. Tan and Y. Y. Yang, *Adv. Mater.*, 2005, **17**, 318-323.
248 M. S. Yavuz, Y. Cheng, J. Chen, C. M. Cobley, Q. Zhang, M. Rycenga, J. Xie, C. Kim, K. H. Song, A. G. Schwartz, L. H. V. Wang and Y. N. Xia, *Nat. Mater.*, 2009, **8**, 935-939.
249 B. Chang, X. Sha, J. Guo, Y. Jiao, C. Wang and W. Yang, *J. Mater.*

Chem., 2011, **21**, 9239-9247.
250 Z. Y. Cheng, R. T. Chai, P. A. Ma, Y. L. Dai, X. J. Kang, H. Z. Lian, Z. Y. Hou, C. X. Li and J. Lin, *Langmuir*, 2013, **29**, 9573-9580.
251 Y. L. Dai, P. A. Ma, Z. Y. Cheng, X. J. Kang, X. Zhang, Z. Y. Hou, C. X. Li, D. M. Yang, X. F. Zhai and J. Lin, *ACS Nano*, 2012, **6**, 3327-3338.
252 X. Zhang, P. P. Yang, Y. L. Dai, P. A. Ma, X. J. Li, Z. Y. Cheng, Z. Y. Hou, X. J. Kang, C. X. Li and J. Lin, *Adv. Funct. Mater.*, 2013, **23**, 4067-4078.
253 N. Graf and S. J. Lippard, *Adv. Drug Delivery Rev.*, 2012, **64**, 993-1004.
254 Y. L. Dai, X. J. Kang, D. M. Yang, X. J. Li, X. Zhang, C. X. Li, Z. Y. Hou, Z. Y. Cheng, P. A. Ma and J. Lin, *Adv. Healthcare Mat.*, 2013, **2**, 562-567.
255 P. Zhao, Y. H. Zhu, X. L. Yang, J. H. Shen, X. Jiang, J. Zong and C. Z. Li, *Dalton Trans.*, 2014, **43**, 451-457.
256 G. Mayer and A. Heckel, *Angew. Chem., Int. Ed.*, 2006, **45**, 4900-4921.
257 Q. N. Lin, Q. Huang, C. Y. Li, C. Y. Bao, Z. Z. Liu, F. Y. Li and L. Y. Zhu, *J. Am. Chem. Soc.*, 2010, **132**, 10645-10647.
258 N. Niu, F. He, P. A. Ma, S. L. Gai, G. X. Yang, F. Y. Qu, Y. Wang, J. Xu and P. P. Yang, *ACS Appl. Mater. Interfaces*, 2014, **6**, 3250-3262.
259 Y. M. Yang, Q. Shao, R. R. Deng, C. Wang, X. Teng, K. Cheng, Z. Cheng, L. Huang, Z. Liu, X. G. Liu and B. G. Xing, *Angew. Chem. Int. Ed.*, 2012, **51**, 3125-3129.
260 S. Sortino, *J. Mater. Chem.*, 2012, **22**, 301-318.
261 G. C. R. Ellis-Davies, *Nat. Methods*, 2007, **4**, 619-628.
262 P. Klán, T. Šolomek, C.G. Bochet, A. Blanc, R. Givens, M. Rubina, V. Popik, A. Kostikov and J. Wirz, *Chem. Rev.*, 2013, **113**, 119-191.
263 Y. H. Chien, Y. L. Chou, S. W. Wang, S. T. Hung, M. C. Liau, Y. J. Chao, C. H. Su and C. S. Yeh, *ACS Nano*, 2013, **7**, 8516-8528.
264 C. J. Carling, F. Nourmohammadian, J. C. Boyer and N. R. Branda, *Angew. Chem., Int. Ed.*, 2010, **49**, 3782-3785.
265 J. V. Garcia, J. P. Yang, D. K. Shen, C. Yao, X. M. Li, R. Wang, G. D. Stucky, D. Y. Zhao, P. C. Ford and F. Zhang, *Small*, 2012, **8**, 3800-3805.
266 P. T. Burks, J. V. Garcia, R. GonzalezIrias, J. T. Tillman, M. T. Niu, A. A. Mikhailovsky, J. P. Zhang, F. Zhang, and P. C. Ford, *J. Am. Chem. Soc.*, 2013, **135**, 18145-18152.
267 B. Yan, J. C. Boyer, D. Habault, N. R. Branda and Y. Zhao, *J. Am. Chem. Soc.*, 2012, **134**, 16558-16561.
268 B. Yan, J.-C. Boyer, N. R. Branda and Y. Zhao, *J. Am. Chem. Soc.*, 2011, **133**, 19714-19717.
269 Y. M. Yang, F. Liu, X. G. Liu and B. G. Xing, *Nanoscale*, 2013, **5**, 231-238.
270 W. Li, J. S. Wang, J. S. Ren and X. G. Qu, *J. Am. Chem. Soc.*, 2014, **136**, 2248-2251.
271 S. Sortino, *Chem. Soc. Rev.*, 2010, **39**, 2903-2913.
272 P. C. Ford, *Nitric Oxide*, 2013, **34**, 56-64.
273 Q. B. Xiao, Y. T. Ji, Z. H. Xiao, Y. Zhang, H. Z. Lin and Q. B. Wang, *Chem. Commun.*, 2013, **49**, 1527-1529.
274 Q. Yuan, Y. F. Zhang, T. Chen, D. Q. Lu, Z. L. Zhao, X. B. Zhang, Z. X. Li, C. H. Yan and W. H. Tan, *ACS Nano*, 2012, **6**, 6337-6344.
275 F. Ercole, T. P. Davisa and R. A. Evans, *Polym. Chem.*, 2010, **1**, 37-54.
276 N. K. Mal, M. Fujiwara and Y. Tanaka, *Nature*, 2003, **421**, 350-353.
277 C.-J. Carling, J.-C. Boyer and N. R. Branda, *J. Am. Chem. Soc.*, 2009, **131**, 10838-10839.
278 J.-C. Boyer, C.-J. Carling, B. D. Gates and N. R. Branda, *J. Am. Chem. Soc.*, 2010, **132**, 15766-15772.
279 T. S. Yang, Q. Liu, J. C. Li, S. Z. Pu, P. Y. Yang and F. Y. Li, *RSC Adv.*, 2014, **4**, 15613-15619.
280 B. F. Zhang, M. Frigoli, F. Angiuli, F. Vetrone and J. A. Capobianco, *Chem. Commun.*, 2012, **48**, 7244-7246.
281 L. Wang, H. Dong, Y. N. Li, C. M. Xue, L. D. Sun, C. H. Yan and Q. Li, *J. Am. Chem. Soc.*, 2014, **136**, 4480-4483.
282 P. Muller, B. Schroder, J. A. Parkinson, N. A. Kratochwil, R. A. Coxall, A. Parkin, S. Parsons and P. J. Sadler, *Angew. Chem., Int. Ed.*, 2003, **42**, 335-339.
283 N. J. Farrer, J. A. Woods, L. Salassa, Y. Zhao, K. S. Robinson, G. Clarkson, F. S. Mackay and P. J. Sadler, *Angew. Chem., Int. Ed.*, 2010, **49**, 8905-8908.
284 F. Chen, S. J. Zhang, W. B. Bu, Y. Chen, Q. F. Xiao, J. N. Liu, H. Y. Xing, L. P. Zhou, W. J. Peng and J. L. Shi, *Chem. Eur. J.*, 2012, **18**, 7082-7090.
285 G. Tian, W. L. Ren, L. Yan, S. Jian, Z. J. Gu, L. J. Zhou, S. Jin, W. Y. Yin, S. J. Li and Y. L. Zhao, *Small*, 2013, **9**, 1929-1938.
286 Y. H. Wang, H. G. Wang, D. P. Liu, S. Y. Song, X. Wang and H. J. Zhang, *Biomaterials*, 2013, **34**, 7715-7724.
287 S. Jin, L. J. Zhou, Z. J. Gu, G. Tian, L. Yan, W. L. Ren, W. Y. Yin, X. D. Liu, X. Zhang, Z. B. Hu and Y. L. Zhao, *Nanoscale*, 2013, **5**, 11910-11918.
288 S. S. Cui, D. Y. Yin, Y. Q. Chen, Y. F. Di, H. Y. Chen, Y. X. Ma, S. Achilefu and Y. Q. Gu, *ACS Nano*, 2013, **7**, 676-688.
289 Q. Chen, C. Wang, L. Cheng, W. W. He, Z. P. Cheng and Z. Liu, *Biomaterials*, 2014, **35**, 2915-2923.
290 L. Zhou, Z. H. Li, Z. Liu, M. L. Yin, J. S. Ren and X. G. Qu, *Nanoscale*, 2014, **6**, 1445-1452.
291 P. Zhang, W. Steelant, M. Kumar and M. Scholfield, *J. Am. Chem. Soc.*, 2007, **129**, 4526-4527.
292 X. F. Qiao, J. C. Zhou, J. W. Xiao, Y. F. Wang, L. D. Sun and C. H. Yan, *Nanoscale*, 2012, **4**, 4611-4623.
293 X. H. Liu, H. S. Qian, Y. P. Ji, Z. Q. Li, Y. Shao, Y. Hu, G. X. Tong, L. C. Li , W. D. Guo and H. C. Guo, *RSC Adv.*, 2012, **2**, 12263-12268.
294 N. M. Idris, M. K. Gnanasammandhan, J. Zhang, P. C. Ho, R. Mahendran and Y. Zhang, *Nat. Med.*, 2012, **18**, 1580-1585.
295 C. Wang, H.Q. Tao, L. Cheng and Z. Liu, *Biomaterials*, 2011, **32**, 6145-6154.
296 A. G. Zhou, Y. C. Wei, B. Y. Wu, Q. Chen and D. Xing, *Mol. Pharmaceutics*, 2012, **9**, 1580-1589.
297 X. M. Liu, M. Zheng, X. G. Kong, Y. L. Zhang, Q. H. Zeng, Z. C. Sun, W. J. Buma and H. Zhang, *Chem. Commun.*, 2013, **49**, 3224-3226.
298 K. Liu, X. M. Liu, Q. H. Zeng, Y. L. Zhang, L. P. Tu, T. Liu, X. G. Kong, Y. H. Wang, F. Cao, S. A. Lambrechts, M. C. G. Aalders and H. Zhang, *ACS Nano*, 2012, **6**, 4054-4062.
299 L. Xia, X. G. Kong, X. M. Liu, L. P. Tu, Y. L. Zhang, Y. L. Chang, K. Liu, D. Z. Shen, H. Y. Zhao and H. Zhang, *Biomaterials*, 2014, **35**, 4146-4156.

300 Y. I. Park, H. M. Kim, J. H. Kim, K. C. Moon, B. Yoo, K. T. Lee, N. Lee, Y. Choi, W. Park, D. Ling, K. Na, W. K. Moon, S. H. Choi, H. S. Park, S. Y. Yoon,Y. D. Suh, S. H. Lee and T. Hyeon, *Adv. Mater.*, 2012, **24**, 5755-5761.
301 G. Y. Chen, J. Shen, T. Y. Ohulchanskyy, N. J. Patel, A. Kutikov, Z. P. Li, J. Song, R. K. Pandey, H. Ågren, P. N. Prasad and G. Han, *ACS Nano*, 2012, **6**, 8280-8287.
302 P. S. Low, W. A. Henne and D. D. Doorneweerd, *Acc. Chem. Res.*, 2008, **41**, 120-129.
303 T. Y. Cao, Y. Yang, Y. A. Gao, J. Zhou, Z. Q. Li and F. Y. Li, *Biomaterials*, 2011, **32**, 2959-2968.
304 N. Erathodiyil and J. Y. Ying, *Acc. Chem. Res.*, 2011, **44**, 925-935.
305 S. Jiang, Y. Zhang, K. M. Lim, E. K. W. Sim and Y. F. Shi, *Nanotechnology*, 2009, **20**, 155101.
306 X. J. Yang, Q. Q. Xiao, C. X. Niu, N. Jin, J. Ouyang, X. Y. Xiao and D. C. He, *J. Mater. Chem. B*, 2013, **1**, 2757-2763.
307 L. M. Pan, Q. J. He, J. N. Liu, Y. Chen, M. Ma, L. L. Zhang and J. L. Shi, *J. Am. Chem. Soc.*, 2012, **134**, 5722-5725.
308 J. N. Liu, W. B. Bu, L. M. Pan, S. J. Zhang, F. Chen, L. P. Zhou, K. L. Zhao, W. J. Peng and J. L. Shi, *Biomaterials*, 2012, **33**, 7282-7290.
309 X. Wang, C. X. Yang, J. T. Chen and X. P. Yan, *Anal. Chem.*, 2014, **86**, 3263-3267.
310 X. Fang and W. Tan, *Acc. Chem. Res.*, 2010, **43**, 48-57.
311 Z. Y. Xiao and O. C. Farokhzad, *ACS Nano*, 2012, **6**, 3670-3676.
312 Q. Yuan, Y. Wu, J. Wang, A. Q. Lu, Z. L. Zhao, T. Liu, X. B. Zhang and W. H. Tan, *Angew. Chem., Int. Ed.*, 2013, **52**, 13965-13969.
313 W. R. Zhao, H. R. Chen, Y. S. Li, L. Li, M. D. Lang and J. L. Shi, *Adv. Funct. Mater.*, 2008, **18**, 2780-2788.
314 D. K. Pan, H. Zhang, T. Fan, J. G. Chen and X. Duan, *Chem. Commun.*, 2011, **47**, 908-910.
315 X. J. Kang, Y. L. Dai, P. A. Ma, D. M. Yang, C. X. Li, Z. Y. Hou, Z. Y. Cheng and J. Lin, *Chem. Eur. J.*, 2012, **18**, 15676-15682.
316 V. V. Mody, A. Cox, S. Shah, A. Singh, W. Bevins and H. Parihar, *Appl. Nanosci.*, 2014, **4**, 385-392.
317 J. Wang, R. R. Deng, M. A. MacDonald, B. L. Chen, J. K. Yuan, F. Wang, D. Z. Chi, T. S. A. Hor, P. Zhang, G. K. Liu, Y. Han and X. G. Liu, *Nat. Mater.*, 2014, **13**,157-162.
318 L. Cheng, C. Wang and Z. Liu, *Nanoscale*, 2013, **5**, 23-27.

Table 1 A summary of recent works on UCNPs-based stimuli-responsive drug delivery systems

Stimuli	Nanoparticles platform	Drug	The style of drug loading	Release experiments	Ref.
pH (PAA)	$NaYF_4$:Yb/Er/Gd @PAA@SiO_2	DOX	electrostatic interaction	*in vitro*	173
	ecc-(*con*-$NaYF_4$:Yb/Er/Gd @mSiO_2)@PAA	DOX	physical adsorption and electrostatic interaction	*in vitro*	174
	$GdVO_4$:Yb/Er@PAA	DOX	electrostatic interaction	*in vitro*	193
	$NaYF_4$:Yb/Er@PAA	DOX	electrostatic interaction	*in vitro*	239
	$NaYF_4$:Yb/Er@γ-AlO(OH)	DOX	physical adsorption	*in vitro*	241
pH (-CONHN=)	$NaYF_4$:Yb/Tm-CONHN=DOX	DOX	covalent bonding	*in vitro*	233
	$BaGdF_5$:Yb/Tm@$BaGdF_5$:Yb -CONHN=DOX	DOX	covalent bonding	*in vitro*	243
thermo (PNIPAM)	$NaYF_4$:Yb/Er@SiO_2@ (PNIPAM-*co*-PAA)	DOX	electrostatic interaction	*in vitro*	251
	$NaYF_4$:Yb/Er@mSiO_2@ (PNIPAM-*co*-PAA)	DOX	physical adsorption and electrostatic interaction	*in vitro*	252
redox (GSH)	$NaYF_4$:Yb/Er-PEI-Pt(IV)	cisplatin	covalent bonding	*in vitro*	254
	$NaYF_4$:Yb/Er-Pt(IV)-mPEG -b-PCL-b-PLL	cisplatin	covalent bonding	*in vitro* and *in vivo*	208
	Fe_3O_4@SiO_2@$NaYF_4$:Yb/Er @MnO_2	Congo red	electrostatic interaction	*in vitro*	255
magnetic	Fe_3O_4@SiO_2@mSiO_2@ $NaYF_4$:Yb/Er	ibuprofen	hydrophobic interaction and Covalent bonding	*in vitro*	160
	Fe_3O_4@SiO_2@volid@ Y_2O_3:Yb/Er	DOX	physical adsorption	*in vitro* and *in vivo*	175
	Fe_3O_4@$NaYF_4$:Yb/Er@ PS_{16}-*b*-PAA_{10}	DOX	polymer encapsulation	*in vitro* and *in vivo*	209

Table 2 A summary of recent works on NIR light-induced photolysis of "caged" compounds

Caged compounds	Photosponsive moieties	Nanoparticles platform	λ_{em} of UCNPs	Active component	Ref.
NB caged oligo(ethylene) glycol	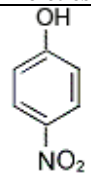 NB	$NaYF_4$:Yb/Tm@ $NaYF_4$@mSiO_2	350 nm	DOX (anticancer drug)	91
NE caged D-luciferin	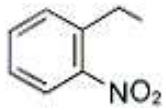 1-(2-nitrophenyl) ethyl (NE)	$NaYF_4$:Yb/Tm@ $NaYF_4$@SiO_2	350 nm	D-luciferin	259
NBA caged folic acid	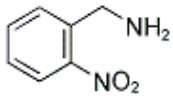 NBA	$NaYF_4$:Yb/Tm@ SiO_2	360 nm	Folic acid (phototarget) and DOX	263
Benzion caged carboxylic acid	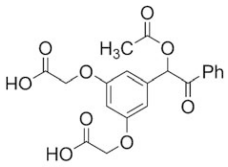 3',5'-di(carboxymethoxy)benzoin	$NaYF_4$:Yb/Tm	290 nm	carboxylic acid	264
Fe_4S_3 $(NO)_7^-$ caged NO	Fe_4S_3 $(NO)_7^-$	$NaYF_4$:Yb/Er@ $NaYF_4$@SiO_2	540 nm	NO	265
		$NaYF_4$:Gd/Yb/Er@ $NaYF_4$-polymer disk	540 nm	NO	266
ONB caged biomacro-molecules	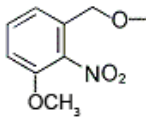 ONB	$NaYF_4$:Yb/Tm@$NaYF_4$-hydrogel	350 nm	Biomacro-molecules	267
ONB caged block copolymer	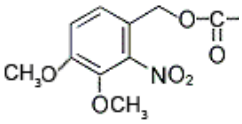 ONB	$NaYF_4$:Yb/Tm@$NaYF_4$-block copolymer	350 nm	Nile Red	268
DMNPE caged siRNA	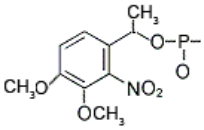 DMNPE	$NaYF_4$:Yb/Tm@ SiO_2@mSiO_2	350 nm	siRNA	269

ONA caged cell adhesion	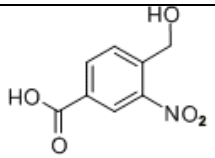 ONA	$NaYF_4$:Yb/Tm	360 nm	Cell release	270

Table 3 A summary of recent works on NIR light-induced photoswitching of photochromic molecules.

Photochromic molecules	Structure transformation	Nanoparticles platform	application	Ref.
azobenzenes	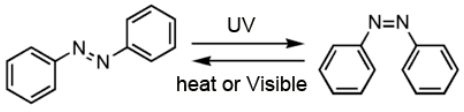 trans form cis-form	$NaYF_4$:Yb/Tm@$NaYF_4$ @$mSiO_2$	DOX release	93
spiropyrans	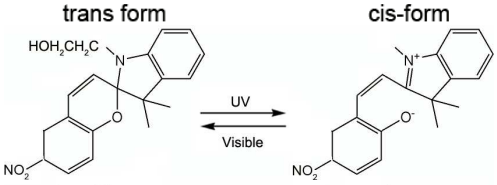 closed form (Spiro, colorless) open form (merocyanine, colored)	hollow $NaYF_4$:Yb/Er	enzyme release	94
diarylethenes	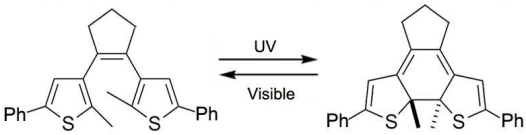 open form colorless closed form colored	$NaYF_4$:Yb/Er (Yb/Tm)	reversible photoswitching	277
diarylethenes	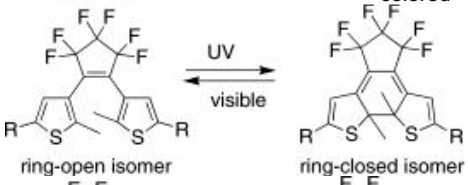 ring-open isomer ring-closed isomer	$NaYF_4$:Yb/Er@ $NaYF_4$:Yb/Tm@$NaYF_4$	reversible photoswitching	278
diarylethenes	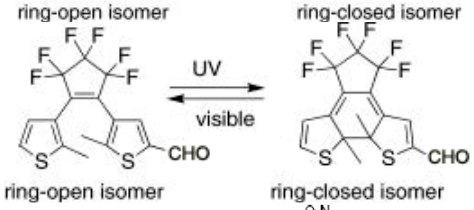 ring-open isomer ring-closed isomer	$NaYF_4$:Yb/Er/Tm	upconversion small animal imaging *in vivo*	279
bis-spiropyrans	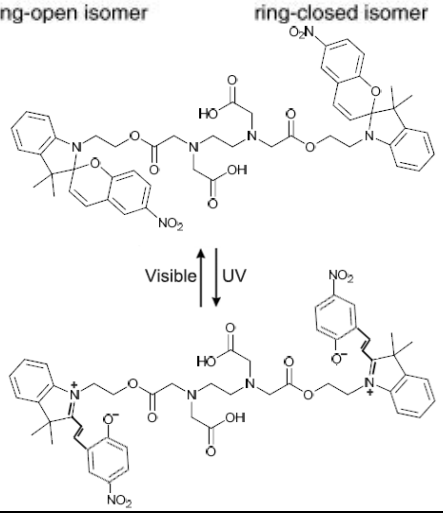	$LiYF_4$:Yb/Tm	reversible photoswitching	280

Azobenzene derivative (chiral molecular)	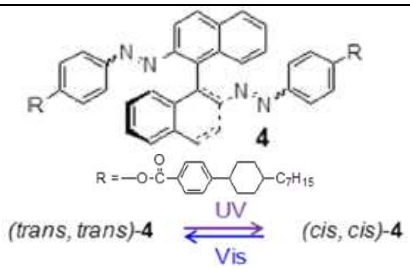	$NaGdF_4$:Yb/Tm@$NaGdF_4$	reversible NIR light directed reflection in a helical superstructure	281

Table 4 A summary of recent works on UCNPs-based PDT system

UCNPs	Surface structure or ligand	PS (Abs_{max})	Incorporated PS to UCNPs	Targeting agent	Ref.
$NaYF_4$:Yb/Er	$mSiO_2$	ZnPc (672 nm)	Silica encapsulation	□□	163
$NaYF_4$:Yb/Er	PAH-DMMA-PEG	Ce6 (663 nm)	Electrostatic adsorption	□□	240
$NaYF_4$:Yb/Er @$NaYF_4$	NGO-PEG	ZnPc (672 nm)	Hydrophobic interaction	□□	286
$NaYbF_4$:Gd/Tm@ $NaGdF_4$	Tween 20	Hypocrellin A (470 nm)	Hydrophobic interaction	□□	287
$NaYF_4$:Yb/Er	Chitosan	ZnPc (672 nm)	Hydrophobic interaction	FA	288
$NaGdF_4$:Yb/Er	BSA	RB (550 nm)	Hydrophobic interaction	□□	289
$NaYF_4$:Yb/Er	Pores	MB (663 nm)	Physical adsorption	□□	290
$NaYF_4$:Yb/Er	SiO_2	MC540 (555 nm)	Silica encapsulation	Antibody	291
$NaYF_4$:Yb/Er	$mSiO_2$	MC540 (555 nm) ZnPc (672 nm)	Silica encapsulation	FA	294
$NaYF_4$:Yb/Er	$C_{18}P_{MH}$-PEG	Ce6 (663 nm)	Hydrophobic interaction	□□	295
$NaYF_4$:Yb/Er	O-Carboxymethy-lated chiosan	PPa (668 nm)	Covalent bonding	c(RGDyK)	296
$NaYF_4$:Yb/Er@ $NaYF_4$:Yb/Tm	PAAM	C_{60}MA	Covalent bonding	FA	297
$NaYF_4$:Yb/Er	AEP	RB (550 nm)	Covalent bonding	FA	298
$NaYF_4$:Yb/Er	Poly(allylamine)	ZnPc (660 nm)	Covalent bonding	FA	299
$NaYF_4$:Yb/Er @$NaGdF_4$	PEG-phospholipids	Ce6 (663 nm)	Hydrophobic interaction and Covalent bonding	□□	300
$NaYF_4$:Yb/Gd/Tm	APBA and HAC_{60}	HAC_{60} (475, 650 nm)	Covalent bonding	APBA and HA	309

5